Variability in Greenhouse Gas Dynamics due to Spatial Heterogeneity and Seasonality in Alaskan Arctic Coastal Wetlands

By

JOSHUA F. HASHEMI
DISSERTATION

Submitted in partial satisfaction of the requirements for the degree of

DOCTOR OF PHILOSOPHY

in

Ecology

a joint program in the

OFFICES OF GRADUATE STUDIES

of the

UNIVERSITY OF CALIFORNIA DAVIS

and

SAN DIEGO STATE UNIVERSITY

Approved:

Walter C. Oechel, Chair

Donatella Zona, Co-Chair

Kyaw Tha Paw U

Committee in Charge

2022

Acknowledgements

For the willingness to provide an opportunity to embark on this path, the means with which to do it and council along the way, I'd like to thank my major professors, Dr. Walter C. Oechel and Dr. Donatella Zona. I'd also like to thank My UC Davis mentor, Dr. Kyaw Tha Paw U, for giving guidance and for his exceptional kindness; Dr. David A. Lipson, for selflessly taking time to be like an additional advisor to me, and importantly, reminding me that the pursuit of knowledge is not to be seen as an encumbrance - but rather, a privilege; Dr. Kyle A. Arndt for being a rare and true friend - for commiseration during moments of failure, and for celebration during those of success; Dr. Aram Kalhori, for her friendship and for encouragement, particularly during the innumerable times of self-doubt. I'd like to thank the global change research group and my cohort for feedback and suggestions.

Finally, I'd like to thank my parents. My mother, Shelley Martin, for her sacrifice and love throughout my life. Her struggles made it possible for me to undertake mine and I owe a debt that I can only hope to repay with my affection. My father, Farizad Hashemi, for his inexhaustible patience and support. I cannot express both the level of admiration I feel toward him nor how much I wish he were here to see the culmination of his efforts on my behalf.

Table of Contents

Abstract

The regional warming of high latitude ecosystems, such as the Arctic tundra, is occurring at an accelerated rate relative to the global average due to a considerable number of positive feedbacks. These ecosystems contain one of the largest terrestrial reservoirs of carbon and nitrogen, locked in the soil column by low temperatures and slow decomposition. However, warming temperatures are increasing emissions of primary greenhouse gases (GHG): carbon dioxide (CO_2), methane (CH_4), and nitrous oxide (N_2O) from these immense Arctic reservoirs. Increased release of greenhouse gases from permafrost dominated regions is providing a strong positive feedback on climate warming.

While attention to GHG dynamics in permafrost regions has increased over the past decade, understanding patterns and controls on GHG emissions due to seasonality and spatial heterogeneity are still poorly understood. This is particularly true for non-CO_2 greenhouse gas fluxes CH_4 and N_2O which are still understudied. Here, I use a combination of data from a network of eddy covariance towers, soil carbon measurements, and chamber flux measurements on the Arctic Coastal Plain to better understand the seasonal and spatial controls on GHG emissions from the Alaskan Arctic. I show that the timing and magnitude of carbon (CO_2 & CH_4) fluxes can be highly variable (77-107 g C-CO_2-eq m^{-2} $year^{-1}$) based on mesoscale (<1 km) hydrological status. While fall CH_4 emissions comprise up to 45% of the annual regional CH_4 budget, there has been uncertainty as to whether emissions of CH_4 during the fall are the product of active methanogenesis or the release of stored methane generated during the prior growing season. Here, I show that fall methane emissions (1100±50 mg C-CH_4

m^{-2}) outweigh methane storage within the soil active layer (106.8±7.9 mg C-CH_4 m^{-2} - 35cm depth). These results indicate that the dominant source of CH_4 emissions during the cold period is likely microbial activity rather than the release of stored methane. Finally, while emissions of N_2O have been thought negligible in Arctic wetlands due to low nitrogen mineralization and high plant-microbe competition for inorganic nitrogen, I show that features of the landscape that are collapsing due to ice wedge and permafrost degradation are important N_2O sources, as high as 38.6 mg N m^{-2} d^{-1}, more than an order of magnitude higher than previously assumed. This understanding of trends, budgets, and drivers of GHG fluxes in the Arctic is intended to help increase accuracy in regional and global climate model projections.

Introduction

Arctic regions contain one of the largest terrestrial reservoirs of carbon and nitrogen on Earth (Hugelius et al., 2014; Voigt et al., 2020), accumulated in permafrost due to cold temperatures and the slow microbial decomposition of soil organic matter. This region, historically a carbon and nitrogen sink, is undergoing accelerated warming, with temperatures having increased by 3.1°C from 1971-2019 in comparison to the global average of 1°C. (AMAP, 2021). The increased rate of warming in the Arctic is due to a number of feedbacks, but with increasing albedo and associated increased heat absorption of the land and sea surface (Serreze and Francis, 2006) being one major factor. Regional warming has already resulted in a number of changes to Arctic regions, including longer fall periods (Arndt et al., 2019), warmer winters (Bekryaev et al., 2010), and shifting hydrology (Liljedahl et al., 2016). Regional warming is beginning to liberate carbon and nitrogen stocks formerly locked in the soil reservoir, increasing emissions of the big three greenhouse gases, carbon dioxide (CO_2), methane (CH_4) and even nitrous oxide (N_2O), thought to be negligible year-round in Arctic ecosystems (Voigt et al., 2017; Voigt et al., 2020; Natali et al., 2021). The climate forcing of these increased emissions stimulates further temperature increase both regionally and globally.

Climate forcing potential, in terms of greenhouse gas emission in the Arctic tundra, involves complex interactions of microbial communities throughout the year and is characterized by large spatial and temporal variability. Until recently, the summer growing season was thought to be the primary period wherein CO_2 and CH_4 atmospheric flux dynamics were significant. Fluxes during the non-growing period were considered to be negligible. However, research has shown that large emissions of both

CO_2 and CH_4 can occur during the non-growing period (Oechel et al., 2014; Zona et al., 2016; Commane et al., 2017; Natali et al., 2019). CH_4 emissions during the non-growing period can be over half of the annual budget. Non-growing period CO_2 emissions can offset much, if not all of, growing season uptake (Hashemi et al., 2021). Non-growing period emissions are primarily associated with early winter in the period during which the soil active layer is freezing, but not entirely frozen. During this period, there is a lens of unfrozen soil around 0°C called the “zero-curtain” (Outcalt et al., 1990; Zona et al., 2016). However, there has been uncertainty if emissions during this fall period are due to current microbial production, or if emissions are simply the release of gas produced during the previous growing season. As Arctic warming is most pronounced during the winter (Bekryaev et al., 2010) and research has shown that the zero-curtain period may be elongating (Arndt et a., 2019), closing this knowledge gap is crucial for long-term climate understanding, prediction and simulations.

Landscape heterogeneity, characteristic of Arctic tundra, can also cause significant variability in GHG dynamics due to changes in oxygen availability, vegetation community, soil composition and soil structure (Butterbach-Bahl et al., 2013; Stewart et al., 2014) among other factors. Arctic tundra on the North Slope of Alaska is comprised of a mosaic of thaw lakes, drained lake basins and polygonized tundra (Hinkel et al., 2003) that can differ significantly in greenhouse gas emission budgets. These factors can cause large variability in emission rates over short distances (Oechel et al., 2014; Commane et al., 2017; Natali et al., 2019). Despite this, ecosystem modelling simulations often operate at coarse resolutions unable to capture this variability (Lara et al., 2020). This creates a mismatch in processes and process input data and results in a

higher model error when both estimating greenhouse gas budgets at a regional scale and the trajectory of Earth's climate at a global scale (Lara et al., 2020).

In the following work, I present three chapters aimed to address some of these critical gaps in knowledge by investigating the variability in greenhouse gas flux strength due to seasonality and spatial heterogeneity. Research took place in an Arctic tundra ecosystem near Utqiagvik, (formerly Barrow), Alaska on the Arctic Coastal Plains. In the first chapter, annual budgets of CH_4 and CO_2 are examined at three close-by sites using continuous year-round eddy-covariance measurements to find the degree of variability in carbon budget dynamics at the mesoscale (<1 km). In the second chapter, soil CH_4 concentrations are compared to mean CH_4 emission totals during the zero-curtain to reveal if emission amounts can be supported by the soil gas reservoir or if microbial production is likely. The third chapter investigates features of the landscape that are strong N_2O sources and identifies some of the controls on emission strength. Ecosystems that are highly sensitive to the effects of climate change are important indicators for climate mitigation efforts. In situ measurements of GHG dynamics from these regions are essential in understanding the trajectory of Earth's climactic fluctuations by informing input parameterizations for global climate simulations. Key is understanding underlying dynamics responsible for the sink-to-source transition currently developing in this vulnerable ecosystem.

Chapter 1

Seasonality buffers carbon budget variability across heterogeneous landscapes in Alaskan Arctic tundra

Joshua Hashemi, Donatella Zona, Kyle Arndt, Aram Kalhori, and Walter C. Oechel

Published in *Environmental Research Letters*

DOI: https://doi.org/10.1088/1748-9326/abe2d1

Abstract

Arctic tundra exhibits large landscape heterogeneity in microtopography, hydrology, and active layer depth. While many carbon flux measurements and experiments are done at or below the mesoscale (≤ 1km), modern ecosystem carbon modeling is often done at scales of 0.25° to 1.0° latitude, creating a mismatch between processes, process input data, and verification data. Here we arrange the naturally complex terrain into mesoscale landscape types of varying microtopography and moisture status to evaluate how landscape types differ in terms of CO_2 and CH_4 balances and their combined warming potential, expressed as CO_2 equivalents (CO_2-eq). Using a continuous four-year dataset of CO_2 and CH_4 fluxes obtained from three eddy covariance towers, we investigate the integrated dynamics of landscape type, vegetation community, moisture regime, and season on net CO_2 and CH_4 fluxes. Eddy covariance towers were situated across a moisture gradient including a moist upland tundra, a heterogeneous polygon tundra, and an inundated drained lake basin. We show that seasonal shifts in carbon emissions buffer annual carbon budget differences

caused by site variability. Of note, high growing season gross primary productivity leads to higher fall zero-curtain CO_2 emissions, reducing both variability in annual budgets and carbon sink strength of more productive sites. Alternatively, fall zero-curtain CH_4 emissions are equal across landscape types, indicating site variation has little effect on CH_4 emissions during the fall despite large differences during the growing season. We find that the polygon site has the largest mean warming potential (107±8.63 g C-CO_2-eq m^{-2} $year^{-1}$) followed by the drained lake basin site (82.12±9.85 g C-CO_2-eq m^{-2} $year^{-1}$) and the upland site (77.19±21.8 g C-CO_2-eq m^{-2} $year^{-1}$), albeit differences were not significant. The highest temperature sensitivities are also at the polygon site with mixed results between CO_2 and CH_4 at the other sites. Results show a similar mean annual net warming effect across dominant landscape types but that these landscape types vary significantly in the amounts and timing of CO_2 and CH_4 fluxes.

Introduction

Arctic tundra is characterized by long non-growing periods punctuated with short growing seasons and a high degree of landscape heterogeneity caused by freeze-thaw cycles. Because these ecosystems are largely inundated or frozen for much of year, soil decomposition is slow, resulting in one of the largest terrestrial reservoirs of labile carbon (C) (Hugelius et al., 2014). Comprising only 15% of the global land surface, Arctic tundra contain close to one third of the Earth's terrestrial soil C (~1500 Pg-C) (Zimov et al., 2006; Tarnocai et al., 2009; Kirschke et al., 2013). As this region is undergoing accelerated warming (Serreze & Francis, 2006), carbon dioxide (CO_2) emissions are increasing, causing a sink-source transition. (Oechel et al., 2014; Natali et al., 2015; Schuur et al., 2015; Commane et al., 2017; Natali et al., 2019). In addition

to CO_2, methane (CH_4) is an important greenhouse gas (GHG) in permafrost and wetland regions as methanogens thrive in areas with large amounts of anaerobic soil (Garcia et al., 2000). Arctic wetlands are responsible for ~15% of global wetland CH_4 emissions and ~4% of all global CH_4 emissions (Kirschke, 2013). As methanogenesis is a temperature sensitive process (Dunfield et al. 1993), it is likely that biogenic CH_4 emissions will increase (Tian et al., 2012; Lawrence et al., 2015). For this reason, attention to natural sources of CH_4 efflux has increased in Arctic regions.

Landscape heterogeneity can contribute to the wide range of estimates in CH_4 emission, ecosystem respiration (ER), and gross primary productivity (GPP) (McGuire et al., 2012, Treat et al., 2018). This heterogeneity is characterized by variability in soil moisture regime and develops from freeze-thaw cycles into a patchwork of polygonized tundra, thaw lakes, drained lake basins and moist upland tundra (Webber, 1978; Zulueta et al., 2011; Liljedahl et al., 2016). Polygonized tundra occurs from the common development of ice wedges in the soil column. As ice wedges degrade, inundated C rich low-centered polygons become drained high-centered polygons and drier upland tundra (Liljedahl et al., 2016). This shift can cause a decrease in CH_4 emissions and an increase in CO_2 emissions (Martin et al. 2017). Degrading ice wedges can also form trough- ponds that facilitate water movement, change the microbial community and, by extension, change GHG fluxes (Koch et al., 2014; Liljedahl et al., 2016). Similarly, thaw lakes form from permafrost thawing and subsequent land subsidence (Jorgensen & Shur, 2007; Huissteden et al., 2011). Thaw lakes drain, forming vegetated drained lake basins (Jorgensen & Shur, 2007). This indicates that over short distances, the effects of

climate change and controls of emissions can be highly variable due to soil moisture content and the resulting plant and microbial communities that develop.

Recent studies have shown emissions of CO_2 and CH_4 occur well into the non-growing season (Euskirchen et al., 2012; Oechel et al., 2014; Zona et al., 2016; Treat, Bloom, & Marushchak, 2018; Arndt et al., 2019a). Cold period emissions of CH_4 can account for nearly 50% of the yearly budget, and largely occur during fall shoulder periods when air and surface soil temperatures are below freezing, and subsurface temperatures are around zero degrees Celsius (20-30%) (Zona et al., 2016; Commane et al., 2017; Taylor et al., 2018). This period is referred to as the “zero-curtain” and is associated with the presence of an unfrozen portion of the active layer during freezing while phase transition occurs (Outcalt, et al.,1990). This highlights the importance of seasonality, yet there is still a paucity of data reflecting how interseasonal C dynamics vary in terms of landscape type.

Quantifying ongoing changes to the pan-Arctic carbon budget is important but cannot be achieved without understanding how variability in landscape scale climate responses affect emissions. By partitioning Arctic tundra ecosystems into sub-landscapes, the variability in timing and magnitude of C fluxes can be better understood. Using a continuous four-year dataset (2014-2017) of CO_2 and CH_4 fluxes obtained from three eddy covariance (EC) towers, each in a distinct landscape type, this study aims to quantify the integrated dynamics involved in CH_4, CO_2, and $CO_2 + CH_4$ (expressed as CO_2 equivalent (CO_2-eq), hereafter referred to as combined C) budgetary contributions due to landscape type, vegetation community composition, and seasonality.

Methodology

Study Area

EC study sites are located on continuous permafrost tundra on the North Slope of Alaska, near Utqiaġvik (Fig. 1(a)). The sites include the Barrow Environmental Observatory (US-Beo) (Fig. 1(b)), Biocomplexity Experiment South (US-Bes) (Fig. 1(c)) and a site near the NOAA Earth System Research Laboratory (US-Brw) (Fig. 1(d)). These sites were chosen for long-term continuous data acquisition as they capture dominant landscape variability of the region. US-Bes is in a drained lake basin containing the wettest soils (Table 1), with the water table above the surface for most of the growing season and is dominated by wet sedges and sphagnum moss (Davidson et al., 2016a). US-Brw is a moist upland tundra containing the driest soils (Table 1) and is dominated by graminoids and lichens (Kwon et al. 2006). US-Beo is characterized by ice wedge polygon formations that arise from the freeze thaw cycle (Webber, 1978). Due to these polygon formations, US-Beo is a mixed landscape, exhibiting both inundated and drained areas and consists of wet sedge/sphagnum moss dominated areas as well as drier graminoid/lichen dominated areas (Davidson et al., 2016a).

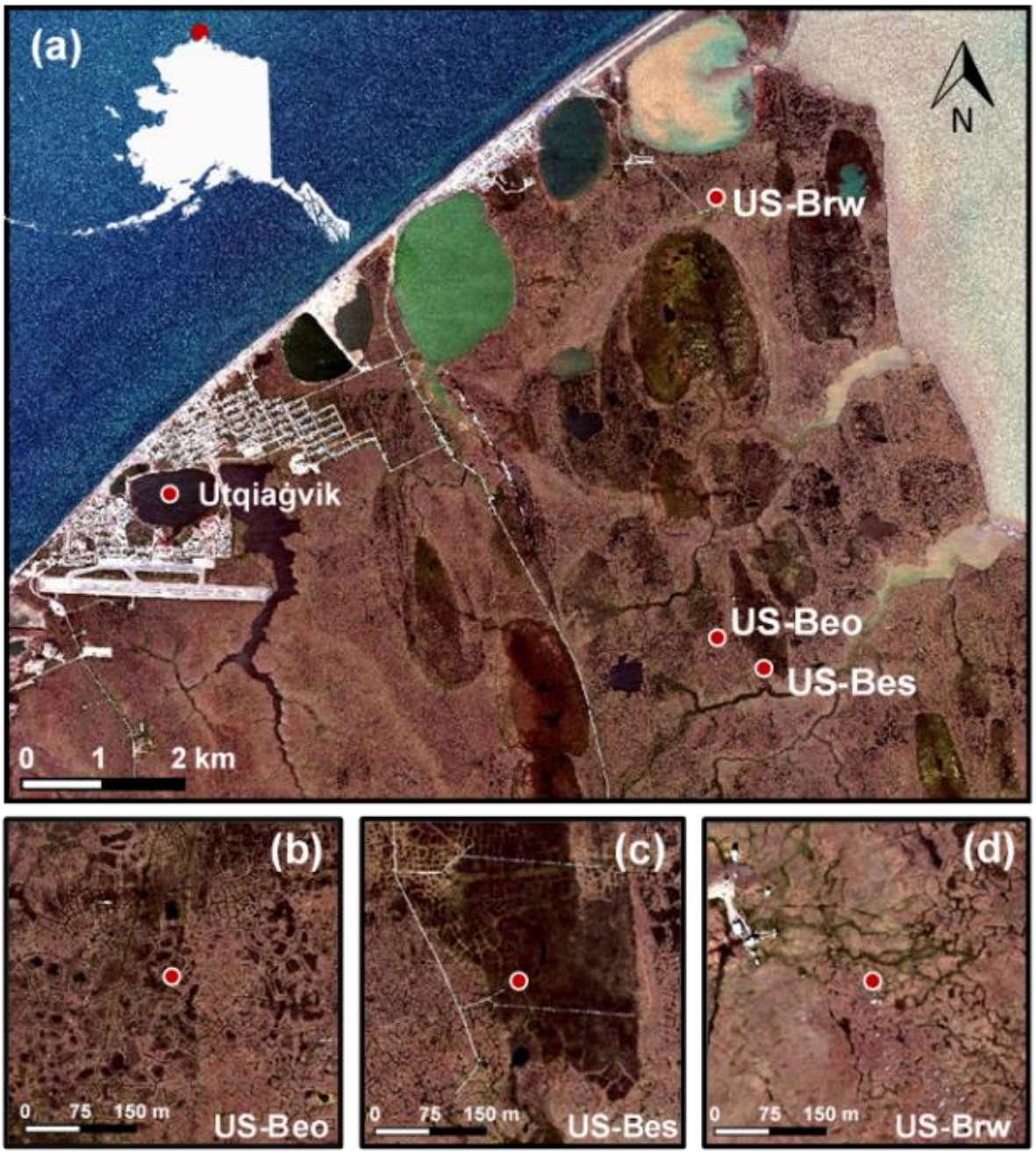

Figure 1: WorldView-3 (Maxar Technologies) imagery acquired 24, July 2016 of Utqiaġvik, AK (a) and the three eddy-covariance experimental sites, US-Beo (b), US-Bes (c), and US-Brw (d). Images generated using Environment for Visualizing Images V5.5 (Harris Geospatial) software.

Eddy Covariance & Meteorological Data

CH_4 and CO_2 fluxes were estimated at half-hourly intervals from year-round data collected at 10 Hz following the procedures outlined from LI-COR® EddyPro®. A double rotation was applied to the axis rotations of three-dimensional wind speeds according to Wilczak et al. (2001) and a block averaging interval was used to define turbulent fluctuations. An in situ/analytic correction, according to Ibrom et al. (2007), was applied to the gas analyzer data as the greenhouse gas analyzer (GGA) has a closed path. Quality flags were output within datasets according to Mauder and Foken (2011) and data that did not pass the quality requirements were removed. An internal chamber pressure of ≥ 20.67 kPa (155 torr) in the GGA indicates line blockage or instrument failure, and these data were eliminated. Additionally, a turbulence threshold was applied, identifying conditions with insufficient turbulence (indicated by low friction velocity ($u^* \leq 0.1$ m/s)), and those data were removed in accordance with Reichstein et al. (2005). A moving window of two weeks was applied and fluxes that were three standard deviations away from the mean were removed as outliers for CH_4 and CO_2 fluxes. EC tower site and instrumentation information can be found in Table 1 (Goodrich et al., 2016; Arndt et al., 2020).

Table 1. Instrumentation and Site Information

Site	Coordinates	Data DOI	EC Height	GGA	Anemometer	MMTD	SWC
US-Brw	71.322 N −156.609 W	10.18739/A2X34MS1B	4.2 m	LGR FGGA	METEK uSonic3 Class A	57±8 cm	47±4%
US-Beo	71.281 N −156.612 W	10.18739/A2X34MS1B	3.1. m	LGR FGGA	Campbell Scientific CSAT3	60±6 cm	H:59±10% T:72±18%
US-Bes	71.280 N −156.596 W	10.18739/A2X34MS1B	2.2 m	LGR FGGA	Campbell Scientific CSAT3	44±5 cm	83±12%

Abbreviations: LGR FGGA – Los Gatos Research Fast Greenhouse Gas Analyzer; MMTD – Mean Maximum Thaw Depth; SWC – Soil Water Content (H – High center, T - Trough). Values represent mean ± standard error over the study period.

Meteorological data were obtained at 30 second intervals and averaged into half hourly means. Each of the three sites had independent meteorological instrumentation and measurements used in defining the peak thaw and zero-curtain period. Meteorological instrumentation used in analysis included soil water content (Campbell Scientific® CS616 Water Content Reflectometer), soil temperature (Omega Engineering™, type T thermocouples), air temperature and humidity (Vaisala, HMP 45), and photosynthetically active radiation (PAR; LI-COR® LI-190R quantum sensor). At each site, soil temperature was measured at 0, -5, -15, and -30 cm from the soil surface and soil moisture probes were inserted from the soil surface to a depth of 20 cm, providing the average soil moisture in the top 20 cm of the soil column. Measurements of soil moisture were taken at one location at US-Brw and US-Bes, and two locations at US-Beo (a high center polygon and polygon trough) for better relief representation then averaged over the growing seasons within the study period. Data from both EC and meteorological instrumentation were collected using datalogger/multiplexer arrays from Campbell Scientific® (i.e., CR-3000, CR-23X & AM-1632). Thaw depth was measured weekly during the growing season by probing the land surface to the extent of the active layer along a transect with a small diameter metal rod.

Data/Statistical Analyses

EC tower footprints were estimated with the analytical footprint model of Korman and Meixner (KM) (2001) using the R package ‘FReddyPro’ v1.0 (Xenakis, 2016). The KM model calculates the density function of the footprint contribution for a two-dimensional area surrounding the EC tower and was used to estimate the landscape area in which 80% of fluxes originated by averaging half-hourly single flux footprints

during 2016. WorldView-3 (Maxar Technologies) imagery (1.24 m multispectral resolution) of Utqiaġvik, AK was used to show variability in the WorldView Normalized Difference Water Index (NDWI) at each of the three sites. As soil water content (SWC) is measured at one to two locations within each EC tower footprint and site hydrology can be variable, NDWI is used in conjunction with SWC to characterize differences in site moisture regime. The WorldView NDWI is calculated as the normalized difference between the coastal band (R_c, 400-450nm) reflectance and the second near infrared band (R_{NIR2}, 860-1040nm) reflectance (Eq. 1). This is because it has been shown that the R_c and R_{NIR2} bands show a better soil-water separation than the typical green (510 - 580 nm) and the first near infrared band (770 - 895 nm) combinations and is indicative of surface water moisture levels (Maglione, Parente, and Vallario, 2014). The NDWI results in values between -1 and 1 where more positive values represent wetter landscapes. Pixels outside of the footprint of the EC towers as well as those representing structures within the tower footprints were masked for statistical analysis. Before calculating statistics, pixels were aggregated into 3x3 pixel grids using the nearest neighbor approach to avoid bias by over sampling and to reduce high variability. A Pairwise Wilcoxon Rank Sum Tests was used to compare NDWI values among sites. Additional imagery for NDWI analysis across study period can be found in Supplementary Information (Fig. S1).

$$NDWI = \frac{R_C - R_{NIR2}}{R_C + R_{NIR2}} \qquad \textbf{Eq. 1}$$

Daily average fluxes were calculated in R V 3.6.2 (R core team, 2019) and R Studio software using the “data.table” package and were calculated with a minimum of

30 half hourly samples per day to ensure proper representation of the diurnal patterns of CH_4 and CO_2 fluxes. Daily averages of CH_4 and CO_2 fluxes for purposes of the examination of site variability and C budgets are beneficial as they show an accurate representation of the systems while qualifying data complexity and size. Data gaps are unavoidable in the harsh conditions characteristic of Arctic environments. These gaps can be a result of power or network outages as well as instrument failure. Total data coverage is between 61-71% depending on the site with the best coverage during the summer and fall periods. Detailed data coverage information by season and annual totals can be found in the supporting information (Table S1). Data gaps were filled using random forest machine learning (R package, “missForest”) utilizing a 300-decision tree design. Model validation can be found in supporting information (Fig. S2). Comparisons of model validation between the default half-hourly data output and daily averages show models perform much better when using a daily average. This method reduces the “noise” and is therefore better equipped to inform machine learning processes.

The beginning of the growing season was defined as the period where the top five cm of the soil are above zero °C, ending at the onset of the zero-curtain. The zero-curtain was defined as the period during the fall shoulder beginning when soil temperature of the top five cm of the soil are less than zero °C for three or more days, ending when the temperature at -15 cm (roughly the middle of the active layer, Table 1) dropped below -0.75°C for three or more days. Non-growing season, as defined here, includes both winter and spring, beginning at the end of the zero-curtain period and ending at the beginning of the growing season.

ER and GPP were partitioned from net ecosystem exchange (NEE) according to Lasslop et. al (2010) using the “REddyproc” package in R (Wutzler et al., 2018), as nighttime data is unobtainable during Arctic summer. Temperature response relationships were calculated using a weekly mean to reduce noise and to better represent annual trends. Models showing temperature response curves for CH_4 were calculated using soil temperature, rather than air temperature, as this has been shown to act as a better predictor for CH_4 fluxes (Arndt et al., 2019a) (Fig. S3). All temperature response curves were linearized by log transformation and compared using analyses of covariance (ANCOVA) to test for homogeneity among the regressions with the “car” R package (Fox and Weisberg, 2019) and Q_{10} values were calculated from temperature response regressions with the “respirometry” R package (Birk, 2020).

Results

Site Moisture Regime

NDWI as well as the KM model footprint of each EC tower were used to establish differences in surface water content within each EC tower footprint (Fig. 2). Using a Pairwise Wilcoxon Rank Sum Tests, NDWI was found to be significantly different ($p<0.001$) among each of the three sites. The results of the NDWI, showing levels of surface moisture, agreed with soil moisture data at the sites (Table 1) with US-Bes showing the wettest conditions (NDWI (mean ± standard error) = -0.079 ± 0.005), US-Beo showing intermediate NDWI levels (NDWI = -0.144 ± 0.003) and US-Brw with the lowest NDWI supporting its position as the driest site in the study (NDWI = -0.204 ± 0.003). Further analyses of NDWI show that imagery acquired July 24, 2016 was representative of site differences and while some variability occurs, these positions are

maintained (Fig. S1) as changes in vegetation community or hydrology at the landscape scale happens over longer periods of time (Arndt et al., 2019b, Liljedahl et al., 2016).

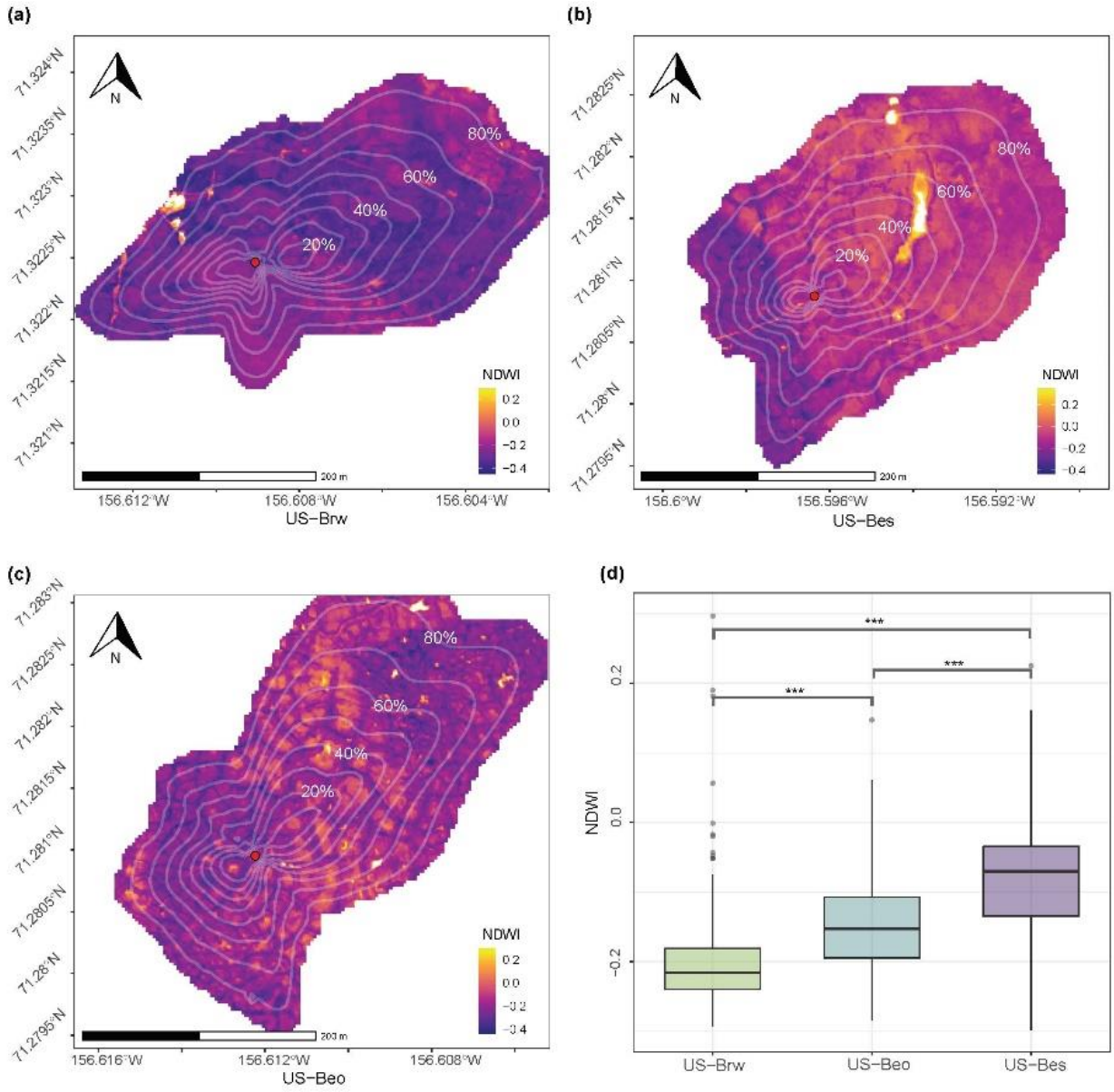

Figure 2: NDWI within EC tower footprints at (a) US-Brw, (b) US-Bes, and (c) US-Brw & NDWI by site (d). Red circles represent EC Tower and isolines are at each 10% and represent cumulative percent of flux contribution. (*** - p<0.001). WorldView-3 (Maxar Technologies) imagery acquired 24, July 2016 of Utqiaġvik, AK.

Seasonal Gas Flux

Peak growing season CH_4 emissions were higher at US-Bes (1.43 ± 0.11 mg C-CH_4 m^{-2} h^{-1}) and US-Beo (1.35 ± 0.31 mg C-CH_4 m^{-2} h^{-1}) in comparison with US-Brw (0.76 ± 0.10 mg C-CH_4 m^{-2} h^{-1}), however, CH_4 fluxes during the zero-curtain period showed lower variability across the three study sites (Fig. 3(a)). The annual average of peak uptake in NEE was greatest at the driest site, US-Brw (75.26 ± 8.9 mg C-CO_2 m^{-2} h^{-1}), followed by US-Beo (60.5 ± 7.9 mg C-CO_2 m^{-2} h^{-1}) and least pronounced at wettest site, US-Bes (39 ± 6.4 mg C-CO_2 m^{-2} h^{-1}). The annual average of peak emission in NEE followed the same order of US-Brw (44.25 ± 4.9 mg C-CO_2 m^{-2} h^{-1}), US-Beo (24.74 ± 5.3 mg C-CO_2 m^{-2} h^{-1}) and US-Bes (13.75 ± 1.7 mg C-CO_2 m^{-2} h^{-1}) (Fig. 3(b)).

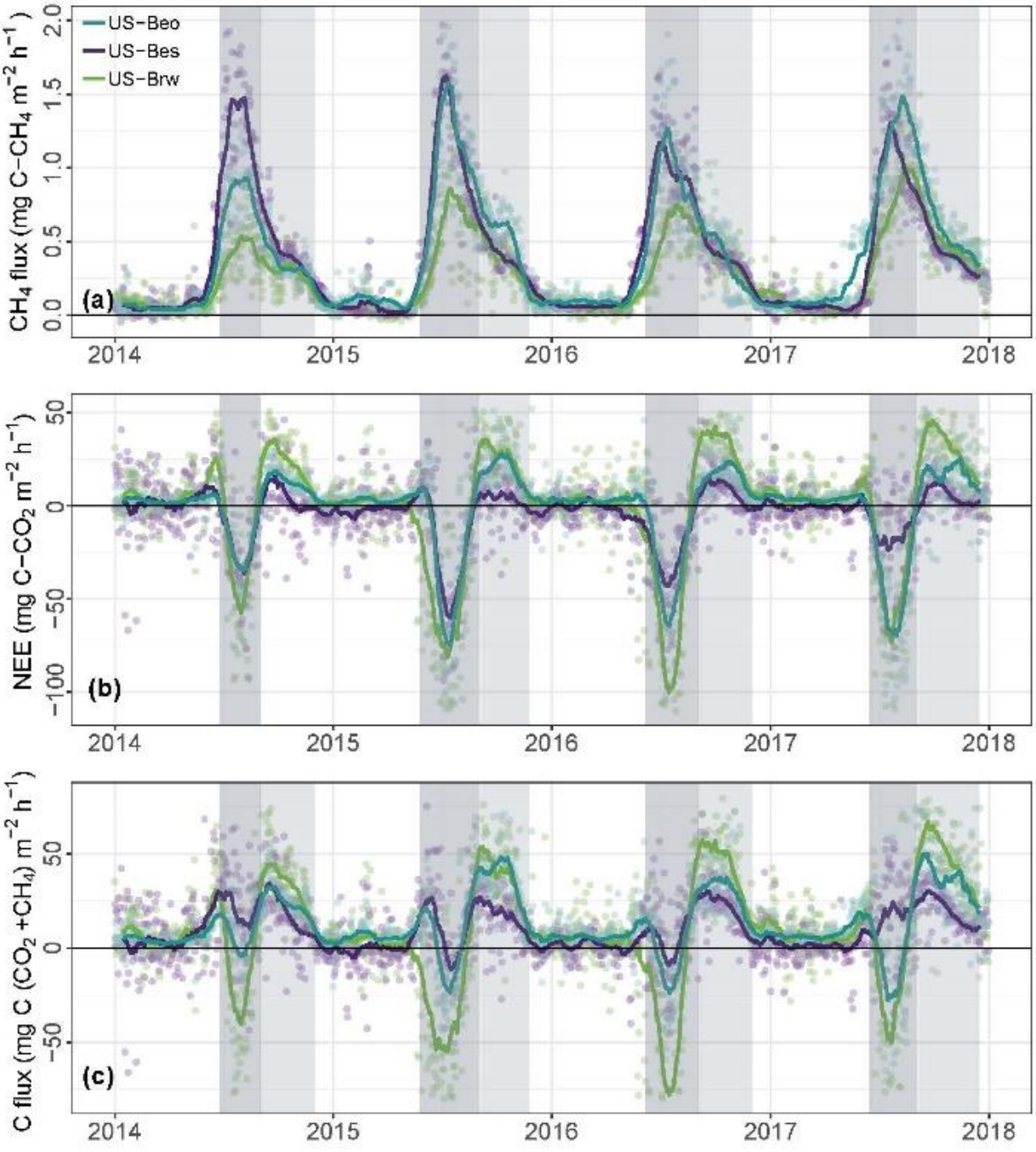

Figure 3: Carbon flux (daily average) of (a) CH_4, (b) CO_2 and (c) CO_2 + CH_4 (with CH_4 expressed as CO_2-eq based on warming potential) at the three EC sites. The darker shaded portion represents the growing season, while the lighter shaded portion represents the zero-curtain period.

Carbon Budget Variability

Seasonal fluctuations (growing season to zero-curtain) of CO_2 budgets are most pronounced at the driest site, US-Brw, and least pronounced at wettest site, US-Bes (Fig. 4(a)). Due to the higher zero-curtain CO_2 emissions dampening growing season CO_2 uptake, US-Brw is the weakest CO_2 sink on average. This trend holds with drier sites generally emitting larger amounts of CO_2 during the zero-curtain offsetting much of the uptake during the growing season (US-Brw: 75%; US-Beo: 62%; US-Bes: 25%). Growing season CH_4 emissions are highest at US-Beo and US-Bes (Fig. 4(b), $p<0.05$). However, zero-curtain CH_4 emissions are roughly equal across all landscapes. This indicates that the percent contribution to local CH_4 budget varies by site during the zero-curtain (US-Brw: 45%; US-Beo: 34%; US-Bes: 32%) and total non-growing season (US-Brw: 56%; US-Beo: 48%; US-Bes: 43%).

Site variability in combined C budgets is most pronounced during the growing season, yet still occur, driven by CO_2 emission, during the zero-curtain period. (Fig. 4(c)). As US-Beo is characterized by low centered polygons, it exhibits characteristics of both US-Brw and US-Bes. This accounts for the larger values observed in CH_4 emission relative to US-Brw and the larger values in net CO_2 uptake relative to US-Bes during the growing season. The effect is that the mixed landscape, US-Beo, is the largest mean C contributor (Table 2). More detailed information regarding C budget by year/season can be found in supplementary information (Table S2).

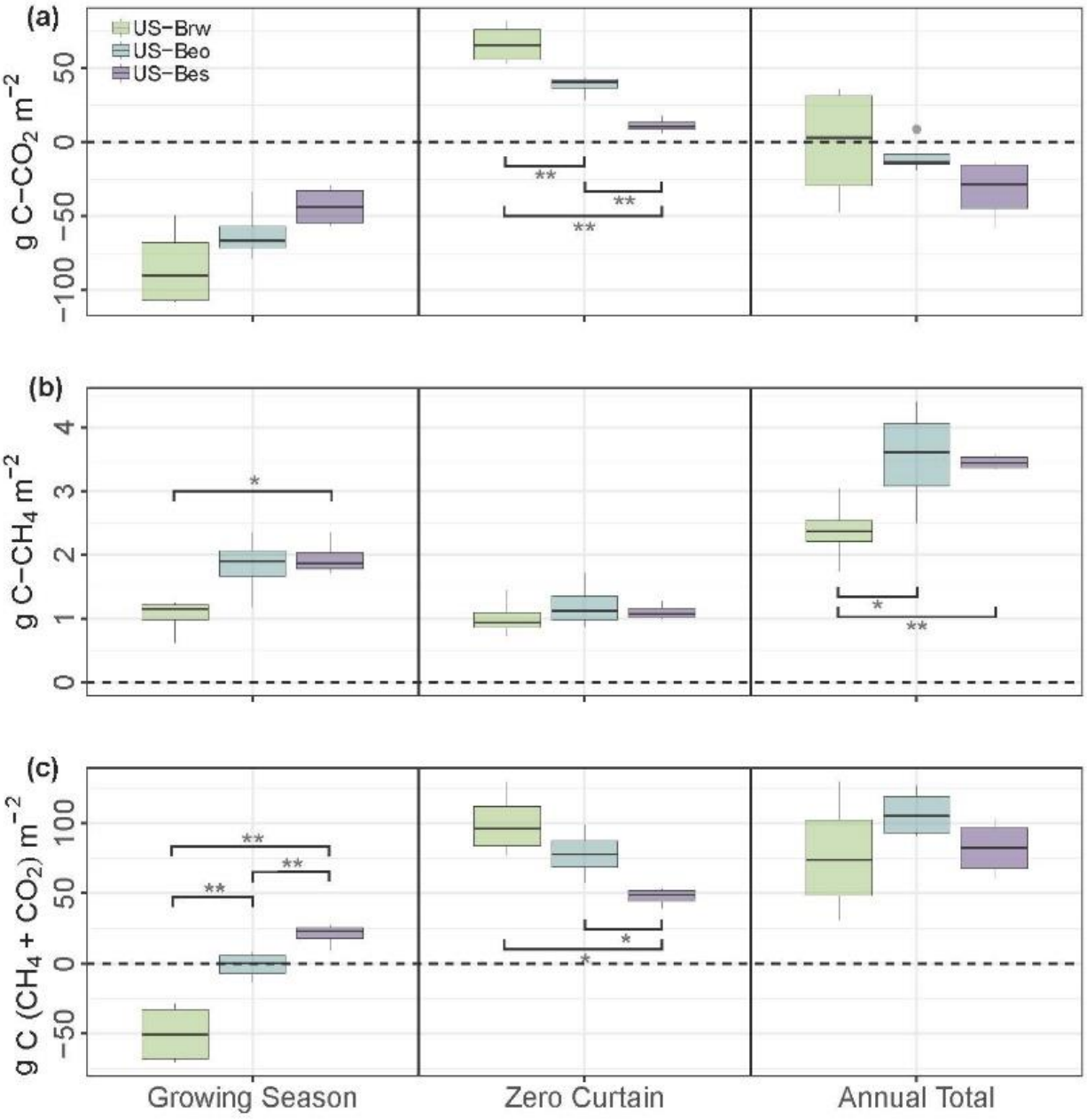

Figure 4: Seasonal and yearly budgetary contributions of (a.) CO_2, (b.) CH_4 and (c.) $CO_2 + CH_4$ (expressed as CO_2-equivalent based on warming potential) at the three EC sites from the growing season, zero-curtain period, and yearly total (* - $p<0.05$; ** - $p<0.01$).

Table 1: Mean Seasonal and annual totals of NEE and CH_4 flux (g C m^{-2} season/$year^{-1}$)

Season	US-Brw			US-Beo			US-Bes		
	NEE	**CH_4**	**C-C**	**NEE**	**CH_4**	**C-C**	**NEE**	**CH_4**	**C-C**
Growing	-84.48±12.2 *GPP: -209.4±24.9* *ER: 125.4±18.1*	1.05±0.12	-49.99±10.8	-61.5±8.3 *GPP: -135±12.4* *ER: 74.6±4.9*	1.83±0.21	-1.02±4.86	-43.52±5.9 *GPP: -104.5±7.8* *ER: 62.7±2.4*	1.95±0.12	20.75±4
Zero-curtain	66.32±5.9	1.01±0.13	99.73±11.51	38.24±2.8	1.2±0.15	77.92±8.66	11.26±2.1	1.11±0.05	47.72±3.27
Non-growing	16.69±5.3	0.33±0.04	27.45±7.47	13.76±1.1	0.5±0.07	30.11±3.82	0.33±3.5	0.4±0.07	13.68±6.31
Annual	**-1.47±17.5**	**2.38±0.23**	**77.19±21.8**	**-9.5±5.3**	**3.53±0.36**	**107±8.63**	**-31.93±9.1**	**3.46±0.05**	**82.12±9.85**

Note: Values indicate mean ± standard error. Positive values indicate release to the atmosphere. C-C represents combined C.

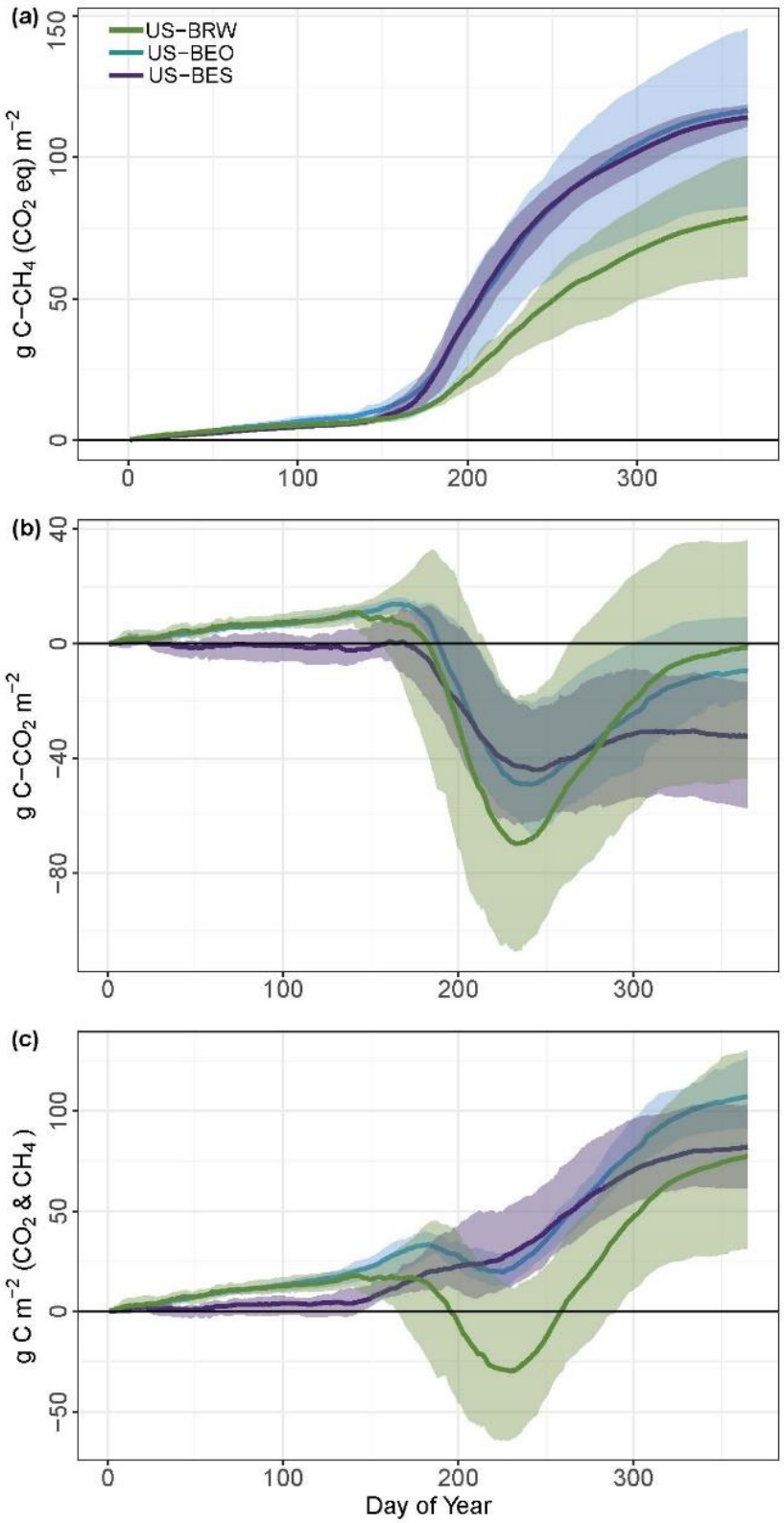

Figure 5: Mean annual cumulative emissions of **(a)** CH_4, **(b)** CO_2 and **(c)** CO_2 + CH_4 (with CH_4 expressed by a CO_2-equivalent) at the three EC sites. Shaded portion represents range of measurements across the 4-year study period.

Yearly cumulative emissions indicate that interannual variability in CH_4 fluxes is limited in inundated sites (Fig. 5(a)). US-Bes exhibited the lowest interannual variability (standard deviation – CO_2-eq (σ)=3.96), followed by US-Brw (σ=15.2) then US-Beo (σ=23.8). Interannual variability in CO_2 fluxes is highest at US-Brw (σ=34.98), followed by US-Bes (σ=18.11) then US-Beo (σ=10.65) (Fig. 5(b)). Most of the variability in combined cumulative C emissions is therefore controlled by variability in CO_2 at US-Brw and US-Bes, and in CH_4 at US-Beo (Fig. 5(c)).

Temperature Response Rates

ER temperature response relationships show that air temperature increases in predictive strength as site wetness decreases (Fig. 6 (a), (b), and (c)). In the inter-site comparison of linearized ER regressions, US-Beo and US-Brw show significant similarity ($p < 0.05$) while US-Bes is significantly different than both US-Brw ($p = 0.12$) and US-Beo ($p = 0.076$). Q_{10} is highest at US-Beo (3.5), followed by US-Brw (2.5) and US-Bes (2.2). Methane temperature response relationships show similar predictive strength across all sites (Fig. 6 (d), (e), and (f)). Q_{10} for CH_4 is again highest at US-Beo (4.6), followed by US-Bes (4.2) and US-Brw (3.1). Contrary to ER, in the inter-site comparison of linearized CH_4 regressions, US-Beo and US-Bes show significant similarity ($p< 0.05$) while US-Brw is significantly different than both US-Beo ($p = 0.11$) and US-Bes ($p = 0.14$).

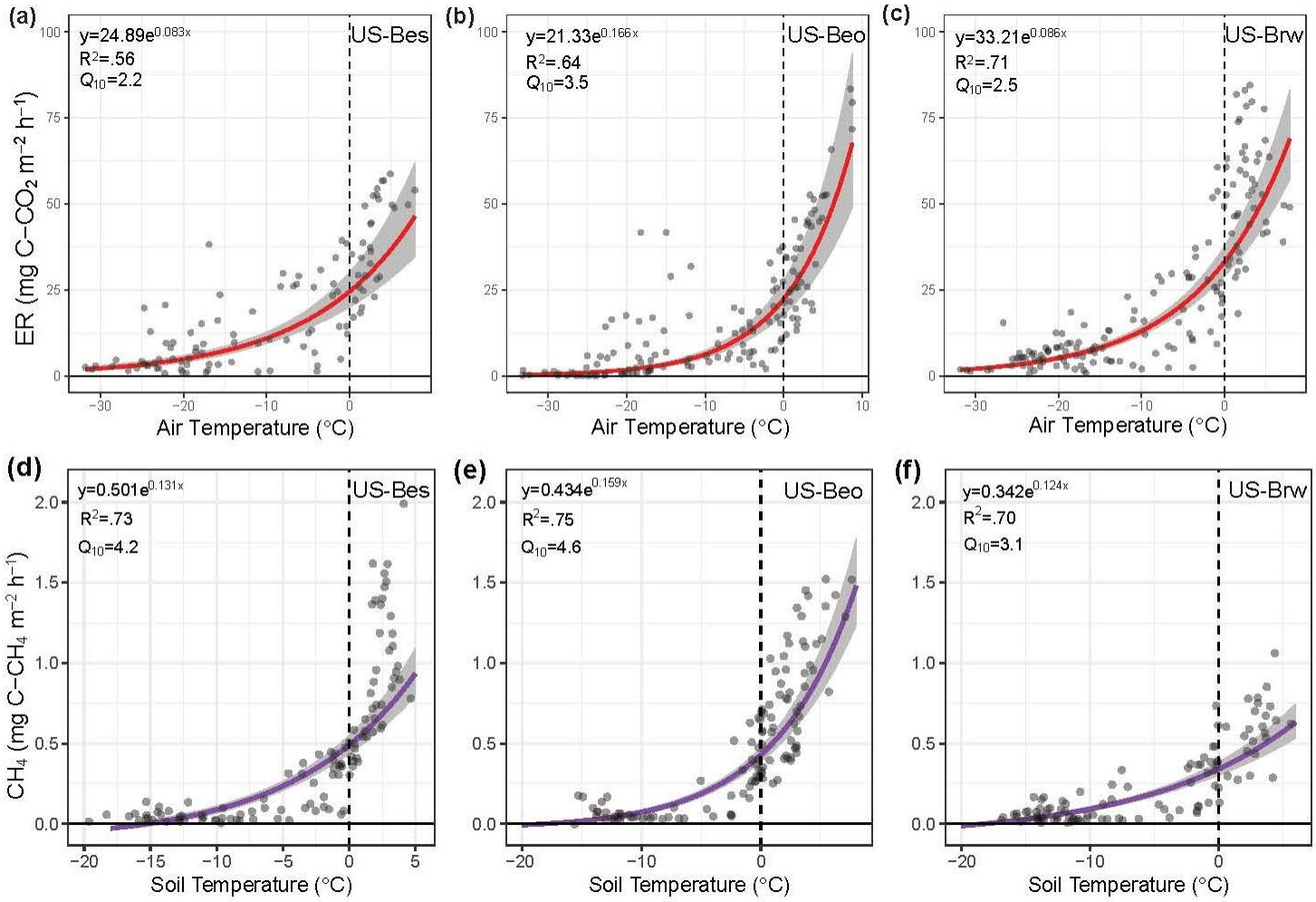

Figure 6: Temperature response curves of ecosystem respiration (ER; a, b, and c (air temperature)) and CH_4 efflux (d, e, and f (soil temperature)) at US-Bes (a and d), US-Beo (b and e), and US-Brw (c and f). All regressions had a p-value of >0.01.

Discussion

CO_2 Seasonality and Annual Budget

Seasonality appears to be the dominant factor in annual variation in NEE; however, we find the magnitude of that effect is dependent on local variation in site hydrology (Fig. 4). US-Brw exhibited the highest GPP yet was the weakest mean annual CO2 sink in comparison with the other wetter sites (Table 2). Conversely, US-Bes exhibited the lowest GPP yet was the strongest mean annual CO2 sink (Table 2). This is because sites with higher summer GPP exhibited larger zero-curtain CO2 emissions. The lower soil water content at US-Brw likely leads to a substantially larger portion of the soil column under oxic conditions, therefore supporting aerobic respiration, increasing CO_2 emissions. While it is probable that this constitutes much of the budget disparity, the contribution of CH_4 oxidation to ER in primarily methanogenic areas has been found to be up to 35% (Nielsen et al., 2019). As US-Brw contained the deepest active layer (Table 1) and largest GPP (Table 2), soils may contain higher amounts of photosynthates and labile C. This can increase methanogenesis rates deeper in the soil column (Dorodnikov et al., 2011) and fuel CO2 producing methanotrophs closer to the surface that would be more active under the oxic conditions in drier areas relative to waterlogged areas (Megonigal & Schlesinger, 2002). Alternatively, as US-Bes is inundated, methanotrophy is likely substantially lower during the zero-curtain period when the highest amount of CO2 loss is observed. Moreover, the lower GPP at US-Bes may result in more recalcitrant C and thus lower ER rates. The US-Beo site exhibited intermediate growing season GPP and zero-curtain CO2 emission relative to the other

two sites likely due to US-Beo exhibiting a mixed landscape regarding the prevalence of drained and inundated areas (Fig. 4 (a)).

Ecosystem respiration temperature response relationships show that US-Beo had the strongest temperature dependence (Q_{10}=3.5) relative to US-Brw and US-Bes (Q_{10}=2.5 & Q_{10}=2.2) (Fig. 6). This may be linked to the intermediate soil moisture of US-Beo. Higher soil water content can limit the temperature sensitivity of soil respiration in wetland regions due to the restriction of oxygen and thus, aerobic respiration (Chen et al., 2018). Alternatively, respiration can be limited by lower soil water content through a reduction in microbial mobility and substrate diffusion (Grant & Rochette, 1994). The temperature sensitivity of belowground respiration can also be dependent on productivity by providing photosynthates as substrates (Hartley et al., 2006). This may contribute to US-Bes having the lowest temperature sensitivity, as this site exhibited the lowest productivity (Table 2).

Similar studies of annual CO_2 budgets show that the largest annual net CO_2 loss is seen during the non-growing season, particularly associated with early winter respiration (Oechel et al. 2014; Commane et al. 2017; Euskirchen et al., 2017), agreeing with data presented here. As early winter respiration comprises a large part of the CO_2 budget, further increases in zero-curtain duration will likely result in winter CO_2 emissions that exceed growing season uptake (Arndt et al., 2019b). Each of the sites in this study were found to act as a weak sink for CO_2, yet others have reported relatively strong annual source signals from similar systems (Eurskirchen et al., 2017; Commane et al., 2017). This highlights the need for the monitoring and greater representation of mesoscale (≤ 1km) processes in climate projections, particularly at sub-grid scales.

CH_4 Seasonality and Annual Budget

Growing season CH_4 emissions are lowest at US-Brw (Fig. 4b). This is likely due to lower soil moisture increasing the volume of soil experiencing aerobic conditions not conducive to methanogenesis (Garcia et al., 2000). The polygon tundra site, US-Beo, had similar CH_4 emissions relative to the inundated US-Bes site despite US-Bes being the site with the higher soil water content (Fig. 4b). This may be related to the vegetation community composition. As US-Bes contains a lower percent cover of sedges (Davidson et al. 2016b.), US-Beo may produce more photosynthates, like acetate, that could leach into surrounding waterlogged soil in polygonal environments, further fueling methanogenesis via acetoclastic methanogenic pathway (King et al., 2002; Dorodnikov et al. 2011). Further, sedge density is positively correlated to CH_4 emissions as sedges provide a pathway for CH_4 through the vegetation to the atmosphere (Andresen et al., 2017; Lai, 2009). Interannual variability in CH_4 emissions is low at US-Bes compared with the other sites (Fig. 5). As US-Bes is consistently inundated, interannual differences in snow melt and rainfall would have a larger impact on soil water content and by proxy, oxygen availability at US-Brw, and US-Beo, possibly explaining this variability.

Contrary to zero-curtain CO_2 emission having site dependent variability, zero-curtain CH_4 emissions are roughly equal across all sites. This may be due to the frozen surface soils, creating an ice “cap”, and limiting oxygen diffusion into the soil column thereby equalizing oxygen availability and by extension, methanogenesis, across sites. This shows that variability in the growing season, rather than the zero-curtain, may have a stronger impact on annual CH_4 variability across different landscapes. However, zero-

curtain emissions may increase as the zero-curtain extends longer into the winter with a warming climate (Arndt et al., 2019a). Zero-curtain CH_4 contributions were found to be higher than in previous works due to the length of the study period capturing the range of annual variability (Zona et al., 2016). Methane temperature response relationships also indicate that temperature dependence was strongest at US-Beo (Q_{10}=4.6), followed by US-Bes (Q_{10}=4.2), and US-Brw (Q_{10}=3.1) (Fig. 6). As US-Beo, like US-Bes, contains large amounts of anaerobic soil, temperature sensitivity of methane production would be stronger than US-Brw where soil moisture is a limiting factor.

Annual Combined Carbon Budget

The largest mean combined C emissions were from the mixed landscape US-Beo, exhibiting both inundated and drained areas. These polygonized landscapes comprise close to 65% of the Alaskan coastal plain (Lara et al., 2018) and contain both anaerobic areas that produce large quantities of CH_4 as well as drained areas where aerobic respiration can readily occur. US-Beo exhibited the strongest temperature response, for both CO_2 and CH_4. On this basis, it is possible that further climate change may disproportionately increase C emissions from polygonized landscapes as rising temperatures will support increased production and emission of CO_2 and CH_4. However, rising temperatures will likely coincide with polygon succession and hydrologic transitions (Liljedahl et al., 2016). These hydrologic transitions can significantly alter annual carbon budgets (Kittler et al., 2017), stressing the importance of monitoring landscape heterogeneity in these regions for carbon budget estimation.

The interplay of CO_2 and CH_4 dynamics are affected strongly by both seasonality and by mesoscale landscape variability. Though the variability in summer C emissions

is significant among the landscapes studied, zero curtain releases of CO_2 and CH_4 tend to offset site differences. This acts as a buffer to variability and leads to similar annual combined C budgets across the sites studied. However, the differences in timing and magnitude of CO_2 and CH_4 fluxes elevate the importance of mesoscale processes for restricting uncertainty in Arctic model projections. Arctic regions make up the largest portion of uncertainty in climate global climate models (IPCC, 2014). Pan-Arctic models are typically run at coarse scales that describe landscape heterogeneity by the dominant landscape. It has been stressed that a higher degree of spatial and temporal coverage is needed (Natali et al., 2019) and that representation of wet and dry tundra at a finer scale (≤ 4 km^2) can result in a threefold reduction in model error (Lara et al., 2020). Data presented here demonstrate the need for this improvement, particularly for models that can represent mesoscale landscape heterogeneity and subsequent differences in seasonal carbon emission patterns.

Conclusions

Although the northern coastal tundra region in Alaska continues to be a weak CO_2 sink in all observed landscapes, CH_4 emissions push the region to have a net warming effect on the atmosphere. Data show the site with the largest mean GPP experienced the lowest mean annual CO_2 uptake, while the site with the lowest mean GPP experienced the highest mean annual CO_2 uptake. This is primarily due to zero-curtain CO_2 emissions and indicates that zero-curtain CO_2 emissions are positively correlated with growing season GPP. Despite site variability in growing season CH_4 emissions, zero-curtain CH_4 emissions are nearly equal across sites. This implies that the percent contribution of zero-curtain CH_4 emissions to annual CH_4 budget varies by

site and can be larger than previously thought, being as high as 45% of the yearly budget from the zero-curtain period alone and over half of the yearly budget from the total non-growing season (including the zero-curtain). Tundra exhibiting both inundated and drained areas are the largest mean annual combined C source and show a stronger ER and CH_4 temperature response than either largely inundated or drained areas. These results show that local variation in site hydrology, seasonality and interannual variability in regional temperature work in tandem to determine carbon balance. This interaction may be indicative of a variable response under further climate change, yet seemingly lacking the strength to cause strong differences in annual C budgets at this time. As both wetting and drying of arctic tundra has been reported, differential landscape development in response to climate change and subsequent C budget divergence may occur. Without improved representation of landscape heterogeneity, this potential divergence would likely confound long term global model predictions further, as changes would occur at sub-grid scales.

Supplementary Material for article “Seasonality buffers carbon budget variability across heterogeneous landscapes in Alaskan Arctic Tundra

This file provides specific details on methods and results referred to in the main text of the above article. Figure S1. shows NDWI by site, Figure S2. shows model cross validation for data imputation, Figure S3. shows linear model regressions of CH_4 and air temperature/soil temperature, Figure S4. shows total cumulative emissions over the study period, Table S1. shows data coverage by season and Table S2. shows yearly budgetary contributions by season and year.

NDWI Boxplots (Fig. S1.) for imagery available during the study period show variability in surface water content by site. Each of the sites exhibited significant differences in NDWI ($p<0.005$) outlining the variability in site water regime. NDWI data is pulled only from EC tower footprints and small structures within EC tower footprint were masked.

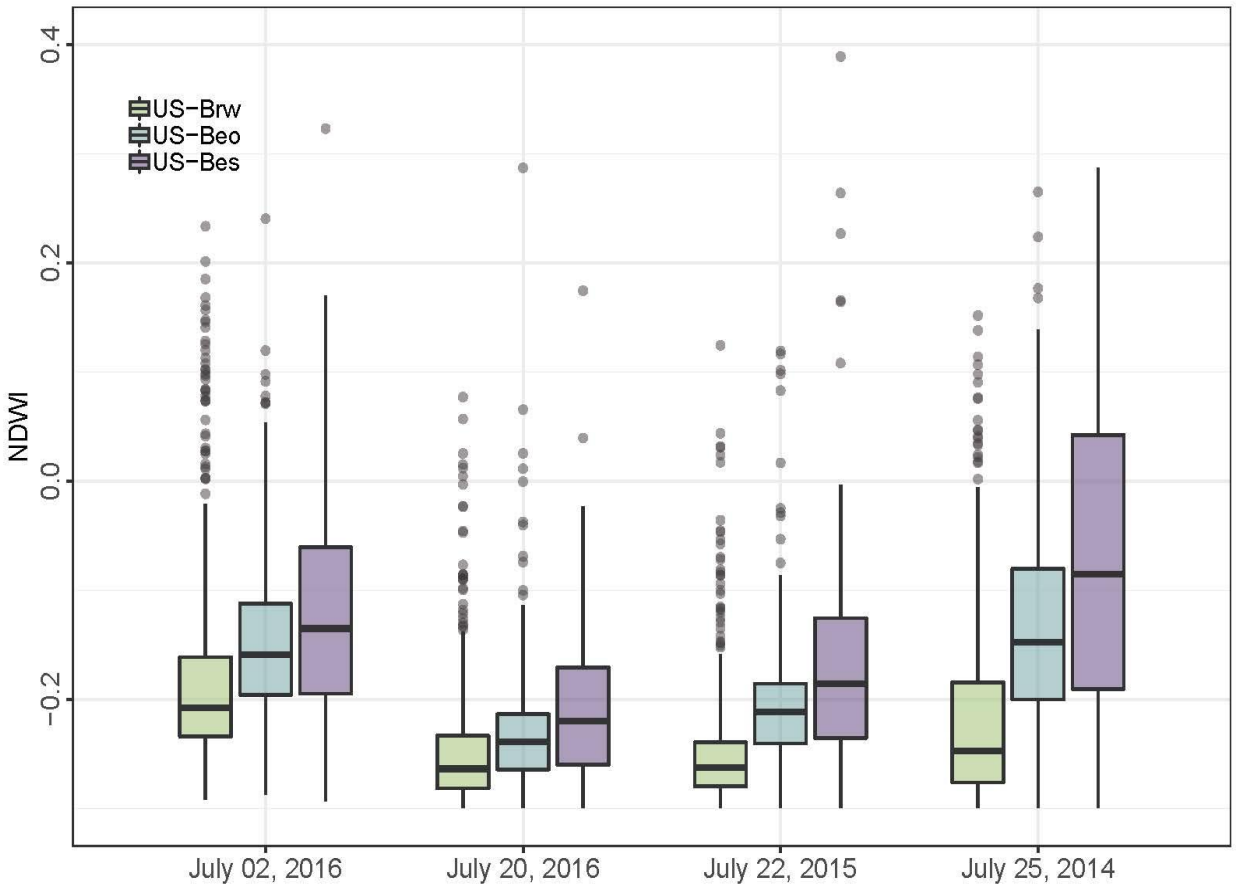

Figure. S1: Boxplots of NDWI for each of the three sites. Calculated from Worldview-3 imagery acquired on July 2nd, 2016, July 20th, 2016, July 22nd, 2015, & July 25th, 2014 from NDWI within EC tower footprints. Each date showed significant difference ($p<0.005$) in NDWI by site.

Model cross validations were made by removing a random 30% of data from dataset using the R package, “data.table”, and imputing missing data with random forest machine learning (R package, “missForest”) utilizing a 300-decision tree design (Fig. S2.). Comparisons of model cross validation between the default half-hourly data output and daily averages show models perform much better when using a daily average. This method reduces the “noise” and is therefore better equipped to inform machine learning processes.

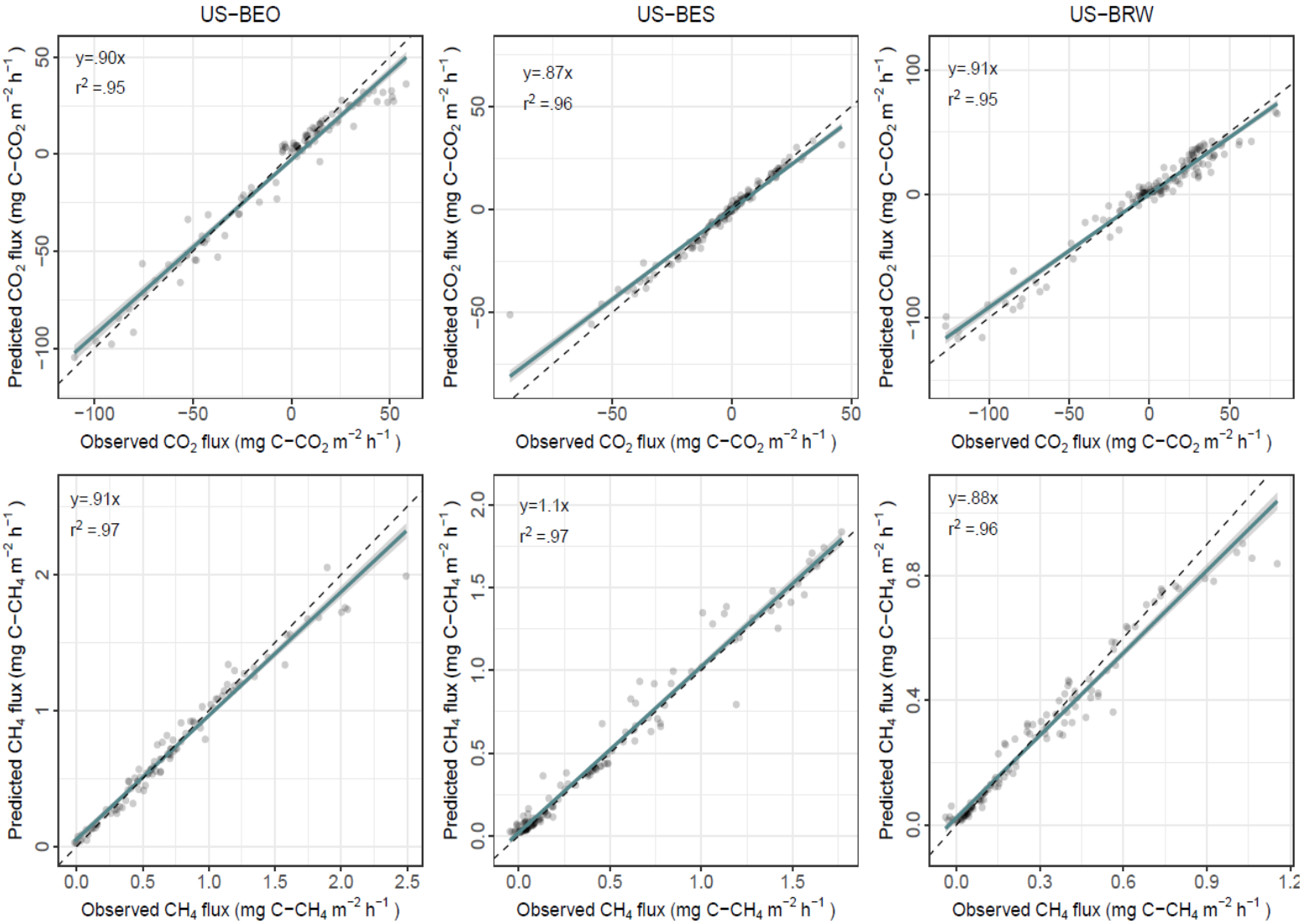

Figure S2: Model cross validation for daily average gap filling. Model validations were performed using daily averages of CH_4 and CO_2 fluxes.

Linear models of temperature response curves of CH_4 emissions using soil temperature (Fig.S3 d., e., & f.) show a stronger relationship than those using air temperature (Fig.S3 a., b., & c.). This is due to methanogenesis occurring deeper in the soil column where variability in temperature is less dynamic. Similar results have been shown in previous work (Arndt et al., 2019).

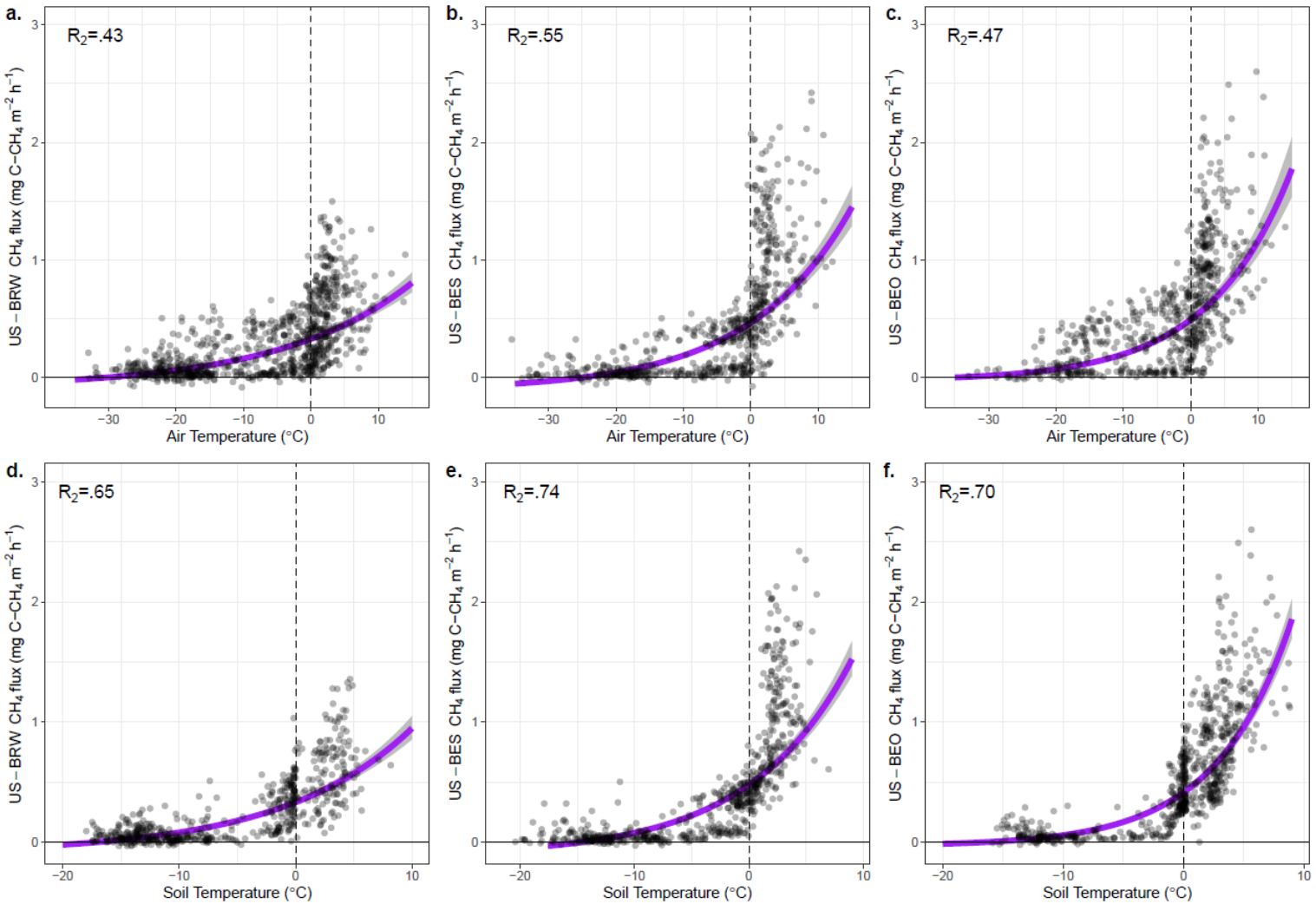

Figure S3: Temperature response regressions of methane efflux with air temperature (a., b., & c.) and methane efflux with soil temperature (d., e., & f.).

Table S1: Seasonal and total percent data coverage over the study period. The winter period (December – February) exhibited the largest amount of data loss due to the frigid temperatures and lack of site accessibility upon power outage or equipment failure.

Table S1. Mean Percent data coverage by season and for total annual

Season	**% Coverage by season/total**		
	US-Brw	**US-Beo**	**US-Bes**
Winter	33.4	21.1	37.2
Spring	79.2	78.7	64.3
Summer	96.5	82.4	83.4
Autumn	75.3	68.1	60.4
Total	**71.1**	**62.5**	**61.3**

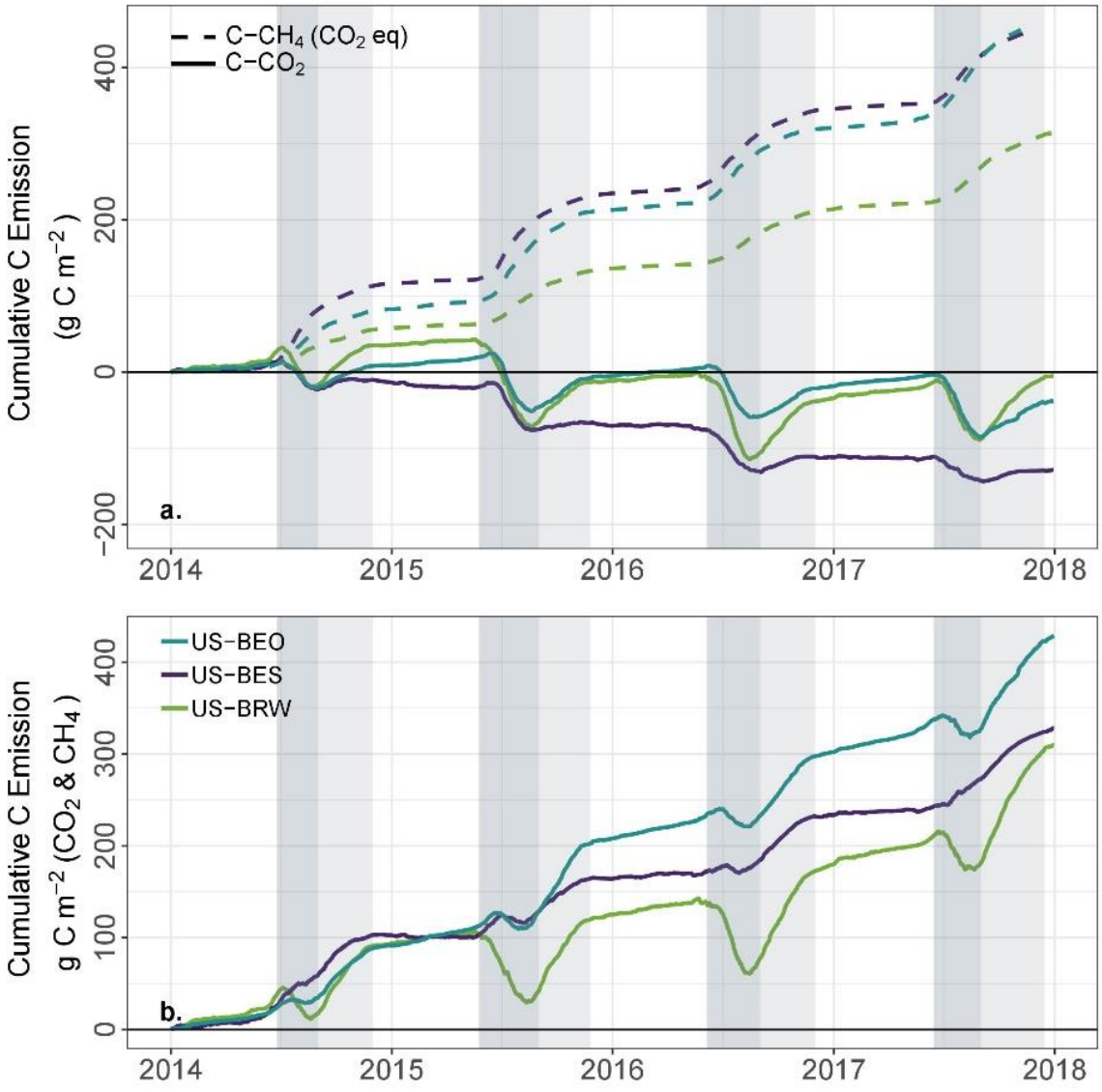

Figure S4: Cumulative emissions of (a.) CH_4 and CO_2 and (c.) CO_2 + CH_4 (with CH_4 expressed by a CO_2 equivalent) at the three EC sites. The darker shaded portion represents the growing season, while the lighter shaded portion represents the zero-curtain period.

Fig. S4. shows cumulative emissions over the entire study period. Trends in CH_4 emissions are similar among US-Beo and US-Bes but diverge from that of US-Brw. This is likely due to the lower soil moisture and by proxy, lower anaerobic soil conditions at US-Brw. Conversely, Trends in CO_2 emissions are similar among US-Brw and US-Beo but diverge from that of US-Bes. This is again, likely due to the increased soil moisture and lower plant biomass within US-Bes. Despite these differences, trends of the combined effect of CO_2 and CH_4 are generally similar across all sites, indicating that despite landscape heterogeneity, there isn't sufficient evidence to suggest that there is currently a differential response, although this may be the case with longer data records. Notably, the largest contributor to carbon emissions over the study period was US-Beo, characterized by an intermediate water regime unlike the inundated US-Bes or the drained US-Brw.

Table S2: Budgetary contributions by site and season/year (g C m^{-2} season/$year^{-1}$)

Season	Year	US-Brw			US-Beo			US-Bes		
		NEE	CH_4	C-C	NEE	CH_4	C-C	NEE	CH_4	C-C
Growing	2014	-49.51 GPP: -161.3 ER: 113.1	0.63	-28.72	-34.02 GPP: -98.21 ER: 64.33	1.18	4.92	-34.1 GPP: -95.12 ER: 61.56	1.8	25.3
Zero Curtain	2014	53.35	0.73	77.44	28.8	0.87	57.51	9.43	1.12	46.39
Non-growing	2014	31.55	0.385	44.26	13.8	0.447	28.55	11.23	0.599	31
Annual	**2014**	**35.39**	**1.745**	**92.98**	**8.58**	**2.497**	**90.98**	**-13.44**	**3.519**	**102.7**
Growing	2015	-108.1 GPP: -194.8 ER: 86.67	1.25	-66.85	-68.75 GPP: -142.1 ER: 75.56	2.34	8.47	-56.59 GPP: -124.6 ER: 69.65	2.35	20.96
Zero Curtain	2015	56.28	0.9	85.98	43.08	1.23	83.67	6.1	1	39.1
Non-growing	2015	4.52	0.221	11.81	11.99	0.374	24.33	-6.74	0.239	1.147
Annual	**2015**	**-47.3**	**2.371**	**30.94**	**-13.68**	**3.944**	**116.5**	**-57.23**	**3.589**	**61.21**
Growing	2016	-106.4 GPP: -279.3 ER: 172.9	1.09	-70.43	-64.73 GPP: -151.3 ER: 87.47	1.83	-4.34	-53.94 GPP: -108.8 ER: 58.36	1.92	9.42
Zero Curtain	2016	74.16	0.98	106.5	38.82	1.01	72.15	17.83	1.02	51.49
Non-growing	2016	8.82	0.292	18.46	12.01	0.433	26.3	-4.81	0.422	9.116
Annual	**2016**	**-23.42**	**2.362**	**54.53**	**-13.9**	**3.273**	**94.11**	**-40.92**	**3.362**	**70.03**
Growing	2017	-73.9 GPP: -202.2 ER: 129.1	1.21	-33.97	-78.49 GPP: -148.4 ER: 71.07	1.98	-13.15	-29.45 GPP: -89.59 ER: 61.09	1.72	27.31
Zero Curtain	2017	81.5	1.44	129	42.24	1.7	98.34	11.67	1.28	53.91
Non-growing	2017	21.85	0.406	35.25	17.25	0.728	41.27	1.65	0.358	13.46
Annual	**2017**	**29.45**	**3.056**	**130.3**	**-19**	**4.408**	**126.5**	**-16.13**	**3.358**	**94.68**

Note: Non-growing seasons contain winter & spring, less the zero-curtain period. C-C represents Combined-C.

Acknowledgements

This work was funded by the NASA ABoVE Program awarded to Walter C. Oechel and Donatella Zona (No. NNX16AF94A) and the National Science Foundation - Office of Polar Programs awarded to Donatella Zona and Walter C. Oechel (Nos. 1204263, and 1702797). Additional logistical support was funded by the National Science Foundation - Office of Polar Programs, the NASA ABoVE Program, NOAA CESSRST EPP awarded to Walter C. Oechel (No. NA16SEC4810008), the European Union's Horizon 2020 research and innovation program awarded to Walter C. Oechel and Donatella Zona (No. 629727890), and from the Natural Environment Research Council (NERC) UAMS Grant awarded to Walter C. Oechel and Donatella Zona (No. NE/P002552/1). Geospatial support for this work (Fig. 1.) provided by the Polar Geospatial Center (under NSF OPP award No.1204263 and 1702797). This research was conducted on land owned by the Ukpeaġvik Inupiat Corporation (UIC) whom we thank for their support. The data that support the findings of this study are openly available at the following URL: https://arcticdata.io/catalog/view/doi:10.18739/A2X34MS1B

References

Andresen, C. G., Lara, M. J., Tweedie, C. E., & Lougheed, V. L. (2017). Rising plant-mediated methane emissions from arctic wetlands. Global Change Biology, 23(3), 1128–1139. https://doi.org/10.1111/gcb.13469

Arndt, K. A., Lipson, D. A., Hashemi, J., Oechel, W. C., & Zona, D. (2020). Snow melt stimulates ecosystem respiration in Arctic ecosystems. Global Change Biology, (May), 1–10. https://doi.org/10.1111/gcb.15193

Arndt, K. A., Santos, M., Ustin, S. L., Davidson, S. J., Stow, D. A., Oechel, W., Tran, T. T. P., Graybill, B. & Zona, D. (2019a). Arctic greening associated with lengthening growing seasons in Northern Alaska. *Environmental Research Letters*.

Arndt, K. A., Oechel, W. C., Goodrich, J. P., Bailey, B. A., Kalhori, A., Hashemi, J., … Zona, D. (2019b). Sensitivity of Methane Emissions to Later Soil Freezing in Arctic Tundra Ecosystems. Journal of Geophysical Research: Biogeosciences, 124(8), 2595–2609. https://doi.org/10.1029/2019jg005242

Birk, M. A. (2020). respirometry: Tools for Conducting and Analyzing Respirometry Experiments. R package version 1.1.0. https://CRAN.R-project.org/package=respirometry

Chen, H., Zou, J., Cui, J., Nie, M., & Fang, C. (2018). Wetland drying increases the temperature sensitivity of soil respiration. Soil Biology and Biochemistry, 120 (July 2017), 24–27. https://doi.org/10.1016/j.soilbio.2018.01.035

Commane, R., Lindaas, J., Benmergui, J., Luus, K. A., Chang, R. Y.-W., Daube, B. C., … Wofsy, S. C. (2017). Carbon dioxide sources from Alaska driven by increasing early winter respiration from Arctic tundra. Proceedings of the National Academy of Sciences, 114(21), 5361–5366. https://doi.org/10.1073/pnas.1618567114

Davidson, S. J., Santos, M. J., Sloan, V. L., Watts, J. D., Phoenix, G. K., Oechel, W. C., & Zona, D. (2016a). Mapping arctic tundra vegetation communities using field spectroscopy and multispectral satellite data in North Alaska, USA. Remote Sensing, 8(12). https://doi.org/10.3390/rs8120978

Davidson, S. J., Sloan, V. L., Phoenix, G. K., Wagner, R., Fisher, J. P., Oechel, W. C., & Zona, D. (2016b). Vegetation Type Dominates the Spatial Variability in CH4 Emissions Across Multiple Arctic Tundra Landscapes. Ecosystems, 19(6), 1116–1132. https://doi.org/10.1007/s10021-016-9991-0

Dorodnikov, M., Knorr, K. H., Kuzyakov, Y., & Wilmking, M. (2011). Plant-mediated CH 4 transport and contribution of photosynthates to methanogenesis at a boreal mire: A 14C pulse-labeling study. Biogeosciences, 8(8), 2365–2375. https://doi.org/10.5194/bg-8-2365-2011

Dunfield, P., Knowles, R., Dumont, R., & Moore, T. R. (1993). Methane production and consumption in temperate and subarctic peat soils: Response to temperature and pH. Soil Biology and Biochemistry, 25(3), 321–326. https://doi.org/10.1016/0038-0717(93)90130-4

Euskirchen, E. S., Bret-Harte, M. S., Scott, G. J., Edgar, C., & Shaver, G. R. (2012). Seasonal patterns of carbon dioxide and water fluxes in three representative tundra ecosystems in northern Alaska. Ecosphere, 3(1), art4. https://doi.org/10.1890/ES11-00202.1

Euskirchen, E. S., Bret-Harte, M. S., Shaver, G. R., Edgar, C. W., & Romanovsky, V. E. (2017). Long-Term Release of Carbon Dioxide from Arctic Tundra Ecosystems in Alaska. Ecosystems. https://doi.org/10.1007/s10021-016-0085-9

Fox, J. & Weisberg, S. (2019). An {R} Companion to Applied Regression, Third Edition. Sage, Thousand Oaks CA.

Garcia, J. L., Patel, B. K. C., & Ollivier, B. (2000). Taxonomic, phylogenetic, and ecological diversity of methanogenic Archaea. Anaerobe, 6(4), 205–226. https://doi.org/10.1006/anae.2000.0345

Goodrich, J. P., Oechel, W. C., Gioli, B., Moreaux, V., Murphy, P. C., Burba, G., & Zona, D. (2016). Impact of different eddy covariance sensors, site set-up, and maintenance on the annual balance of CO2 and CH4 in the harsh Arctic environment. Agricultural and Forest Meteorology, 228-229, 239–251. https://doi.org/10.1016/j.agrformet.2016.07.008

Grant R. F., Rochette P. (1994) Soil microbial respiration at different water potentials and temperatures: theory and mathematical modeling. *Soil Science Society of America Journal*, 58, 1681–1690.

Hartley IP, Armstrong AF, Murthy R et al. (2006). The dependence of respiration on photosynthetic substrate supply and temperature: integrating leaf, soil and ecosystem measurements. Global Change Biology, 12, 1954–1968.

Huissteden, J., Berrittella, C., Parmentier, F. et al*.* (2011). Methane emissions from permafrost thaw lakes limited by lake drainage. Nature Climate Change **1,** 119–123. https://doi.org/10.1038/nclimate1101

Holland, M. M., & Bitz, C. M. (2003). Polar amplification of climate change in coupled models. Climate Dynamics, 21(3–4), 221–232. https://doi.org/10.1007/s00382-003-0332-6

Hugelius, G., Strauss, J., Zubrzycki, S., Harden, J. W., Schuur, E. A. G., Ping, C. L., … Kuhry, P. (2014). Estimated stocks of circumpolar permafrost carbon with quantified uncertainty ranges and identified data gaps. Biogeosciences, 11(23), 6573–6593. https://doi.org/10.5194/bg-11-6573-2014

Ibrom, A., Dellwik, E., Flyvbjerg, H., Jensen, N. O., & Pilegaard, K. (2007). Strong low-pass filtering effects on water vapour flux measurements with closed-path eddy correlation systems. Agricultural and Forest Meteorology, 147(3), 140–156. https://doi.org/10.1016/j.agrformet.2007.07.007

IPCC 2013. Climate Change 2013: The Physical Science Basis. Contribution of Working Group I to the Fifth Assessment Report of the Intergovernmental Panel on Climate Change. In: Stocker, T. F., D. Qin, G.-K. Plattner, M. Tignor, S.K. Allen, J. Boschung, A. Nauels, Y. Xia, V. Bex and P.M. Midgley (ed.). United Kingdom and New York, NY, USA.

IPCC. Climate Change 2014: Synthesis Report. Contribution of Working Groups I, II and III to the Fifth Assessment Report of the Intergovernmental Panel on Climate Change.

Jorgenson, M. T., & Shur, Y. (2007). Evolution of lakes and basins in northern Alaska and discussion of the thaw lake cycle. Journal of Geophysical Research: Earth Surface, *112*(2). https://doi.org/10.1029/2006JF000531

King, J. Y., Reeburgh, W. S., Thieler, K. K., Kling, G. W., Loya, W. M., Johnson, L. C., & Nadelhoffer, K. J. (2002). Pulse-labeling studies of carbon cycling in Arctic tundra ecosystems: The contribution of photosynthates to methane emission. Global Biogeochemical Cycles, 16(4), 10-1-10–18. https://doi.org/10.1029/2001gb001456

Kirschke, S., Bousquet, P., Ciais, P., Saunois, M., Canadell, J. G., Dlugokencky, E. J., … Zeng, G. (2013). Three decades of global methane sources and sinks. Nature Geoscience, 6(10), 813–823. https://doi.org/10.1038/ngeo1955

Kittler, F., Heimann, M., Kolle, O., Zimov, N., Zimov, S., & Göckede, M. (2017). Long-term drainage reduces CO2uptake and CH4emissions in a Siberian permafrost ecosystem. Global Biogeochemical Cycles, 31, 1704–1717. https://doi.org/10.1002/2017GB005774

Koch, J. C., Gurney, K., & Wipfli, M. S. (2014). Morphology-Dependent Water Budgets and Nutrient Fluxes in Arctic Thaw Ponds. Permafrost and Periglacial Processes, 25(2), 79–93. https://doi.org/10.1002/ppp.1804

Korman R, Meixner F (2001) An analytical footprint model for non-neutral stratification. Boundary-Layer Meteorology. 99:207–224

Kwon, H.-J., Oechel, W. C., Zulueta, R. C., & Hastings, S. J. (2006). Effects of climate variability on carbon sequestration among adjacent wet sedge tundra and moist tussock tundra ecosystems. Journal of Geophysical Research, 111, G03014. https://doi.org/10.1029/ 2005JG000036

Lai, D. Y. F. 2009. Methane dynamics in northern peatlands: A review. *Pedosphere.* 19(4): 409–421. https://doi.org/10.1016/S1002-0160(09)00003-4

Lara, M. J., Nitze, I., Grosse, G. & David McGuire, A. (2018). Data descriptor: tundra landform and vegetation productivity trend maps for the Arctic Coastal Plain of Northern Alaska. Sci. Data https://doi.org/10.1038/sdata.2018.58

Lara, M.J., McGuire, A.D., Euskirchen, E.S. *et al.* (2020). Local-scale Arctic tundra heterogeneity affects regional-scale carbon dynamics. *Nature Communications.* 11, 4925 https://doi.org/10.1038/s41467-020-18768-z

Lasslop, G., Reichstein, M., Papale, D., Richardson, A.D., Arneth, A., Barr, A., Stoy, P. And Wohlfahrt, G. (2010), Separation of net ecosystem exchange into assimilation and respiration using a light response curve approach: critical issues and global evaluation. Global Change Biology, 16: 187-208. doi:10.1111/j.1365-2486.2009.02041.x

Lawrence, D. M., Koven, C. D., Swenson, S. C., Riley, W. J., & Slater, A. G. (2015). Permafrost thaw and resulting soil moisture changes regulate projected high-latitude CO2 and CH4 emissions. Environmental Research Letters, 10(9). https://doi.org/10.1088/1748-9326/10/9/094011

Liljedahl, A. K., Boike, J., Daanen, R. P., Fedorov, A. N., Frost, G. V., Grosse, G., … Zona, D. (2016). Pan-Arctic ice-wedge degradation in warming permafrost and its influence on tundra hydrology. Nature Geoscience, 9(4), 312–318. https://doi.org/10.1038/ngeo2674

Maglione, P., Parente, C. & Vallario, A. 2014. Coastline extraction using high resolution WorldView-2 satellite imagery. *European Journal of Remote Sensing,* 47, 685-699.

Martin, A. F., Lantz, T. C., & Humphreys, E. R. (2018). ARTICLE Ice wedge degradation and CO 2 and CH 4 Northwest Territories. 145(October 2017), 130–145.

Mastepanov, M., Sigsgaard, C., Dlugokencky, E. J., Houweling, S., Ström, L., Tamstorf, M. P., & Christensen, T. R. (2008). Large tundra methane burst during onset of freezing. Nature, 456(7222), 628–630. https://doi.org/10.1038/nature07464

Mauder, M., & Foken, T. (2011). Documentation and instruction manual of the eddy-covariance software package TK3. In (Vol. 46). Bayreuth.

McGuire, A. D., Christensen, T. R., Hayes, D., Heroult, A., Euskirchen, E., Kimball, J. S., … Yi, Y. (2012). An assessment of the carbon balance of Arctic tundra: Comparisons among observations, process models, and atmospheric inversions. Biogeosciences, 9(8), 3185–3204. https://doi.org/10.5194/bg-9-3185-2012

Megonigal, J. P., and Schlesinger, W. H.. (2002). Methane-limited methanotrophy in tidal freshwater swamps. Global Biogeochemical Cycles, 16(4), 1088. doi:10.1029/2001GB001594, 2002.

Natali, S. M., Schuur, E. A. G., Mauritz, M., Schade, J. D., Celis, G., Crummer, K. G., … Webb, E. E. (2015). Permafrost thaw and soil moisture driving CO_2 and CH_4 release

from upland tundra. Journal of Geophysical Research: Biogeosciences, 120(361), 1–13. https://doi.org/10.1002/2014JG002872.

Natali, S. M., Watts, J. D., Rogers, B. M., Potter, S., Ludwig, S. M., Selbmann, A.-K., … Zona, D. (2019). Large loss of CO2 in winter observed across the northern permafrost region. Nature Climate Change, 9(11), 852–857. https://doi.org/10.1038/s4155 8-019-0592-8

Nielsen, C. S., Hasselquist, N. J., Nilsson, M. B., Öquist, M., Järveoja, J., & Peichl, M. (2018). A Novel Approach for High-Frequency in-situ Quantification of Methane Oxidation in Peatlands. Soil Systems, 3(1), 4. http://dx.doi.org/10.3390/soilsystems3010004

Oechel, W. C., Laskowski, C. A., Burba, G., Gioli, B., & Kalhori, A. A. M. (2014). Annual patterns and budget of CO 2 flux in an Arctic tussock tundra ecosystem. Journal of Geophysical Research: Biogeosciences, 119(3), 323–339. https://doi.org/10.1002/2013JG002431

Outcalt, S.I., Nelson, F.E. and Hinkel, K.M., 1990. The zero-curtain effect: Heat and mass transfer across an isothermal region in freezing soil. Water Resources Research, 26(7), pp.1509-1516.

R Core Team. (2019). R: A language and environment for statistical computing. Vienna, Austria: R Foundation for Statistical Computing. Retrieved from https://www.R-proje ct.org/

Reichstein, M., Falge, E., Baldocchi, D., Papale, D., Aubinet, M., Berbigier, P., et al. (2005). On the separation of net ecosystem exchange into assimilation and ecosystem respiration: Review and improved algorithm. Global Change Biology, 11(9), 1424–1439. https://doi.org/ 10.1111/j.1365-2486.2005.001002.x

Schuur, E. A. G., Abbott, B. W., Bowden, W. B., Brovkin, V., Camill, P., Canadell, J. G., … Zimov, S. A. (2013). Expert assessment of vulnerability of permafrost carbon to climate change. Climatic Change. https://doi.org/10.1007/s10584-013-0730-7

Serreze, M.C., Francis, J.A. The Arctic Amplification Debate. Climatic Change. 76**,** 241–264 (2006). https://doi.org/10.1007/s10584-005-9017-y

Sturtevant, C. S., & Oechel, W. C. (2013). Spatial variation in landscape-level CO 2 and CH 4 fluxes from arctic coastal tundra: Influence from vegetation, wetness, and the thaw lake cycle. Global Change Biology, 19(9), 2853–2866. https://doi.org/10.1111/gcb.12247

Tamocai, C., Canadell, J. G., Schuur, E. A. G., Kuhry, P., Mazhitova, G., & Zimov, S. (2009). Soil organic carbon pools in the northern circumpolar permafrost region. Global Biogeochemical Cycles, 23(2), 1–11. https://doi.org/10.1029/2008GB003327

Taylor, M. A., Celis, G., Ledman, J. D., Bracho, R., & Schuur, E. A. G. (2018). Methane Efflux Measured by Eddy Covariance in Alaskan Upland Tundra Undergoing Permafrost Degradation. Journal of Geophysical Research: Biogeosciences, 123(9), 2695–2710. https://doi.org/10.1029/2018JG004444

Tian, H., Lu, C., Chen, G., Tao, B., Pan, S., Del Grosso, S. J., … Prior, S. A. (2012). Contemporary and projected biogenic fluxes of methane and nitrous oxide in North American terrestrial ecosystems. Frontiers in Ecology and the Environment, 10(10), 528–536. https://doi.org/10.1890/120057

Treat, C. C., Bloom, A. A., & Marushchak, M. E. (2018). Nongrowing season methane emissions-a significant component of annual emissions across northern ecosystems. Global Change Biology, 24(8), 3331–3343. https://doi.org/10.1111/gcb.14137

Treat, C. C., Marushchak, M. E., Voigt, C., Zhang, Y., Tan, Z., Zhuang, Q., Virtanen, T. A., Rasanen, A., Biasi, C., Hugelius, G., Kaverin, D., Miller, P. A., Stendel, M., Romanovsky, V., Rivkin, F., Martikainen, P. J. & Shurpali, N. J. (2018). Tundra landscape heterogeneity, not interannual variability, controls the decadal regional carbon balance in the Western Russian Arctic. Glob Chang Biol, 24, 5188-5204.

Von Fischer, J. C., Rhew, R. C., Ames, G. M., Fosdick, B. K., & Von Fischer, P. E. (2010). Vegetation height and other controls of spatial variability in methane emissions from the Arctic coastal tundra at Barrow, Alaska. Journal of Geophysical Research: Biogeosciences, 115(3), 1–11. https://doi.org/10.1029/2009JG001283

Webber, P. J. 1978. Spatial and Temporal Variation of the Vegetation and Its Production, Barrow, Alaska. In: Tieszen, L. L. (ed.) Vegetation and Production Ecology of an Alaskan Arctic Tundra. New York, NY: Springer New York.

Wilczak, J. M., Oncley, S. P., & Stage, S. A. (2001). Sonic anemometer tilt correction algorithms. Boundary-Layer Meteorology, 99(1), 127–150. https://doi.org/10.1023/a:10189 66204465

Wutzler, T., Lucas-Moffat, A., Migliavacca, M., Knauer, J., Sickel, K., Šigut, L., … Reichstein, M. (2018). Basic and extensible post-processing of eddy covariance flux data with REddyProc. Biogeosciences, 15(16), 5015–5030. https://doi.org/10.5194/bg-15-5015-2018

Xenakis, G. (2016). FREddyPro: Post-processing EddyPro full output file. R package version 1.0.

Zhang, X., He, J., Zhang, J., Polyakov, I., Gerdes, R., Inoue, J., & Wu, P. (2013). Enhanced poleward moisture transport and amplified northern high-latitude wetting trend. Nature Climate Change, 3(1), 47–51. https://doi.org/10.1038/nclimate1631

Zimov, S. A., Schuur, E. A. G., & Stuart Chapin, F. (2006). Permafrost and the global carbon budget. Science, 312(5780), 1612–1613. https://doi.org/10.1126/science.1128908

Zona, D., Gioli, B., Commane, R., Lindaas, J., Wofsy, S. C., Miller, C. E., … Oechel, W. C. (2016). Cold season emissions dominate the Arctic tundra methane budget. Proceedings of the National Academy of Sciences, 113(1), 40–45. DOI: 10.1073/pnas.1516017113

Zulueta, R.C., Oechel, W.C., Loescher, H.W., Lawrence, W.T. And Paw U, K.T. (2011), Aircraft-derived regional scale CO_2 fluxes from vegetated drained thaw-lake basins and interstitial tundra on the Arctic Coastal Plain of Alaska. Global Change Biology, 17: 2781-2802. https://doi.org/10.1111/j.1365-

Chapter 2

Early Winter Methane Emissions Exceed Active Layer Gas Reservoir in Arctic Wetlands

Joshua Hashemi, David Lipson, Kyle Arndt, Guadalupe Barajas, Aram Kalhori, Walter C. Oechel & Donatella Zona

Abstract

Cold season methane (CH_4) emissions account for about half of the annual CH_4 budget in Arctic tundra. Despite their importance, it is currently unknown if these cold season CH_4 emissions are a result of active methanogenesis or the release of stored CH_4 generated during the prior growing season. Here, we show that CH_4 emissions outweigh CH_4 storage within the soil active layer (~35cm depth) during early winter at a drained lake basin near Utqiaġvik, Alaska. Soil CH_4 concentrations during early winter were 106.8±7.9 mg C-CH_4 m^{-2} (per active layer depth) while mean cumulative zero-curtain methane emissions were over 1100±50 mg C-CH_4 m^{-2}. Soil concentrations were higher in spring (417.3±282.3 mg C-CH_4 m^{-2} (per active layer depth)) than in early winter, illustrating additions of CH_4 to the soil column over the cold period. These results suggest that the dominant source of CH_4 emissions during the cold period is likely microbial activity rather than the release of stored CH_4.

Plain Language Summary

The Arctic is undergoing warming twice that of the global average due to positive feedback loops involving snow and ice loss. This is altering seasonality and greenhouse

gas dynamics in tundra regions, where a large carbon reservoir exists in tundra soils. The effects of Arctic warming are most pronounced in the cold period (October – April). This is crucial as the cold period in Arctic tundra environments can account for half of annual emissions of methane (CH_4), a powerful greenhouse gas with ~30 times the warming potential than that of carbon dioxide by mass over a 100-year time horizon, and much more over a 20-year time period. The majority of cold season CH_4 emissions occur in early winter when soils are not completely frozen and temperatures hover around 0° C during the transition from liquid to solid. This is referred to as the zero-curtain period. There is uncertainty regarding whether CH_4 emissions during the zero-curtain period are due to active microbial production of CH_4 or merely the result of CH_4 escaping that was generated during the prior summer season. Our study suggests that microbial activity occurs during the zero-curtain period, as emissions of CH_4 far exceed the concentrations of CH_4 within the soil column at the onset of winter. Moreover, soil concentrations of CH_4 are higher in spring than at the beginning of winter, suggesting additions of CH_4 to the soil column over the cold period.

Introduction

The Arctic region contains one of the largest terrestrial reservoirs of organic carbon (~1000 Pg-C in just the top three meters) stored in tundra soils (Hugelius et al., 2020; Mishra et al., 2021). As this region continues to warm at an accelerated rate, disproportionate to the global average (Serreze & Francis, 2006), these soils are experiencing increased thawing and decomposition, potentially mobilizing and releasing a substantial amount of carbon to the atmosphere, fueling further warming (Commane et al., 2017; Schuur et al., 2013, 2015; Natali et al., 2015, 2019). Arctic warming has

been most pronounced during the nongrowing season leading to both warmer winters (Bekryaev et al., 2010) and an extension of the duration of zero-curtain period (Arndt et al., 2019), when phase transition occurs while the soil freezes during early winter (Outcalt et al. 1990). Methane (CH_4), a potent greenhouse gas, is particularly important in large swaths of the Arctic characterized by inundated soils. In these arctic tundra ecosystems, surface waters restrict the availability of oxygen, creating favorable conditions for anaerobic methanogenesis (Garcia et al., 2000; Lipson et al., 2012). Acetoclastic methanogenesis, an acetate dismutation forming carbon dioxide (CO_2) and CH_4 is most important in anaerobic freshwater sediments and is the dominant pathway of methanogenesis in Arctic tundra (Metje and Frenzel, 2007; Throckmorton et al., 2015). Methane dynamics in Arctic wetlands during the nongrowing season has been a research focal point over the last several years (Mastepanov et al., 2008, Zona et al., 2016; Taylor et al., 2018; Arndt et al., 2019). This is because the nongrowing season can account for over half of the annual CH_4 budget, primarily due to emissions during the zero-curtain period (Zona et al., 2016; Hashemi et al. 2021).

Arctic tundra exhibits a large degree of landscape heterogeneity with one of the dominant landform types being vegetated drained lake basins (DLB) (Hinkel et al, 2003; Zulueta et al, 2011). These DLBs comprise around half of the landscape in the Alaskan Arctic Coastal Plain, and form because of permafrost degradation and subsequent land subsidence (Jorgensen and Shur, 2007; van Huissteden et al, 2011). DLBs typically have a water table at or above the ground surface for most or all of the year, making them particularly strong sources of CH_4 (Garcia et al., 2000) and among the strongest emitters of CH_4 during the zero-curtain period (Zona et al, 2016). Many studies have

been conducted observing early winter CH_4 emissions in Arctic wetlands, yet few have examined the mechanisms controlling these emissions Bao et al., 2021). This is due in part to the challenging conditions intrinsic to data collection during the cold period in the Arctic. The portion of the soil column undergoing phase transition is between downward and upward freezing fronts making sample collection or in situ measurements are difficult to obtain. Consequently, there is still uncertainty regarding whether the majority of zero-curtain CH_4 emissions are a result of microbial activity or the release of CH_4 stored in the gas reservoir of the soil column from the previous growing season. It has been suggested that these cold season emissions are due to active winter CH_4 production (Pirk et al., 2015; Raz-Yaseef et al., 2016) and that it may be due to burst emissions from cracks as the soil column becomes pressurized during freezing (Tagesson et al., 2012; Mastepanov et al., 2013). Additionally, aerenchamatous vegetation, known to play a large role in CH_4 dynamics via plant mediated transport of CH_4 to the atmosphere (Whalen et al., 2005) and of oxygen to the soil (Ström et al., 2005), may also contribute to these fall zero-curtain emissions. However, little is known of plant mediated transport outside of the growing season.

Data from $\delta^{13}C$-CH_4 analysis indicates that the renewed growth of global CH_4 concentrations since 2007 is dominated by significant increases in biogenic CH_4 production and is attributed, in the Arctic, to increased late summer CH_4 emissions from wetland regions (Fisher et al., 2011; Sriskantharajah et al., 2012; Nisbet et al., 2016). While it has been shown that microbial activity can occur in subzero conditions (Mikan, Schimel and Doyle, 2002; Jansson and Taş, 2014) there is a paucity of in-situ data combining soil microbial measurements to ecosystem scale fluxes in Arctic tundra

systems, particularly during early winter. High latitude wetlands have been estimated to contribute only around 4-5% of global CH_4 emissions (Kirschke et al., 2013). However, terrestrial CH_4 enhancement in Arctic tundra is trending upwards in the fall (Sweeny et al., 2016) and has been linked to subsurface soils freezing later in the year (Arndt et al., 2019). As Arctic warming is causing an elongation of the zero-curtain period (Arndt et al., 2019), it follows that if zero-curtain CH_4 emissions are predominantly due to microbial activity, then annual CH_4 emissions will also continue to increase. This highlights the importance of understanding the mechanisms involved in CH_4 emissions during early winter. Here, we used a combination of eddy covariance data, chamber flux measurements, isotopic analysis, and soil gas concentrations to estimate the turnover rate of the active layer CH_4 reservior during the cold season. Our multi-faceted study is designed to elucidate the sources and dynamics of CH_4 emissions spanning the cold season .

Materials and Methods

Study site and eddy covariance data

Measurements were taken at a medium aged (50-300 years since drained) (Hinkel et al., 2003) DLB near Utqiaġvik on the North Slope of Alaska in the Barrow Environmental Observatory (BEO) (Fig. 6). The DLB is the location of a longterm year-round eddy covariance tower (US-Bes) and is dominated by mosses (*Sphagnum sp.* - 95% cover), sedges (*C. aquatilis* – 3% cover) and grasses (*E. russeolum* - <1%) (Davidson et al., 2016). This site was chosen as DLBs are one of the dominant landform types of the Northern Alaskan Arctic (Hinkel et al., 2003; 2005), are primarily methanogenic areas - characterized by shallow inundation and a distinct start of the

zero-curtain period, and have been shown to have very low interannual variability (± 4.5% from 2014-2017) providing a more reliable estimation of annual emissions. Soil temperature was used to determine the initiation of the zero-curtain period (when surface soil temperature drops below freezing) using a Type T thermocouple (Omega Engineering) array with 5 cm resolution (from +10 to -55 cm relative to the soil surface). Eddy covariance data from the zero-curtain period are averaged seasonal emissions over 2014-2017 and are taken from Hashemi et al. (2021).

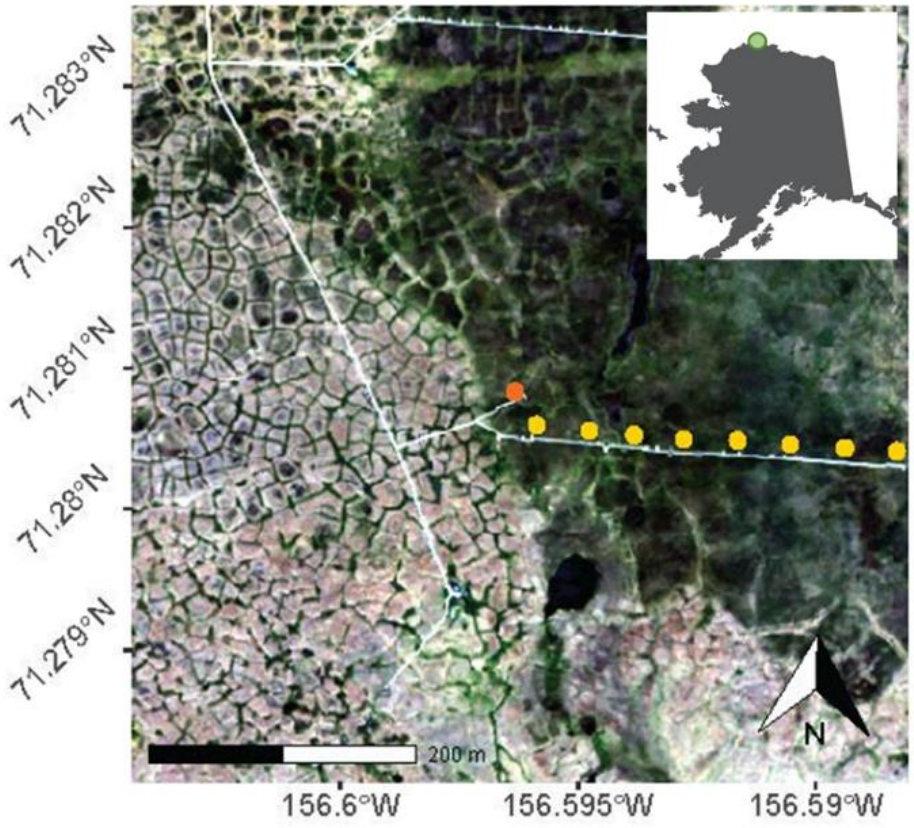

Figure 7: Map of the drained lake basin site near Utqiġavik, AK. Orange circle represents location of the US-Bes eddy covariance tower. Yellow circles represent locations of chambers used for acetate injection and chamber flux measurements. Imagery acquired from WorldView-3 (Maxar Technologies) on July 24, 2016.

CH_4 production

Methane production via acetoclastic methanogenesis was investigated using ^{13}C isotopically labelled sodium acetate soil injections during the growing season. We installed eight chambers along a transect in the DLB in August 2019. Chambers were constructed from PVC pipes (10 cm diameter) inserted into the soil through the extent of the active layer (~35 cm), equipped with 1.5 cm diameter PVC access ports attached at an angle to allow label injection and water sampling at 15 cm soil depth without disturbing the soil surface. Chambers were placed over areas containing only mosses and areas containing both sedges and mosses to represent the naturally occurring vegetation in the DLB. Based on the approximate volume of soil water enclosed in each chamber (~2 L) and average acetate concentrations measured previously in the landscape (50 µM), a mixture of 2-^{13}C-labeled and unlabeled acetate was added to each soil to attain a final acetate concentration of 100 µM enriched to 100 ‰. 50 mL of 1.9956 mM unlabeled sodium acetate with 4.4 µM 99% 2-^{13}C sodium acetate was injected through the injection port using a syringe equipped with a stainless-steel tube (2 mm D), and injection ports were sealed with end caps. Before injection of the labeled acetate, soil water samples were collected from 15 cm depth, and 1 mL of each was injected into evacuated 10 ml glass vials for dissolved gas analysis. Gas samples were taken from the chamber headspace after one hour of incubation with chamber lids (10 cm D end caps fitted with foam tape for seal and fitted with septa for syringe sampling). Headspace samples were taken before injection and on the 1st, 2nd, 3rd, 4th, 5th, 7th, and 10th day following injection. Gas samples were stored in 10 cc exetainers, which were sealed in Bitran ziplock bags until analysis. A final set of water samples from 15

cm depth was collected after the last time point. Gas samples were sent to the Stable Isotope Facility at the University of California, Davis for analysis of $\delta^{13}CH_4$ by mass spectrometry. The ^{13}C content was reported as ‰ relative to the Vienna Pee Dee Belemnite Standard (VPDB) and the mean standard deviation was 0.14‰ over 29 samples. During October of 2019, PVC pipes were covered for a period of 24 hours at which point air samples were taken and measured for concentration to try to capture stochastic burst emission events and to show estimations of CH_4 emission differences during the zero-curtain depending on vegetation composition.

Active Layer CH_4 Concentrations

Methane concentrations in the active layer of the soil column were collected using a combination of equilibrium headspace sampling of water extracted from the soil column and gas extraction from frozen soil cores depending on the season. During the zero-curtain period of Oct 2019, water samples were collected from 4 locations with a syringe fitted with a stainless-steel sampling tube from depth ranges of 5-10, 15-20, and 30-35 cm and placed into tubes without headspace. The frozen surface layer (7.5-10 cm depth) was collected with a hole saw and electric drill. Subsamples of the water samples were injected into N_2-flushed 10 mL tubes. Frozen soils were sealed in two layers of Bitran bags and kept frozen until analysis. During summer 2021, water samples were collected from six locations at depth ranges of 0, 0-6, 6-12, 12-18 and 18-24 cm. Water samples were transported to San Diego, CA where headspace gas concentrations were measured by gas chromatography (SRI 8610 GC with methanizer and flame ionization detector) within one week of collection. During spring 2021, three frozen soil cores were collected using a SIPRE auger and gas-powered drill head soil.

Soil cores were vacuum sealed and shipped frozen to San Diego, CA for further processing. Soil cores were sliced into 5 cm subsections using a band saw, and subsamples of each layer (0-5, 5-10, 10-15, 15-20, 20-25, and 25-30 cm) were used for determinations of trapped CO_2 and CH_4. Frozen soil samples (~ 25 g) were placed in 0.473 L jars on ice, and flushed with N_2. 100 mL of N_2-degassed deionized water was injected into each jar, and jars were then placed in a 40°C water bath and swirled to rapidly thaw soils, releasing trapped gases with minimal time for biological activity (5-15 minutes). Immediately after thawing, headspace was sampled by syringe into evacuated tubes and analyzed by gas chromatography (SRI 8610 GC with methanizer and flame ionization detector). Remaining subsamples of soil from the layers were analyzed for organic matter, water content, and bulk density (Lipson et al., 2013) to allow calculation of trapped gases per unit volume. To estimate CH_4 storage from soil and soil water concentrations, we used linear interpolation to estimate concentrations between measured depths. Total soil CH_4 concentrations are reported in C-CH_4 mg m^{-2} over the active layer depth (35 cm determined by the depth of maximum thaw) for easy comparison to eddy covariance data.

Statistical analysis

All data processing, organization and analysis was performed in R (R v4.0.2, R Core Team, 2020). An analysis of variance was used to test for differences in seasonal CH_4 concentrations and emissions and a t-test was used to test for differences in CH_4 fluxes based on vegetation community. Graphics were generated using the raster (Hijmans, 2020), ggplot2 (Wickham, 2016) and cowplot (Wilke, 2019) R packages.

Results

^{13}C labelled sodium acetate was used for observations of soil CH_4 production from acetoclastic methanogenesis. Isotopic analysis shows $\delta^{13}C$-CH_4 levels at -54.5 ± 2.99 ‰ at the time of injection, immediately increasing to near maximum values within hours of injection, peaking at -40.32 ± .80 ‰ at five days and beginning decline at seven days after injection (Fig. 8). showing evidence of immediate production and emission of CH_4.

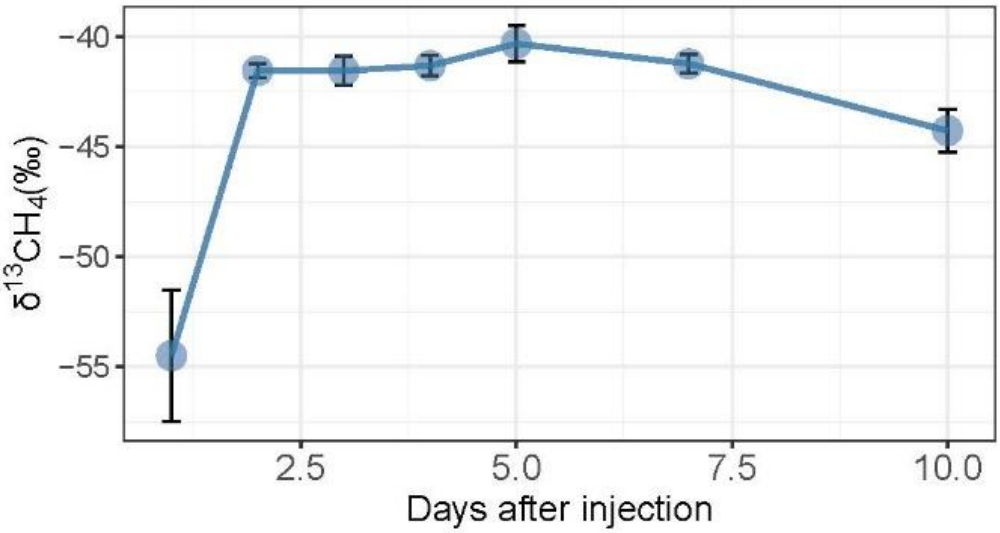

Figure 8: $\delta^{13}C$-CH4 at and following ^{13}C acetate injection. Error bars represent ± standard error

Measurements of zero-curtain soil CH_4 concentrations took place when the soil surface consistently reached temperatures below 0°C. After the start of the zero-curtain, subsurface temperatures can remain at ~0°C for months, sometimes approaching the following calendar year. Methane concentrations within the soil column increased with depth during the summer ranging from 24.92 ± 10 µM at the soil surface to 808.68 ±

316.32 µM at -25 cm. During the zero-curtain period, concentrations ranged from 0.76 ± 0.12 µM just beneath the freezing front (-2.5 cm) to 47.69 ± 36.52 µM at -32.5 cm. Spring concentrations ranged from 25.73 ± 20.96 µM at the soil surface to 349.88 ± 294.14 µM at -25 cm, suggesting that CH_4 was added to the soil column over the winter (Fig. 9a). Total CH_4 storage within the active layer (35 cm depth) was highest during the summer at 1115.69 ± 299.57 mg m^{-2} and decreased to 106.83 ± 7.86 mg m^{-2} at the start of the zero-curtain period. Seasonal totals calculated from eddy covariance tower flux data show emissions during the zero curtain to be an order of magnitude higher (1100 ± 50 mg/m2 (Fig. 9b)) than active layer storage at the beginning of the zero-curtain period. Soil storage during spring was 417.3 ± 282.3 mg m^{-2}, showing an increase over the winter period.

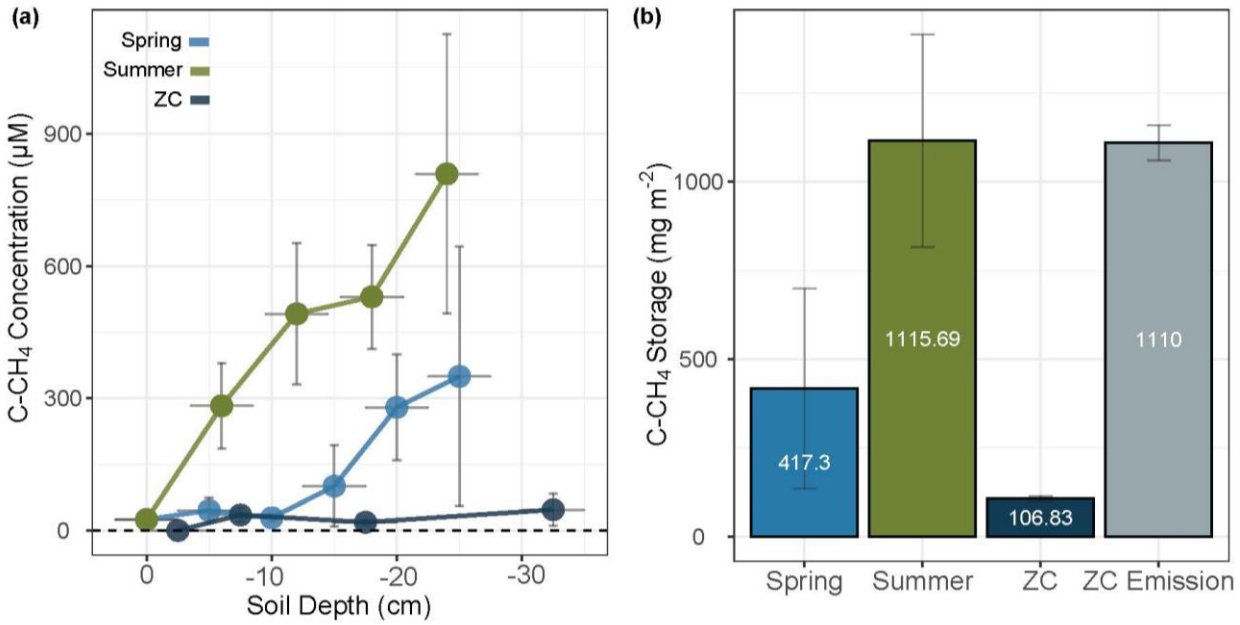

Figure 9: (a) CH_4 concentrations (µM) through the active layer during Spring, Summer and the zero-curtain period); (b) C-CH_4 storage (mg/m^2) in active layer reservoir and mean total zero-curtain emissions over 2014-2017 ($p<0.01$ for comparison of Spring, Summer and zero-curtain concentration). Error bars represent ± standard error.

Results show that plant mediated CH_4 transport occurs into the zero-curtain period, after surface soils freeze, providing an explanation for transport other than stochastic burst events. Measurements of CH_4 emissions during the zero-curtain period in October of 2019 show that areas comprised with high percent cover in sedges (186.11 ± 58.22 µg m^{-2} hr^{-1}) have methane emissions two orders of magnitude higher than areas comprised only of mosses (1.74 ± .72 µg m-2 hr-1) (Fig. 10).

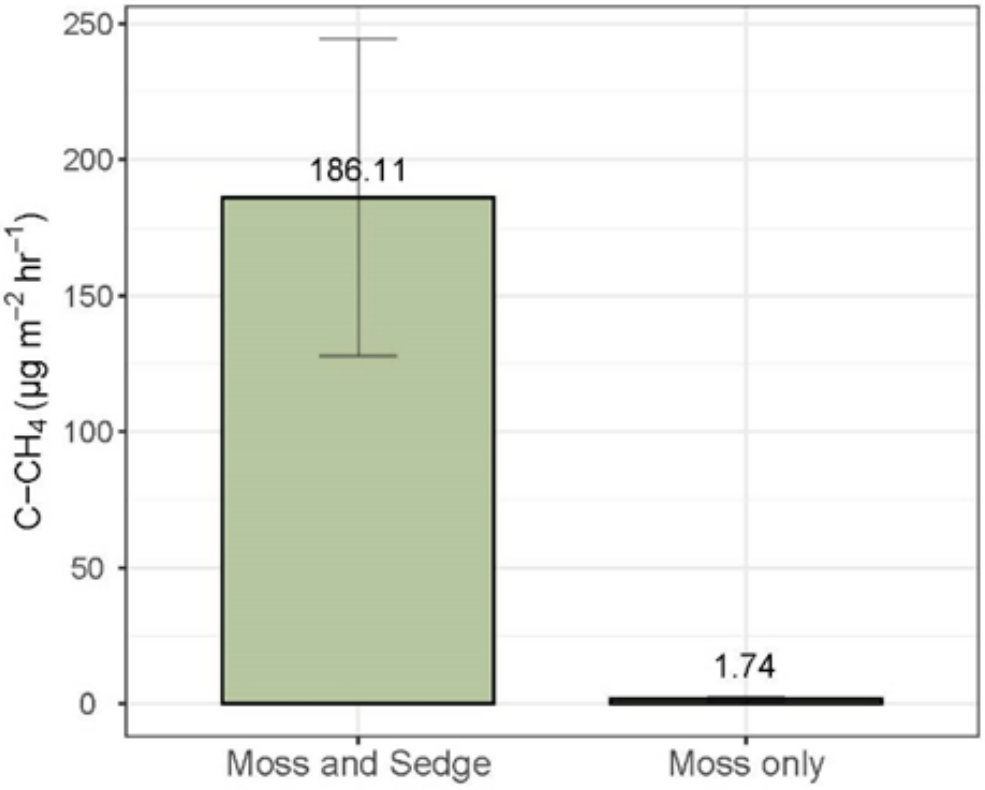

Figure 10: CH_4 flux during October 2019 from areas of comprised only of mosses and areas comprised of both mosses and sedges ($p<0.001$). Error bars represent ± standard error.

Discussion

Our study shows evidence supporting consistent production of CH_4 during the cold season. Both aerobic and anaerobic CH_4 oxidation in the soil column substantially reduce CH_4 emission at up to 90% and 25% of production respectively (Le Mer and Roger, 2001; Miller et al., 2019). Methane production rates at the US-Bes DLB have been found to be around 1.64 nmol cc^{-1} hr^{-1} (Lipson et al., 2012) and summer emissions at 0.24 nmol cc^{-1} hr^{-1} (based on emissions from Zona et al., 2016 over 35 cm active layer depth) showing oxidation within the soil column to be around 85%. Isotopic analysis indicates that production begins only hours after the introduction of labeled acetate and continues for around seven days before labeled concentrations begin to decline (Fig. 8). This rapid CH_4 turnover agrees with calculations based on CH_4 storage (1115.69 mg m^{-2}) (Fig. 9b) divided by mean seasonal emission (1.45 mg C-CH¬4 m^{-2} hr^{-1}) (Hashemi et al., 2021) at the US-Bes DLB, resulting in the estimated CH_4 residence time within the soil at a range of 6.4-8 days using a CH_4 oxidation of 80-85% of soil concentrations. These results suggest that prolonged CH_4 storage is unlikely leading up to the zero-curtain period as the reservoir from which emissions originate undergoes rapid turnover.

Concentrations of CH_4 within the soil column increased with soil depth with a higher degree of variability in the deepest areas of the active layer during the growing season (Fig. 9a). These concentrations are greatly reduced at the beginning of the zero-curtain period, approaching winter, and do not exhibit a similar relationship with soil depth. This may be due to (1) losses from the soil reservoir as a result of pressurized soils during initial freeze-up (Mastepanov et al., 2008); (2) methanogenesis occurring at

a slower rate due to temperature decline as this is a temperature dependent process (Dunfield et al., 1993); and (3) the reduction in oxygen diffusion through the top layer of ice (Hemmingsen, 1958) dampening the oxygen gradient and thus the relationship of depth and CH_4 concentration in the soil column, as methanotrophy would be hindered. Methane concentrations in the spring increased with depth below the top ten cm (Fig. 9a). This is likely due to methanogenesis occurring throughout the zero-curtain period. Once the surface layer of ice is thick enough, CH_4 emission may become limited resulting in a pocket of CH_4 being trapped below the top freezing front during winter. Total soil column concentrations are expectedly highest during the growing season (1115.69 ± 299.57 mg C-CH_4 m^{-2}) and decrease to 106.83 ± 7.86 mg m^{-2} at the beginning of the zero-curtain (Fig. 9b). However, CH_4 emissions during the zero-curtain far exceed this (1110 ± 50 mg C-CH_4 m^{-2} $season^{-1}$). While studies involving the temperature sensitivity of methanogens have shown that they have a similar temperature response to methanotrophs (Metje & Frenzel, 2007), methanotrophy largely takes place in aerobic surface soils that are frozen during this time (Reim et al., 2012). This may explain the large emissions during the zero-curtain, as CH_4 production may be less inhibited than consumption during this time, though more research is beginning to show the importance of anaerobic methane oxidation (Fan et al., 2021). Nonetheless, soil CH_4 would undergo some level of oxidation before emission, decreasing the reservoir further, illustrating that cold season emissions are not solely the release of trapped CH_4. Total soil column concentrations during the spring corroborate the likelihood of microbial production as data show an increase from fall

concentrations to 417.3 ± 282.3 mg m^{-2}, revealing an addition to the soil gas reservoir over the cold season.

The zero-curtain period begins when surface soils freeze leaving an unfrozen portion of the active layer for months into the winter. As the landscape begins to freeze during this transition, CH_4 emissions can occur through stochastic burst events caused by CH_4 that is squeezed through cracks created by frost action (Mastepanov et al., 2008). However, it has also been shown that emissions during the zero-curtain period are often steady through freeze-up (Zona et al., 2016; Commane et al. 2019; Natali et al., 2019; Arndt et al, 2020; Hashemi et al., 2021) indicating continuous release. This is likely due, in part, to the presence of aerenchymatous vegetation in wetlands. It has been well documented that CH_4 transport can occur through aerenchyma of vascular plants in Arctic wetlands, particularly *Carex aquatilis*, which possess aerenchyma and are abundant in these regions (Kutzbach et al., 2004; Davidson et al., 2016; Andresen et al., 2017). However, no studies to our knowledge have been conducted on plant mediated CH_4 transport during early winter in Arctic wetlands. Measurements show areas containing aerenchymatous vegetation exhibit CH_4 emissions two orders of magnitude higher than those only containing mosses (Fig. 10). This is likely due to plant mediated transport continuing to occur during the zero-curtain period as vegetation extends from the soil column through the layer of surface ice. This may describe the dominant physical pathway of CH_4 emissions in DLBs during this time and also explain the high degree of variability in storage during spring. In areas where there was little or no aerenchymatous vegetation, CH_4 could build up leading to release or oxidation during the snowmelt period of the following spring (Arndt et al., 2020) while areas with

an abundance of aerenchymatous vegetation may experience more rapid CH_4 loss to both emission and oxidation during the zero-curtain period, though lateral movement of CH_4 could occur confounding clear relationships with surface vegetation.

In primarily methanogenic areas, CH_4 oxidation can account for up to 35% of ecosystem respiration (Nielson et al., 2019), though during the zero curtain, oxygen may become increasingly limited in the soil column. Aerenchymae not only allow for CH_4 transport to the atmosphere but also allow for oxygen transport into the soil column. This would serve as a route for CH_4 oxidation, likely having a lowering effect on levels of CH_4 approaching the surface of the active layer during spring (Fig. 9a) and a portion of the CO_2 emissions characteristic of Arctic wetlands during the zero-curtain period (Oechel et al., 2014; Commane et al., 2017; Euskirchen et al., 2017; Natali et al., 2019). Further research into changes in percent CH_4 oxidation from the growing season to the zero-curtain and into the percent contribution of CH_4 oxidation to ecosystem respiration is needed to understand these mechanisms. These data could help decrease error in regional model parameterizations using sedge density.

Despite the paucity of data in the literature directly showing biological activity during the zero-curtain period, our data show strong evidence in support of its occurrence and that this process along with stochastic burst emission events and plant mediated transport extending into winter operate simultaneously. Correspondingly, this study begins to describe some of the possible mechanisms and research directions to elaborate further on cold season emission dynamics in Arctic wetlands. Specifically, (1) studies examining cold-adapted methanogenic communities during the zero-curtain period and the associated temperature response of CH_4 production can help predict

emission dynamics under further warming and (2) data from chamber flux studies with measurements capturing the heterogeneity in hydrology and vegetation communities during the zero-curtain period can be upscaled to improve regional annual budgets estimations and lead to a reduction in model error.

Acknowledgments

This work was funded by the NASA ABoVE Program (No. NNX16AF94A) and the National Science Foundation—Office of Polar Programs (Nos. 1204263 and 1702797). Additional logistical support was funded by the National Science Foundation—Office of Polar Programs, the NASA ABoVE Program, NOAA CESSRST EPP (No. NA16SEC4810008), the European Union's Horizon 2020 research and innovation program (No. 629727890), and from the Natural Environment Research Council (NERC) UAMS Grant (No. NE/P002552/1). The first author was supported by the Joint Doctoral Program in Ecology. We would like to thank the Ukpeaġvik Inupiat Corporation (UIC) for the ability to conduct this research on UIC owned land.

References

Andresen, C. G., & Lougheed, V. L. (2015). Disappearing Arctic tundra ponds: Fine-scale analysis of surface hydrology in drained thaw lake basins over a 65 year period (1948-2013). *Journal of Geophysical Research: Biogeosciences*, *120*(3), 466–479. https://doi.org/10.1002/2014JG002778

Arndt, K. A., Lipson, D. A., Hashemi, J., Oechel, W. C., & Zona, D. (2020). Snow melt stimulates ecosystem respiration in Arctic ecosystems. *Global Change Biology*, *26*(9), 5042–5051. https://doi.org/10.1111/gcb.15193

Arndt, K. A., Oechel, W. C., Goodrich, J. P., Bailey, B. A., Kalhori, A., Hashemi, J., … Zona, D. (2019). Sensitivity of Methane Emissions to Later Soil Freezing in Arctic Tundra Ecosystems. *Journal of Geophysical Research: Biogeosciences*, *124*(8), 2595–2609. https://doi.org/10.1029/2019jg005242

Bao, T, Xu, X, Jia, G, Billesbach, DP, Sullivan, RC. Much stronger tundra methane emissions during autumn freeze than spring thaw. *Glob Change Biol*. 2020; 27: 376– 387. https://doi.org/10.1111/gcb.15421

Bekryaev, R. V., Polyakov, I. V., & Alexeev, V. A. (2010). Role of polar amplification in long-term surface air temperature variations and modern arctic warming. *Journal of Climate*, *23*(14), 3888–3906. https://doi.org/10.1175/2010JCLI3297.1

Commane, R., Lindaas, J., Benmergui, J., Luus, K. A., Chang, R. Y.-W., Daube, B. C., … Wofsy, S. C. (2017). Carbon dioxide sources from Alaska driven by increasing early winter respiration from Arctic tundra. *Proceedings of the National Academy of Sciences*, *114*(21), 5361–5366. https://doi.org/10.1073/pnas.1618567114

Davidson, S. J., Santos, M. J., Sloan, V. L., Watts, J. D., Phoenix, G. K., Oechel, W. C., & Zona, D. (2016). Mapping arctic tundra vegetation communities using field spectroscopy and multispectral satellite data in North Alaska, USA. *Remote Sensing*, *8*(12). https://doi.org/10.3390/rs8120978

Davidson, S. J., Sloan, V. L., Phoenix, G. K., Wagner, R., Fisher, J. P., Oechel, W. C., & Zona, D. (2016). Vegetation Type Dominates the Spatial Variability in CH4 Emissions Across Multiple Arctic Tundra Landscapes. *Ecosystems*, *19*(6), 1116–1132. https://doi.org/10.1007/s10021-016-9991-0

Dunfield, P., Knowles, R., Dumont, R., & Moore, T. R. (1993). Methane production and consumption in temperate and subarctic peat soils: Response to temperature and pH. *Soil Biology and Biochemistry*, *25*(3), 321–326. https://doi.org/10.1016/0038-0717(93)90130-4

Euskirchen, E. S., Bret-Harte, M. S., Shaver, G. R., Edgar, C. W., & Romanovsky, V. E. (2017). Long-Term Release of Carbon Dioxide from Arctic Tundra Ecosystems in Alaska. *Ecosystems*. https://doi.org/10.1007/s10021-016-0085-9

Fan, L., Dippold, M. A., Thiel, V., Ge, T., Wu, J., Kuzyakov, Y., & Dorodnikov, M. (2022). Temperature sensitivity of anaerobic methane oxidation versus methanogenesis in paddy soil: Implications for the CH4 balance under global warming. *Global Change Biology*, *28*(2), 654–664. https://doi.org/10.1111/gcb.15935

Fisher, R. E., Sriskantharajah, S., Lowry, D., Lanoisellé, M., Fowler, C. M. R., James, R. H., … Nisbet, E. G. (2011). Arctic methane sources: Isotopic evidence for atmospheric inputs. *Geophysical Research Letters*, *38*(21), 1–7. https://doi.org/10.1029/2011GL049319

Garcia, J. L., Patel, B. K. C., & Ollivier, B. (2000). Taxonomic, phylogenetic, and ecological diversity of methanogenic Archaea. *Anaerobe*, *6*(4), 205–226. https://doi.org/10.1006/anae.2000.0345

Hashemi, J., Zona, D., Arndt, K. A., Kalhori, A., & Oechel, W. C. (2021). Seasonality buffers carbon budget variability across heterogeneous landscapes in Alaskan Arctic tundra. *Environmental Research Letters*, *16*(3). https://doi.org/10.1088/1748-9326/abe2d1

Hemmingsen, E. (1959) Permeation of Gases through Ice, *Tellus, 11:3*, 355-359, DOI: 10.3402/tellusa.v11i3.9311

Hijmans (2020). raster: Geographic Data Analysis and Modeling. R package version 3.3-13. https://CRAN.R-project.org/package=raster

Hinkel, K. M., Eisner, W. R., Bockheim, J. G., Nelson, F. E., Peterson, K. M., & Dai, X. (2003). Spatial Extent, Age, and Carbon Stocks in Drained Thaw Lake Basins on the Barrow Peninsula, Alaska. *Arctic, Antarctic, and Alpine Research*, *35*(3), 291–300. https://doi.org/10.1657/1523-0430(2003)035[0291:SEAACS]2.0.CO;2

Hinkel, K. M., Frohn, R. C., Nelson, F. E., Eisner, W. R., & Beck, R. A. (2005). Morphometric and spatial analysis of thaw lakes and drained thaw lake basins in the western Arctic Coastal Plain, Alaska. *Permafrost and Periglacial Processes*, *16*(4), 327–341. https://doi.org/10.1002/ppp.532

Hugelius, G., Loisel, J., Chadburn, S., Jackson, R. B., Jones, M., MacDonald, G., … Yu, Z. (2020). Large stocks of peatland carbon and nitrogen are vulnerable to permafrost thaw. *Proceedings of the National Academy of Sciences of the United States of America*, *117*(34), 20438–20446. https://doi.org/10.1073/pnas.1916387117

Jansson, J. K., & Taş, N. (2014). The microbial ecology of permafrost. *Nature Reviews Microbiology*, *12*(6), 414–425. https://doi.org/10.1038/nrmicro3262

Jorgenson, M. T., & Shur, Y. (2007). Evolution of lakes and basins in northern Alaska and discussion of the thaw lake cycle. *Journal of Geophysical Research: Earth Surface*, *112*(2). https://doi.org/10.1029/2006JF000531

Kirschke, S., Bousquet, P., Ciais, P., Saunois, M., Canadell, J. G., Dlugokencky, E. J., … Zeng, G. (2013). Three decades of global methane sources and sinks. *Nature Geoscience*, *6*(10), 813–823. https://doi.org/10.1038/ngeo1955

Kutzbach, L., Wille, C., & Pfeiffer, E. M. (2007). The exchange of carbon dioxide between wet arctic tundra and the atmosphere at the Lena River Delta, Northern Siberia. *Biogeosciences*, *4*(5), 869–890. https://doi.org/10.5194/bg-4-869-2007

Le Mer, J., & Roger, P. (2001). Production, oxidation, emission and consumption of methane by soils: A review. *European Journal of Soil Biology*, *37*(1), 25–50. https://doi.org/10.1016/S1164-5563(01)01067-6

Lipson, D. A., Zona, D., Raab, T. K., Bozzolo, F., Mauritz, M., & Oechel, W. C. (2012). Water-table height and microtopography control biogeochemical cycling in an Arctic coastal tundra ecosystem. *Biogeosciences*, *9*(1), 577–591. https://doi.org/10.5194/bg-9-577-2012

Lipson, D.A., Raab, T.K., Goria, D. and Zlamal, J., 2013. The contribution of Fe (III) and humic acid reduction to ecosystem respiration in drained thaw lake basins of the Arctic Coastal Plain. *Global Biogeochemical Cycles*, *27*(2), pp.399-409.

Mastepanov, M., Sigsgaard, C., Dlugokencky, E. J., Houweling, S., Ström, L., Tamstorf, M. P., & Christensen, T. R. (2008). Large tundra methane burst during onset of freezing. *Nature*, *456*(7222), 628–630. https://doi.org/10.1038/nature07464

Mastepanov, M., Sigsgaard, C., Tagesson, T., Ström, L., Tamstorf, M. P., Lund, M., and Christensen, T. R. (2013) Revisiting factors controlling methane emissions from high-Arctic tundra. *Biogeosciences, 10*, 5139–5158. https://doi.org/10.5194/bg-10-5139-2013.

Metje, M., & Frenzel, P. (2007). Methanogenesis and methanogenic pathways in a peat from subarctic permafrost. *Environmental Microbiology*, *9*(4), 954–964. https://doi.org/10.1111/j.1462-2920.2006.01217.x

Mikan, C. J., Schimel, J. P., & Doyle, A. P. (2002). Temperature controls of microbial respiration in arctic tundra soils above and below freezing. *Soil Biology and Biochemistry*, *34*(11), 1785–1795. https://doi.org/10.1016/S0038-0717(02)00168-2

Miller, K., Lai, C.-T., Dahlgren, R., & Lipson, D. (2019). Anaerobic Methane Oxidation in High-Arctic Alaskan Peatlands as a Significant Control on Net CH4 Fluxes. *Soil Systems*, *3*(1), 7. https://doi.org/10.3390/soilsystems3010007

Mishra, U., Hugelius, G., Shelef, E., Yang, Y., Strauss, J., Lupachev, A., … Orr, A. (2021). Spatial heterogeneity and environmental predictors of permafrost region soil organic carbon stocks. *Science Advances*, *7*(9), 1–13. https://doi.org/10.1126/sciadv.aaz5236

Natali, S. M., Schuur, E. A. G., Mauritz, M., Schade, J. D., Celis, G., Crummer, K. G., … Webb, E. E. (2015). Journal of Geophysical Research: Biogeosciences. *Journal of Geophysical Research: Biogeosciences*, *120*(361), 1–13. https://doi.org/10.1002/2014JG002872.Received

Natali, S. M., Watts, J. D., Rogers, B. M., Potter, S., Ludwig, S. M., Selbmann, A. K., … Zona, D. (2019). Large loss of CO2 in winter observed across the northern permafrost region. *Nature Climate Change*, *9*(11), 852–857. https://doi.org/10.1038/s41558-019-0592-8

Nielsen, C. S., Hasselquist, N. J., Nilsson, M. B., Öquist, M., Järveoja, J., & Peichl, M. (2019). A novel approach for high-frequency in-situ quantification of methane oxidation in peatlands. *Soil Systems*, *3*(1), 1–14. https://doi.org/10.3390/soilsystems3010004

Nisbet, E. G., Dlugokencky, E. J., Manning, M. R., Lowry, D., Fisher, R. E., France, J. L., … Ganesan, A. L. (2016). Rising atmospheric methane: 2007-2014 growth and isotopic shift. *Global Biogeochemical Cycles*, *30*(9), 1356–1370. https://doi.org/10.1002/2016GB005406

Oechel, W. C., Laskowski, C. A., Burba, G., Gioli, B., & Kalhori, A. A. M. (2014). Annual patterns and budget of CO 2 flux in an Arctic tussock tundra ecosystem. *Journal of Geophysical Research: Biogeosciences*, *119*(3), 323–339. https://doi.org/10.1002/2013JG002431

Outcalt, S. I., Arbor, A., Nelson, F. E., & Hinkel, K. M. (1990). The zero-curtain effect: heat and mass transfer across an isothermal region in freezing soil. *Water Resources*, *26*(7), 1509–1516.

Pirk, N., T. Santos, C. Gustafson, A. J. Johansson, F. Tufvesson, F.-J. W. Parmentier, M. Mastepanov, and T. R. Christensen (2015), Methane emission bursts from permafrost environments during autumn freeze-in: New insights from ground-penetrating radar. *Geophys. Research Letters., 42*, 6732–6738. doi:10.1002/2015GL065034

Raz-Yaseef, N., Torn, M. S., Wu, Y., Billesbach, D. P., Liljedahl, A. K., Kneafsey, T. J., … Wullschleger, S. D. (2016). Large CO2 and CH4 emissions from polygonal tundra during spring thaw in northern Alaska. *Geophysicial Research Letters*, 504–513. https://doi.org/10.1002/2016GL071220.

Reim, A., Lüke, C., Krause, S., Pratscher, J., & Frenzel, P. (2012). One millimetre makes the difference: High-resolution analysis of methane-oxidizing bacteria and their specific activity at the oxic-anoxic interface in a flooded paddy soil. *ISME Journal*, *6*(11), 2128–2139. https://doi.org/10.1038/ismej.2012.57

Schuur, E. A. G., Abbott, B. W., Bowden, W. B., Brovkin, V., Camill, P., Canadell, J. G., … Zimov, S. A. (2013). Expert assessment of vulnerability of permafrost carbon to climate change. *Climatic Change*. https://doi.org/10.1007/s10584-013-0730-7

Schuur, E. A. G., McGuire, A. D., Schädel, C., Grosse, G., Harden, J. W., Hayes, D. J., … Vonk, J. E. (2015). Climate change and the permafrost carbon feedback. *Nature*, *520*(7546), 171–179. https://doi.org/10.1038/nature14338

Serreze, M. C., & Francis, J. A. (2006). The arctic amplification debate. *Climatic Change*, *76*(3–4), 241–264. https://doi.org/10.1007/s10584-005-9017-y

Sriskantharajah, S., Fisher, R. E., Lowry, D., Aalto, T., Hatakka, J., Aurela, M., … Nisbet, E. G. (2012). Stable carbon isotope signatures of methane from a Finnish subarctic wetland. *Tellus, Series B: Chemical and Physical Meteorology*, *64*(1), 1–8. https://doi.org/10.3402/tellusb.v64i0.18818

Ström, L., Ekberg, A., Mastepanov, M., & Christensen, T. R. (2003). The effect of vascular plants on carbon turnover and methane emissions from a tundra wetland. *Global Change Biology*, *9*(8), 1185–1192. https://doi.org/10.1046/j.1365-2486.2003.00655.x

Sweeney, C., Dlugokencky, E., Miller, C. E., Wofsy, S., Karion, A., Dinardo, S., et al. (2016). No significant increase in long-term CH4 emissions on North Slope of Alaska despite significant increase in air temperature. *Geophysical Research Letters, 43*, 6604–6611. https:// doi.org/10.1002/2016GL069292

Tagesson, T., Mölder, M., Mastepanov, M., Sigsgaard, C., Tamstorf, M. P., Lund, M., et al. (2012). Land-atmosphere exchange of methane from soil thawing to soil freezing in a high-Arctic wet tundra ecosystem. *Global Change Biology, 18(6*), 1928–1940. https://doi.org/ 10.1111/j.1365-2486.2012.02647.x

Taylor, M. A., Celis, G., Ledman, J. D., Bracho, R., & Schuur, E. A. G. (2018). Methane Efflux Measured by Eddy Covariance in Alaskan Upland Tundra Undergoing Permafrost Degradation. *Journal of Geophysical Research: Biogeosciences*, *123*(9), 2695–2710. https://doi.org/10.1029/2018JG004444

Throckmorton, H. M., Heikoop, J. M., Newman, B. D., Altmann, G. L., Conrad, M. S., Muss, J. D., … Wilson, C. J. (2015). Global Biogeochemical Cycles of stable isotopes. *Global Biogeochemical Cycles*, *29*, 1893–1910. https://doi.org/10.1002/2014GB005044.

Van Huissteden, J., Berrittella, C., Parmentier, F. J. W., Mi, Y., Maximov, T. C., & Dolman, A. J. (2011). Methane emissions from permafrost thaw lakes limited by lake drainage. *Nature Climate Change*, *1*(2), 119–123. https://doi.org/10.1038/nclimate1101

Whalen, S. C. (2005). Natural Wetlands and the Atmosphere. *Environmental Engineering Science*, *22*(1), 73–94. https://doi.org/10.1089/ees.2005.22.73

Wickham, H. (2016) ggplot2: Elegant Graphics for Data Analysis. Springer-Verlag New York.

Wilke, C. O. (2020). cowplot: Streamlined Plot Theme and Plot Annotations for 'ggplot2'. R package version 1.1.0. https://CRAN.R-project.org/package=cowplot

Zona, D., Gioli, B., Commane, R., Lindaas, J., Wofsy, S. C., Miller, C. E., … Oechel, W. C. (2016). Cold season emissions dominate the Arctic tundra methane budget. *Proceedings of the National Academy of Sciences*, *113*(1), 40–45. https://doi.org/10.1073/pnas.1516017113

Zulueta, R. C., Oechel, W. C., Loescher, H. W., Lawrence, W. T., & Paw U, K. T. (2011). Aircraft-derived regional scale CO2 fluxes from vegetated drained thaw-lake basins and interstitial tundra on the Arctic Coastal Plain of Alaska. *Global Change Biology*, *17*(9), 2781–2802. https://doi.org/10.1111/j.1365-2486.2011.02433.x

Chapter 3

Collapsing polygons are strong sources of N_2O in Alaskan Arctic tundra.

Joshua Hashemi, David Lipson, Kyle Arndt, Scott Davidson, Walter Oechel and Donatella Zona

Abstract

Nitrous oxide (N_2O) emissions have been considered negligible in permafrost regions. Many of these regions are characterized by a variety of distinct landscape types formed by the freeze-thaw cycle. Large portions of the landcover have developed into polygonized tundra that can exhibit cracking and collapse due to permafrost degradation and cryoturbation, exposing unvegetated soil protruding above the water table. Here we show strong N_2O emissions from unvegetated features (mean (range) = 4.5 (.06-38.9) mg N_2O-N m^{-2} d^{-1}), more than an order of magnitude higher than mean rates previously reported for Arctic tundra wetlands, bolstered by lower soil water content, low bulk density and high soil temperature. Isotopic enrichment of ^{15}N in unvegetated soil areas indicates a greater loss of N via microbial processes, in absence of plant uptake. Based on our results, N_2O emissions from unvegetated areas within these features are three times higher than those of CO_2, in terms of warming. Though barren soil features are currently about 12% of the Arctic landscape, climate change is increasingly causing permafrost degradation and this coverage may increase, with the potential to substantially affecting the global N_2O budget.

Introduction

Greenhouse gas (GHG) dynamics in permafrost ecosystems have been shifting due to increasing global temperatures, associated environmental changes, and subsequent positive feedbacks accelerating regional warming (Natali et al., 2021). As permafrost soils make one of the largest terrestrial reservoirs of carbon (C) and nitrogen (N) (Hugelius et al., 2014; Harden et al., 2012; Tarnocai et al., 2009), accumulated over many years due to low temperatures and slow decomposition (Post et al., 1982), increased attention has been given to GHG dynamics in permafrost regions over the last several years (Natali et al., 2019; Bruhwiler et al., 2021; Miner et al., 2022). The majority of regional GHG studies have focused on carbon emissions (i.e., CO_2 and CH_4), outlining effects of, among others, seasonality (Commane et al., 2017; Taylor et al., 2018), landscape heterogeneity (Treat et al., 2018), vegetation composition (Davidson et al., 2016) and vegetation density (Andresen et al., 2017). However, few studies have reported the flux dynamics of nitrous oxide (N_2O), an ozone depleting substance and powerful greenhouse gas with a 100-year global warming potential (GWP_{100}) 298 times that of carbon dioxide (CO_2) and 12 times that of methane (CH_4) (IPCC, 2013). N_2O emissions have often been considered negligible in permafrost regions, and particularly Arctic tundra, because of limited N bioavailability due to cold and wet environmental conditions (Voigt et al., 2020). Low rates of N mineralization are often associated with permafrost soils and can act as a bottleneck to subsequent pathways to N_2O production (i.e., nitrification and denitrification). However, N mineralization rates in permafrost soil active layers can be of similar magnitude to those in temperate and tropical systems

(Ramm et al., 2021). Warming can release organic matter, and therefore N, previously locked in the permafrost and make it available for N mineralization. Additions of bioavailable N can stimulate N mineralization and subsequent N_2O production (Butterbach-Bahl et al., 2013). Strong plant-microbe competition for available inorganic N (ammonium (NH_4^+), nitrite (NO_2^-), and nitrate (NO_3^-)) can also reduce the production and emission of N_2O (Subbarao et al., 2009) in vegetated areas. Plants absorb most of the bioavailable N due to rapid microbial turnover in comparison to plant root tissue (Hodge et al., 2000). However, unvegetated areas common in Arctic regions (Repo et al., 2009; Marushchak et al., 2011; Abbot et al., 2015; Voigt et al., 2017) removes competition for N and can result in higher rates of N_2O producing processes (i.e., nitrification and denitrification) (Palmer et al., 2012; Gil et al., 2017). Emissions of N_2O can be difficult to capture and quantify as the production process requires aerobic and anaerobic steps. These processes are more common during rapid fluctuations in soil conditions that can be highly variable both spatially and temporally (Bernhardt et al., 2017). These “hot spots” and “hot moments” contribute to the difficulty in upscaling N_2O budgets, particularly in regions thought to be of low significance, as data collection campaigns are sparse. Despite this, research is emerging, suggesting that N_2O emissions from permafrost ecosystems may have a significant and growing impact on the global N_2O budget, contributing up to an estimate of 1.27 Tg N_2O-N per year (7% of global budget) (Voigt et al., 2020). Increasing soil temperatures and landscape change due to permafrost degradation are facilitating conditions favorable for increased N cycling, thus a better understanding of the response of N dynamics to warming in permafrost regions is needed.

There is still large uncertainty in high latitude N_2O budgets due to the small number of published regional observations from potential N_2O sources. A recent summary of the published research on this topic (Voigt et al., 2020) showed no measurements of N_2O emissions in the Arctic Coastal Plain in Arctic Alaska. The Arctic Coastal Plain region is characterized by a patchwork of landscape features that includes lakes and ponds, drained lake basins, drained upland tundra and polygonized tundra (Hinkel et al., 2003; Zulueta et al., 2011). Landscape heterogeneity in this region is due in part to freeze-thaw dynamics and permafrost degradation (Liljedahl et al., 2016). In particular, polygonized tundra, extending to an estimated 65% of the Arctic Coastal Plain (Hinkel et al., 2003), can result in significant variability in vegetation composition (Webber, 1978; Davidson et al., 2016), hydrology (Jorgensen and Shur, 2007; Liljedahl et al., 2016), GHG dynamics (Martin et al., 2018; Taş et al., 2018), and a wide range of GHG budget estimations (McGuire et al., 2012; Euskirchen et al., 2017; Zona et al., 2016). Surface relief is created by the common development and growth of ice wedges that, over time, lift areas of the soil, creating ridges and forming distinct polygonal patterns across the landscape that vary in position of the water table (Liljedahl et al., 2016). Polygons follow a succession that can lead to large soil mounds that protrude above the water table, referred to as high-centered polygons (Liljedahl et al., 2016). Permafrost degradation and abrupt thaw processes can destabilize and shift overlying soil structures (Jorgenson et al., 2001; Turetsky et al., 2020), causing high-centered polygons to crack and collapse, similar to palsa mires in lower latitude subarctic peatlands (Zuidhoff and Kolstrup, 2005). This can result in areas of exposed, unvegetated soil that can affect microbial communities and GHG dynamics (Olefeldt et al., 2016).

Here, we report the first magnitude of N_2O fluxes from collapsed polygon surfaces and outline some of the dominant factors controlling variability in emission strength. Further, we address whether these polygon features have a larger climate forcing potential than previously assumed, when accounting for the much larger warming power of N_2O (IPCC 2013). GHG fluxes were estimated using the static chamber technique on the Barrow Environmental Observatory (BEO), a polygonized tundra south of Utqiaġvik, Alaska (Fig. 11a). In this study we report fluxes of both N_2O and CO_2 to show the combined climate forcing potential of two of the main GHGs in these high latitude systems. Measurements were taken at collapsing polygon surfaces (Fig 11b.) both without vegetation cover (Fig. 11c), and nearby vegetated areas (Fig. 11d) experiencing similar environmental conditions. The aim of this study was to identify the role of progressive thermokarst development on N_2O emissions with the expectation that areas of no vegetation cover exhibit higher levels of N_2O emission supported by increased oxygen availability due to lower soil moisture and soil bulk density. Given the drier conditions of the areas selected for this study, CH_4 emissions were negligible and not reported in this study. These data may begin to describe an unaccounted-for feedback and help to constrain estimates of N_2O emissions from permafrost regions.

Results and Discussion

In-situ GHG fluxes.

Flux measurements show collapsing unvegetated areas in high-centered polygons are strong emitters of N_2O (Fig. 12a). Locations where measurements were taken exhibited no significant differences in soil temperature, thaw depth, soil water content

and water table (Supplementary Fig. S6). Unvegetated areas on collapsed polygons show significantly stronger ($p < 0.001$) emissions of N_2O (mean ± standard error = 4.51 ± 0.4 mg N_2O-N m^{-2} d^{-1}) in comparison with vegetated areas (0.82 ± 0.29 mg N_2O-N m^{-2} d^{-1}) (Fig 12a.) and are more than an order of magnitude higher than the mean rate associated with pristine Arctic tundra wetlands (0.125 mg N_2O-N m^{-2} d^{-1}) (Voigt et al., 2020). By unit area, N_2O emission rates from unvegetated surfaces of collapsing features are comparable to those of tropical forest soils (1.5 mg N_2O-N m^{-2} d^{-1}) and are substantially higher than mean emissions measured from peatlands and upland tundra (0.596 & 0.211 mg N_2O-N m^{-2} d^{-1}, respectively) (Voigt et al., 2020), highlighting the importance of permafrost regions and Arctic wetlands in the global N_2O cycle. Emission rates of N_2O at vegetated areas on collapsing high-centered polygons are also higher in comparison to previous estimations for Arctic wetlands. This may have a relationship with frost heaved permafrost N in high-centered polygon development as increased soil N content is generally linked to increased N_2O production (Butterbach-Bahl et al., 2013). Cryoturbation, permafrost degradation, and abrupt thaw may enrich soils by increasing mineralization rates and mixing N from deeper soil layers thereby increasing N availability (Marushchak et al., 2021). Moreover, vegetation on these structures is dominated by moss and lichen communities that are associated with biological nitrogen fixation that can stimulate increases in the soil inorganic N pool (Diáková et al., 2016; Stewart et al., 2011).

Emissions of CO_2 were also significantly larger from unvegetated surfaces ($p < 0.001$), showing these areas to be a source (0.91 ± 0.05 g C-CO_2 m^{-2} d^{-1}) compared to a weak sink at adjacent vegetated areas (-0.16 ± 0.08 g C m^{-2} d^{-1}) (Fig 12b). Fluxes of

CO_2 from vegetated areas and unvegetated areas fall within the range of previous estimations of net ecosystem exchange and ecosystem respiration respectively (Arndt et al., 2020). In estimations of the global warming potential of these collapsed high center polygons in the arctic continuous permafrost, the inclusion of N_2O more than tripled the climate forcing potential (>3.5 g CO_2eq m^{-2} d^{-1}) when compared to that of CO_2 alone. The prevalence of landscape features that are characterized by sparsely vegetated or unvegetated areas such as high-center polygons, make up an estimated 12% of the Arctic tundra region, north of the tree line (Walker et al., 2005). Moreover, the percent cover of these features may substantially increase with an increase in permafrost degradation due to ground subsidence (Liljedahl et al., 2016). Results presented here begin to reconcile differences in assumed rates of N_2O emissions and those observed at the landscape scale in the North Slope of Alaska using aircraft eddy covariance showing an average of 3.8 mg N_2O m^{-2} d^{-1} (Wilkerson et al., 2019).

Variability in N_2O emission strength.

Regression analyses indicates that soil water content (Fig. 13a), bulk density (Fig. 13b) and soil temperature (Fig. 13c) are significantly correlated to N_2O fluxes ($p < 0.001$ for all) in unvegetated areas. None of these relationships were found to be significant in vegetated areas. Bulk density was significantly lower ($p < 0.001$) in unvegetated soil areas (73.3 ± 6.3 g cm^{-3}) than in vegetated areas (119.1 ± 6.3 g cm^{-3}), possibly allowing for increased oxygen penetration into the soil column and thus, conditions more favorable for nitrification. Multivariate regression showed that the combined effect of bulk density and soil water content was an important predictor of N_2O flux at unvegetated soil

locations, explaining 66% of the variability in N_2O emissions (Supplementary Table S3) under these conditions. The inclusion of mean soil temperature in multivariate linear regression models only slightly improved model performance, revealing soil temperature as a lesser control for the temperature ranges reported here. Though there is an obvious influence of temperature over N_2O emissions, as presented here, N_2O emissions in permafrost regions have been found to be dominantly controlled by conditions associated with oxygen availability, such as soil moisture and soil pore size (Stewart et al., 2014). This may also be due to a limited range in mean soil temperature per collar relative to regressions with all soil temperature data. Soil water content and bulk density are tightly related to soil redox potential and oxygen availability, as soil diffusivity increases with lower bulk density and soil water content (Butterbach-Bahl et al., 2013). Thaw depth showed both weak association and predictive strength (Supplementary Fig. S7) and decreased multivariate model performance. Correlations of N_2O emissions with thaw depth are generally observed with permafrost thaw rather than seasonally thawing active layer, as observed here (Voigt et al., 2017).

Soil environment

Soil samples from areas with no vegetation were significantly higher in both $\delta^{15}N$ (30 ± 2.34 ‰) and $\delta^{13}C$ (-4.74 ± 3.2 ‰) content than in vegetated soils ($\delta^{15}N$: 14.58 ± 3.3 ‰; $\delta^{13}C$: = -21.32 ± 2.8 ‰) (Fig 14a & b). Isotopic enrichment of ^{15}N in unvegetated soil areas indicates a greater loss of N via microbial processes, as plant uptake does not occur. Production pathways of N_2O in Arctic regions are predominantly nitrification, where N_2O is produced in the oxidation of NH_4^+, and denitrification, where N_2O is an

intermediate in the reduction of NO_2^- and NO_3^- to produce dinitrogen (N_2) gas. Both of these pathways are highly sensitive to changes in oxygen availability and due to the variable nature of hydrology in polygonized tundra (Liljedahl et al., 2016), microsite variability in moisture content may support high rates of N_2O production through both nitrification and denitrification. However, as nitrification is an aerobic process and denitrification is largely anaerobic dominated (Butterbach-Bahl, 2011), it is likely that emissions of N_2O from collapsing polygon features were primarily from nitrification due to the strong relationship with properties governing oxygen availability. Data from $\delta^{15}N$ and $\delta^{13}C$ in unvegetated areas showed no relationship with depth in the top 15 cm of the soil column, likely as differences would develop in areas of substantially different oxygen availability, or close to the permafrost (Supplementary Fig. S8).

Significantly lower C:N ratios ($p = 0.03$) were found in unvegetated soils (14.82 ± 0.52) than in vegetated (17.63 ± 1.1) (Fig. 14c). This supports N_2O emissions patterns as higher N content is associated with higher N bioavailability (Liimatainen et al., 2018). Differences in C:N ratio were driven by a higher N content in unvegetated areas (17.6 ± 0.7 mg N g^{-1}) than in vegetated soils (10.3 ± 1.4 mg N g^{-1}) (Supplementary Fig S9). Total C and N content per volume was not significantly different when standardizing with mean bulk density measurements (Supplementary Fig. S10). In vegetated soil areas, C:N ratios generally decreased with depth in the top 15 cm of the soil column (Supplementary Fig. S11), likely related to plant N uptake occurring at increased rates closer to the surface where plant root tissue is more abundant (Subbarao et al., 2009; Hodge et al., 2000).

Implications of N_2O fluxes on collapsing tundra feature for the N budget.

Data presented here have important implications for regional estimations of future N_2O emissions due to the substantial hydrological change of high latitude ecosystems and the increased permafrost degradation with climate change. Arctic wetlands maintain water tables at or above the soil surface for most or all of the year, due to limited drainage created by the permafrost barrier, facilitating anaerobic conditions in the soil column (Lipson et al., 2011). However, as regional warming continues, permafrost degradation could translate into increased drainage, lateral movement of water and drainage of polygon tundra (Oelke et al., 2004; Liljedahl et al., 2016). This can increase the prevalence of block eroding polygon features that develop with permafrost thaw and degradation of polygon ice cores, thereby increasing the potential of Arctic wetlands to be globally significant emitters of N_2O.

This work highlights the need for additional N_2O flux measurements across a wide range of sites in heterogeneous tundra environments to represent the variability of emissions due to terrain relief and vegetation composition. Results show that parts of the landscape in the Arctic coastal plains can be strong N_2O sources if vegetation cover is limited, particularly in drier porous soils. There is currently a paucity of in situ data over longer time periods making upscaling to regional estimates very challenging. N_2O emission events can be stochastic and therefore difficult to capture as conditions favorable for N_2O production and release, such as redox potential, soil texture, and nutrient availability can rapidly change or be highly spatially variable (Siewert et al., 2021). As a result, rates observed here are only representative of the growing season and the annual contribution to the global N_2O budget from these regions is still currently

unknown. In particular, N_2O flux data from outside of the growing season is needed. Year-round flux measurements at the landscape level, i.e., eddy covariance, are needed to sufficiently constrain seasonal budget dynamics and to better inform model parameterizations. Arctic wetlands exhibit strong emissions of both CO_2 and CH_4 during seasonal shoulder periods, notably in the autumn during soil freezing (Oechel et al., 2014; Mastepanov et al., 2013; Zona et al., 2016). As plant-microbe competition for inorganic N should be more limited during this time, due to lower plant productivity and plant senescence, emissions of N_2O may occur over a larger area. Data collected during the spring could reveal large budgetary contributions as the thaw period has been associated with peak N_2O emission (Voigt et al., 2017). A budgetary understanding of regional emissions of N_2O will likely increase warming potential estimates of Arctic wetlands and account for an additional warming feedback.

Materials and methods

Study site.

This study was performed near Utqiaġvik, Alaska at a well-developed polygonized tundra, consisting of high and low-center polygons, on the BEO (71 16’ 51’’N, 156 26’ 44’’W) (Fig. 11). The BEO is on the Arctic Coastal Plain in the North Slope of Alaska and is predominantly (65%) polygon tundra (Hinkel et al., 2003). Soils in the BEO are gelisols (turbels: 71%; orthels: 8%; organic soils: 1%) (Davison et al., 2016). Soil organic matter is also variable and ranges from 0 - 30 cm (Davidson et al., 2016). Vegetation consists of wet sedges and *Sphagnum* mosses in heavily inundated areas such as low center polygons and troughs, and *Polytrichum* moss/lichen dominated communities in

high-center polygon and ridge areas (Davidson et al., 2016). The water table is variable dependent on landscape relief and can be as high as 20 cm above the ground surface and as low as 50 cm below the ground surface. Collar locations were only in collapsing high-center polygons with unvegetated soil or adjacent vegetated areas also on collapsing high center polygons. All collapsing polygon features had a water table below the thaw depth throughout the study period. Mean maximum thaw depth in these features was 40 cm.

Flux and ancillary measurements.

Static chamber fluxes were measured with a Gasmet GT5000 Terra Fourier transform infrared (FTIR) greenhouse gas analyzer (GGA) and a clear, cylindrical polycarbonate chamber (50 cm height and 20cm diameter) (Supplementary Fig. S12) in a closed system at a 1Hz sampling rate. The FTIR GGA is capable of measuring concentrations of multiple gases simultaneously by scanning the full infrared spectrum and calculating the concentrations of each gas in the sample based on its absorption (San Martin Ruiz et al., 2021; Elpelt-Wessel et al., 2022). Chamber collars were made of PVC (15 cm height and 20 cm diameter) and installed 3 days prior to greenhouse gas measurements at a depth of 10 cm. Following chamber placement, measurements were recorded over 7 minutes to obtain a stable increase in GHG concentration. Fluxes were calculated according to the linear slope fitting technique (McEwing et al., 2015). Fluxes were measured at 30 locations – 10 vegetated replicates and 20 unvegetated soil replicates – whenever weather permitted over July 2021 (4th, 5th, 7th, 10th, 11th, 12th, 15th, 16th, 19th, 22nd, & 25th) for a total of 263 measurements. The consistent emissions rates across the

30 plots suggested that the sample size properly captured the emission rates of these land cover types. Detailed information or the measurement locations can be found in SI Materials and Methods, Fig. S4 and Table S2. Ancillary measurements included soil temperature, bulk density, thaw depth, soil water content, stable isotope ratios, and carbon to nitrogen (C:N) ratios. Soil water content, soil surface temperature, and thaw depth were measured at the time of each chamber measurement at the flux collar throughout the study period (n = 263). Soil water content was measured with a Fieldscout 300 TDR soil moisture meter The conditions during summer 2021 were within the ranges reported by the long-term mean (Zona et al., 2014), further supporting the representativeness of these measurements of longer-term emission rates. Soil surface temperature was measured with an infrared thermometer. Depth of thaw was measured with a small diameter metal rod. Bulk density was measured from soil samples of the top 15 cm of the soil column, collected at each collar location at the end of the study period, for a total of 30 data points. Samples were dried for 24 hours at 60 C in a drying oven and weighed per volume.

Stable isotope analysis.

Soil samples from the top 15 cm of the soil column were removed at both vegetated and unvegetated areas near where fluxes were measured using a handheld soil sampling corer (7 cm diameter, 15 cm height) at the end of the experiment. Soil samples consisted of four profiles with three depths for a total of 24 samples. Samples were frozen and shipped to San Diego State University for stable isotope analysis. Samples were then separated into 5 cm depth segments (to check relationship with depth) using a band

saw, placed in a drying oven at 65 C for 48 hours, then homogenized with a vibratory ball mill. The abundance of ^{15}N, ^{13}C, and C:N ratios were measured using a continuous flow isotope ratio mass spectrometer (IRMS, Delta V Advantage, Thermo Fisher Scientific). A laboratory standard (USGS41, L-glutamic acid) was used as a reference material for the calibration of stable carbon and nitrogen measurements. Isotope values are reported in standard δ notation (‰) relative to Vienna PeeDee Belemnite ($\delta^{13}C$) and air-N_2 ($\delta^{15}N$).

Data analysis.

All data analyses were performed in R software (R Core Team, 2019). Data organization was performed using the 'data.table' (Dowle and Srinivasan, 2021) R package. Repeated measures ANOVAs were used for comparisons of N_2O and CO_2 fluxes using collar location as a random variable to represent hierarchical structure, controlling for the pseudo replication related to measuring the same plots multiple times during the summer. Univariate linear regressions were used to examine the relationship of N_2O fluxes with soil water content, bulk density, and soil temperature (Fig. 13). Regressions of N_2O fluxes with soil water content and bulk density were performed with log linearized data given the skewed distribution of the N2O fluxes (Fig. 13). Multivariate linear regression models were used to explain combined variability in N_2O fluxes. Assumptions of normality and homoscedasticity were verified with residual diagnostic tests. All model variables for multivariate linear regression models were checked for multicollinearity using the 'olsrr' R package (Hebbali, 2020). Graphics were generated using the 'ggplot2' (Wickham, 2016), 'ggsignif' (Ahlmann-Eltze and Patil, 2021), and 'cowplot' (Wilke, 2020)

packages. As bulk density measurements were taken once per collar, univariate linear regression analysis using bulk density was performed using mean N_2O flux per collar and therefore does not capture the single-point variability of each measurement location throughout the study period. For the same reason, multivariate linear regression models including bulk density were conducted using per-collar averages of N_2O flux, soil water content, and soil temperature. T-tests were used for comparisons of stable isotope content and C:N Ratios (Fig. 14).

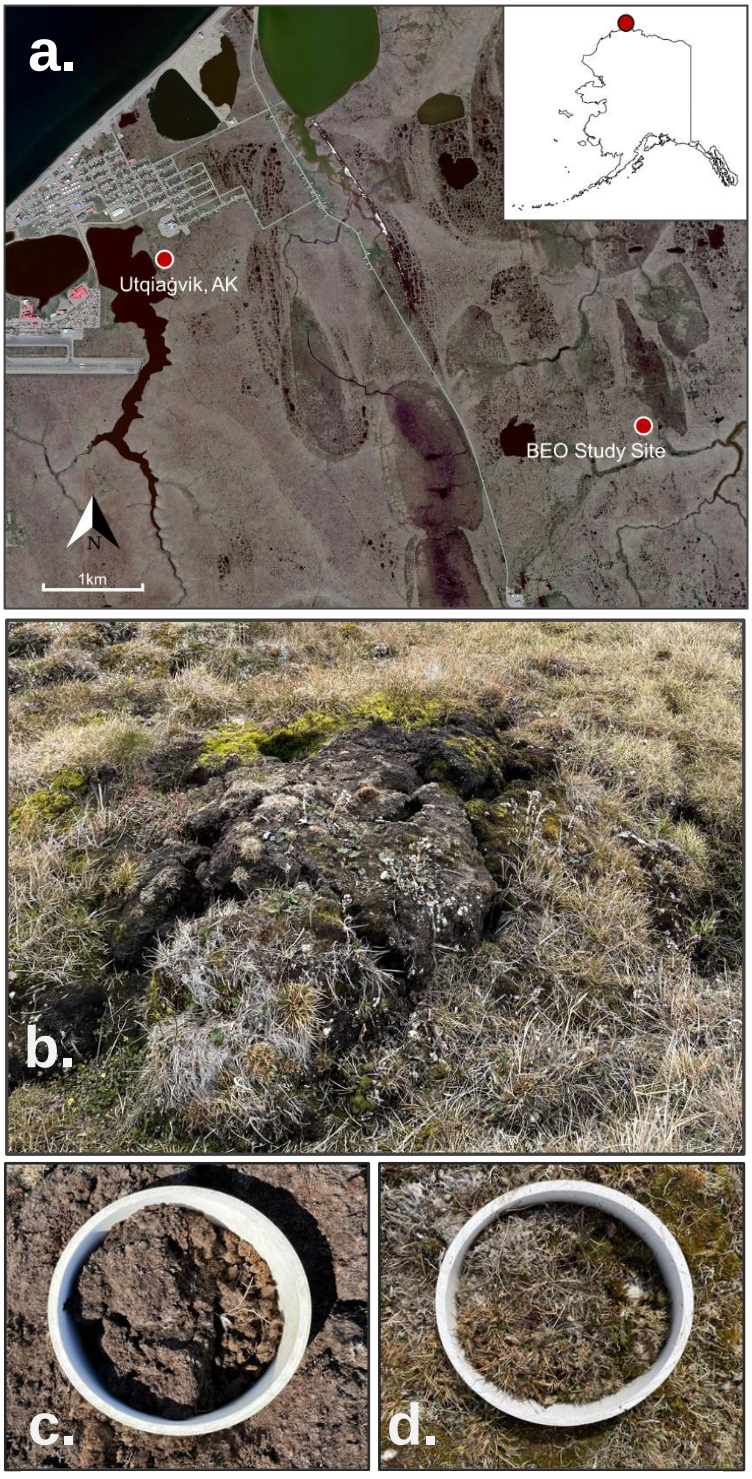

Figure 11. (a) Map of study area near Utqiaġvik, AK and (b) collapsing polygon landscape feature with photos of collars with (c) unvegetated and (d) vegetated surface. Imagery is from Google, provided by Maxar Technologies.

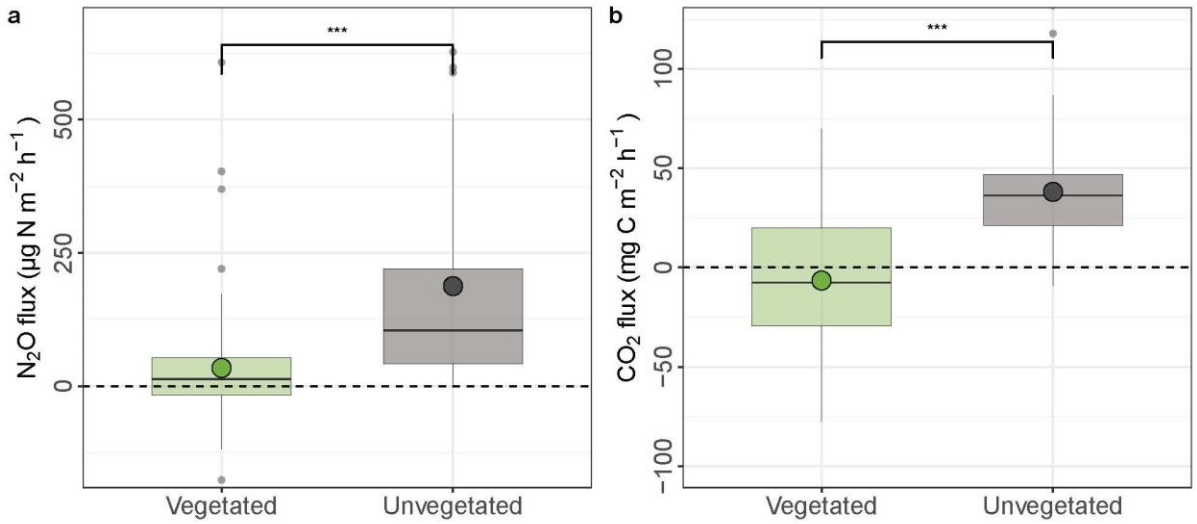

Figure 12. Comparison of fluxes of (a) N2O (µg N m-2 hr-1) and (b) CO2 (mg C m-2 hr-1) at areas with vegetated and unvegetated soil surfaces. Circles represent means. *** = p<0.001.

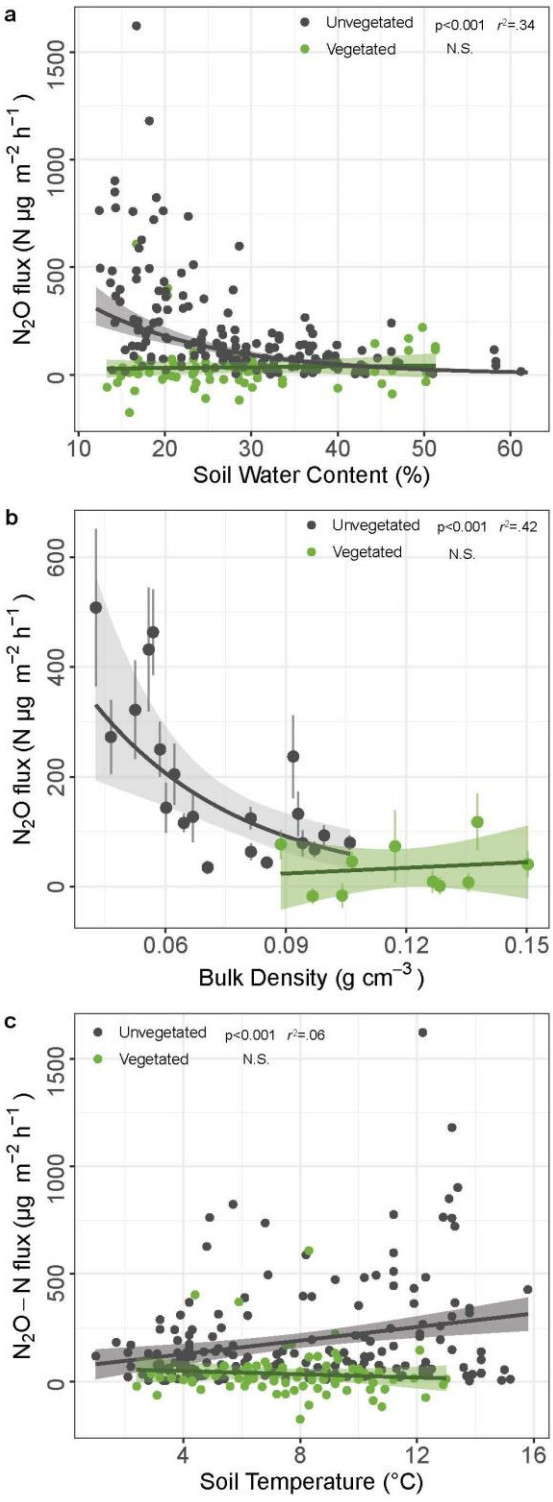

Figure 13. Linear regressions of dominant controlling variables (a) soil water content, (b) bulk density and (c) soil temperature. Bulk density is measured per collar location with N2O flux represented as mean per collar. Error bars represent ± standard error. All regressions were significant in unvegetated soils ($p<0.001$) and not significant (N.S.) for vegetated soils. For regressions with soil water content and bulk density, r^2 values are reported for log linearized data.

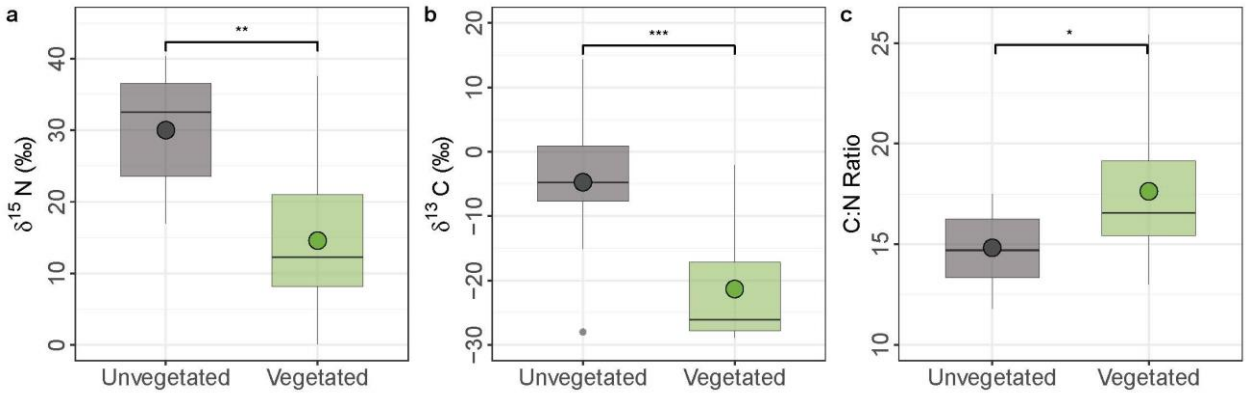

Figure 14. Comparison of mean (a) $\delta^{15}N$, (b) $\delta^{13}C$, and (c) C:N ratio from soil samples with unvegetated and vegetated surface. *=p<0.01; **=p<0.005; ***=p<0.001.

Supplementary Material for article "Collapsing polygons are strong sources of N_2O in Alaskan Arctic tundra."

Supplementary Figure 5. Photos of collapsing polygon surfaces on the Barrow environmental observatory, near Utqiaġvik, AK.

Supplementary Figure 6. Comparisons of soil temperature, soil water content, thaw depth, and bulk density at vegetated and unvegetated areas on collapsing polygons.

Supplementary Figure 7. Regression of thaw depth and N_2O fluxes at vegetated and unvegetated areas on collapsing polygons.

Supplementary Figure 8. Nitrogen (^{15}N) and carbon (^{13}C) stable isotope ratios and variability with soil depth at vegetated and unvegetated areas on collapsing polygons.

Supplementary Figure 9. Total soil nitrogen and carbon content and variability with soil depth at vegetated and unvegetated areas on collapsing polygons both raw data and corrected with mean bulk density.

Supplementary Figure 10. Carbon to nitrogen ratios and variability with soil depth at vegetated and unvegetated areas on collapsing polygons.

Supplementary Figure 11. Comparisons of soil content per volume of N and C and soil depth at vegetated and unvegetated areas on collapsing polygon features

Supplementary Figure 12. Static flux chamber and Fourier transform infrared greenhouse gas analyzer setup.

Supplementary Table 3. Multivariate regression model performance

Supplementary Figures

Figure S5. Photos of landscape and a collapsing high-centered polygon exhibiting both block erosion and vegetation disturbance at the surface.

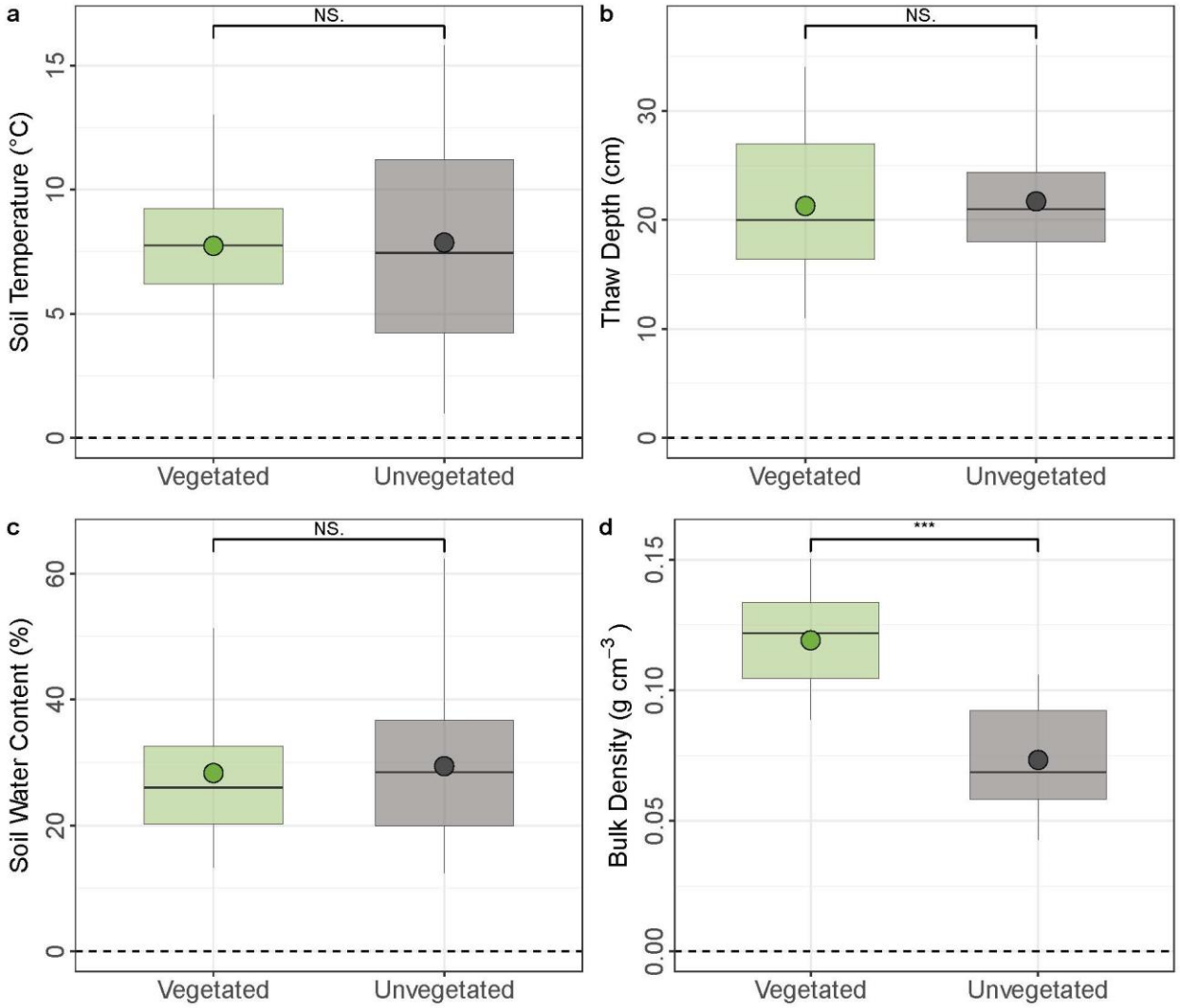

Figure S6. Comparisons of soil parameters at vegetated and unvegetated areas on collapsing polygon features including (a) soil temperature, (b) thaw depth, (c) soil water content and (d) bulk density. *** = p<0.001 and NS. indicates no significance.

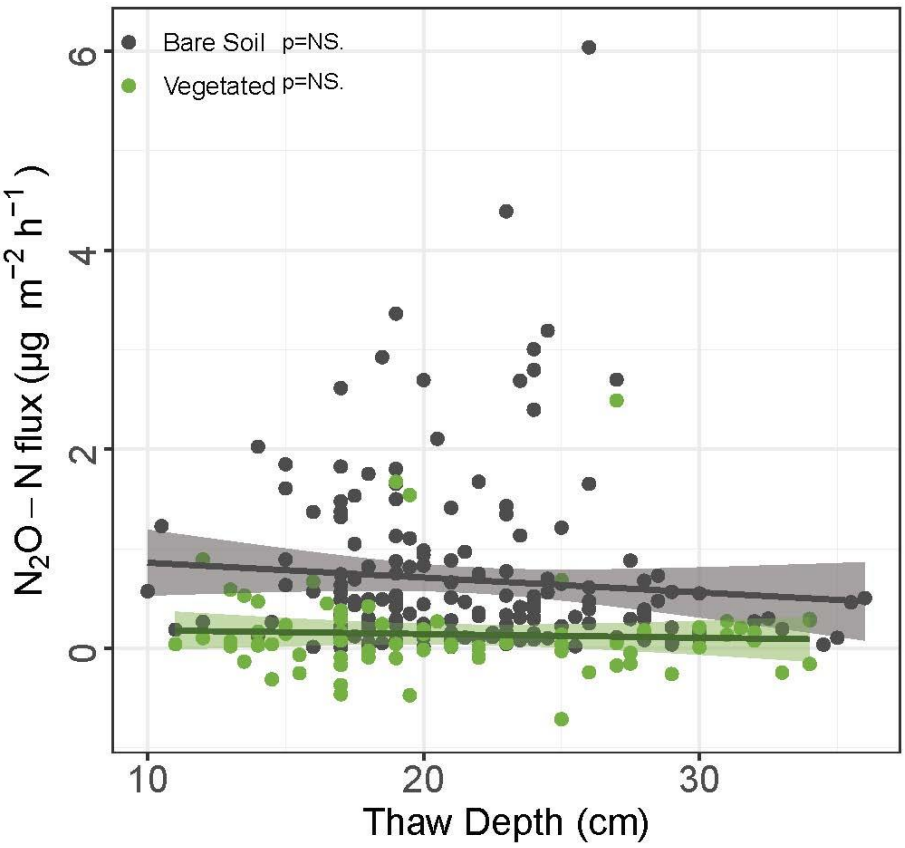

Figure S7. Linear regression of N_2O flux and thaw depth a at vegetated and unvegetated areas on collapsing polygon features. NS. Indicates not significant.

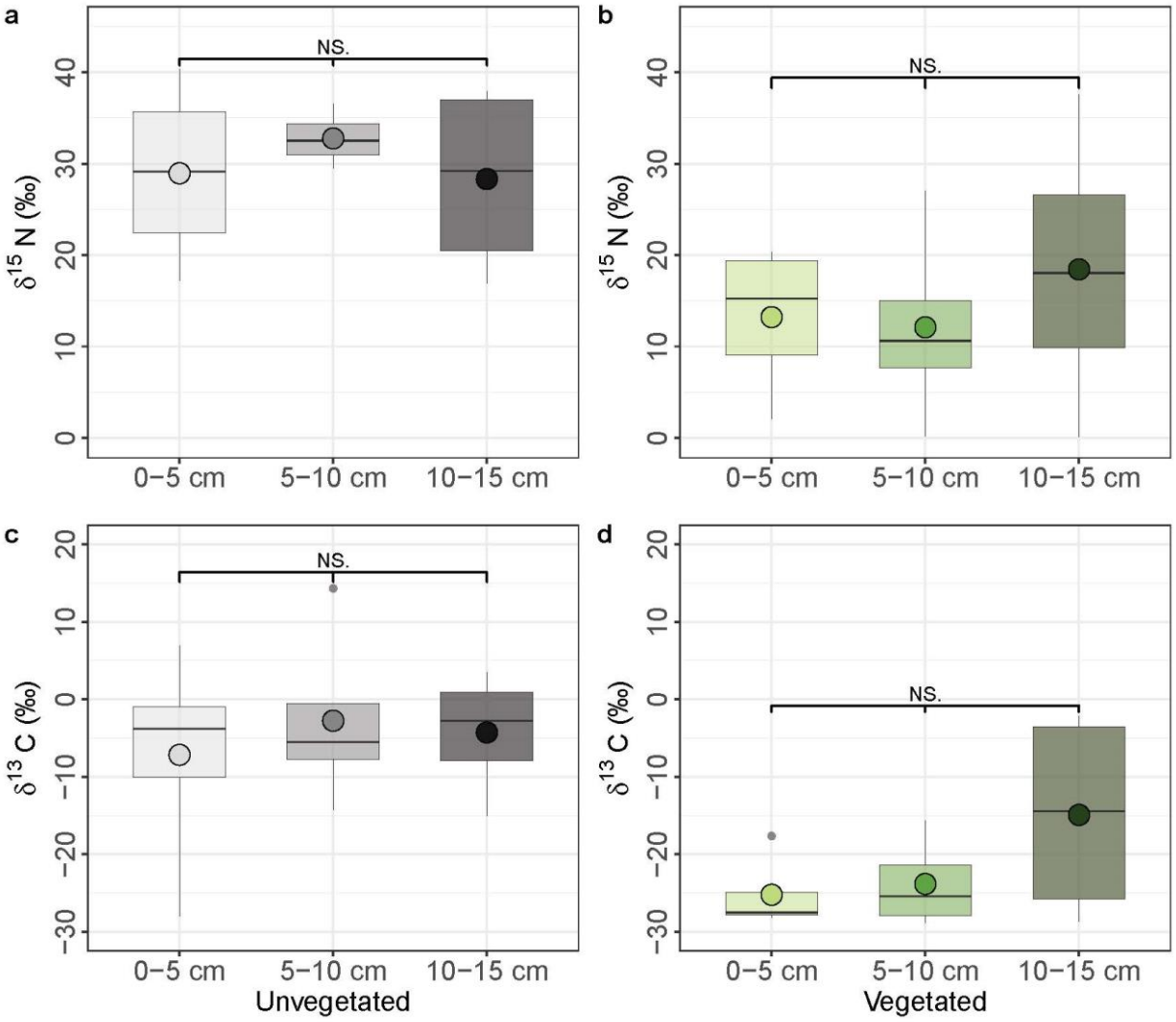

Figure S8. Comparisons of stable isotope ratios of $d^{15}N$ (a & b) and $d^{13}C$ (c & d) and soil depth at vegetated and unvegetated areas on collapsing polygon features. NS. indicates no significance.

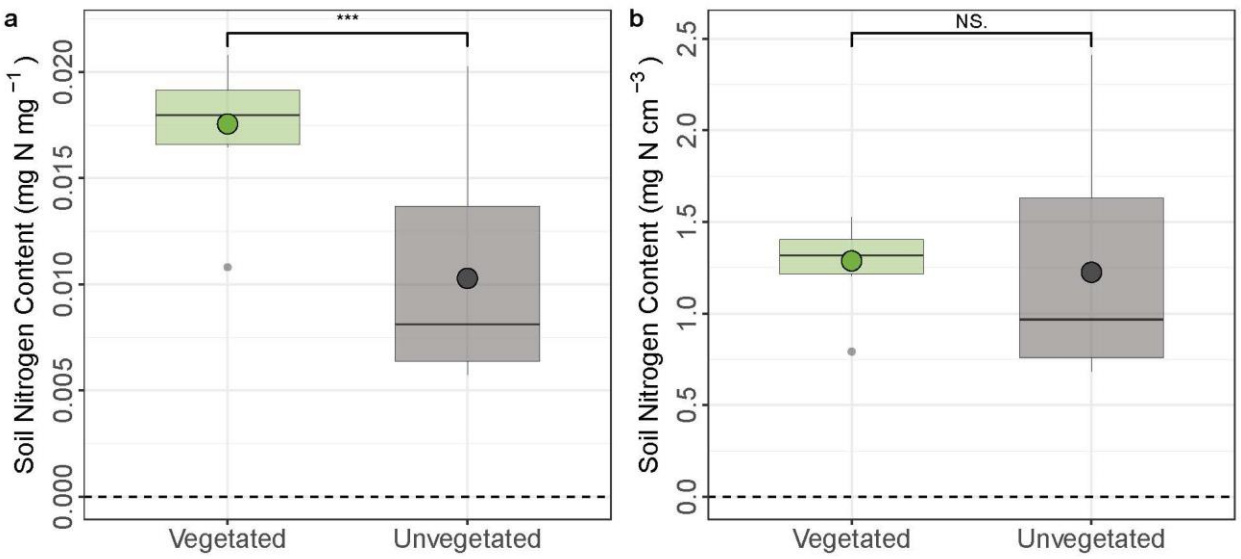

Figure S9. Comparisons of soil nitrogen content by (a) weight and (b) volume at vegetated and unvegetated areas on collapsing polygon features. NS. indicates no significance.

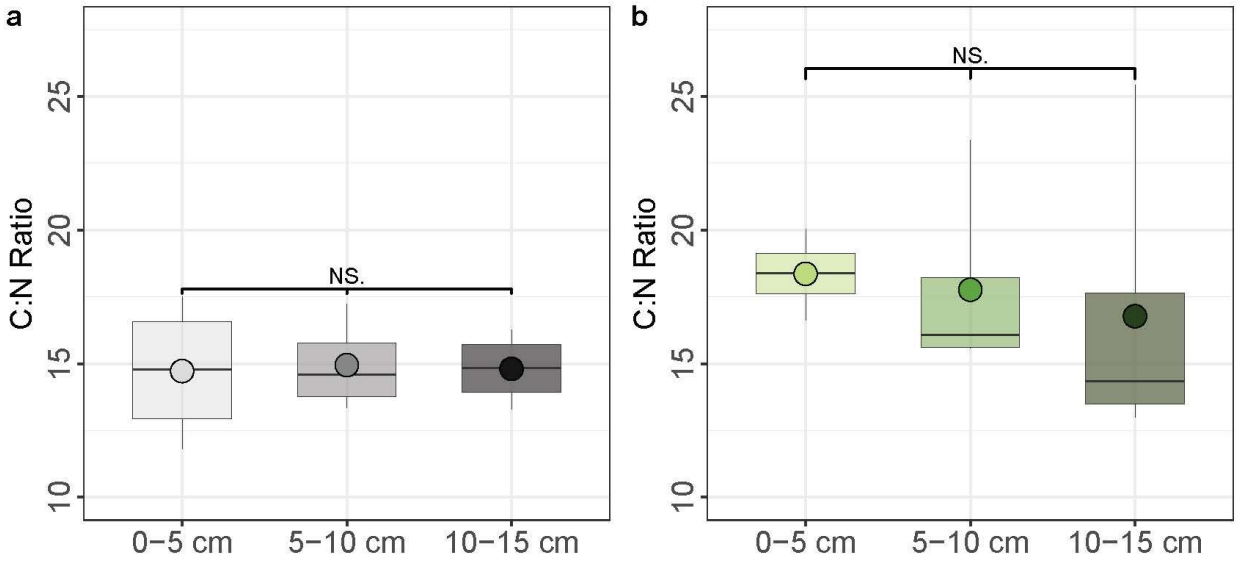

Figure S10. Comparisons of carbon to nitrogen ratios and soil depth at (a) unvegetated and (b) vegetated areas on collapsing polygon features. NS. indicates no significance.

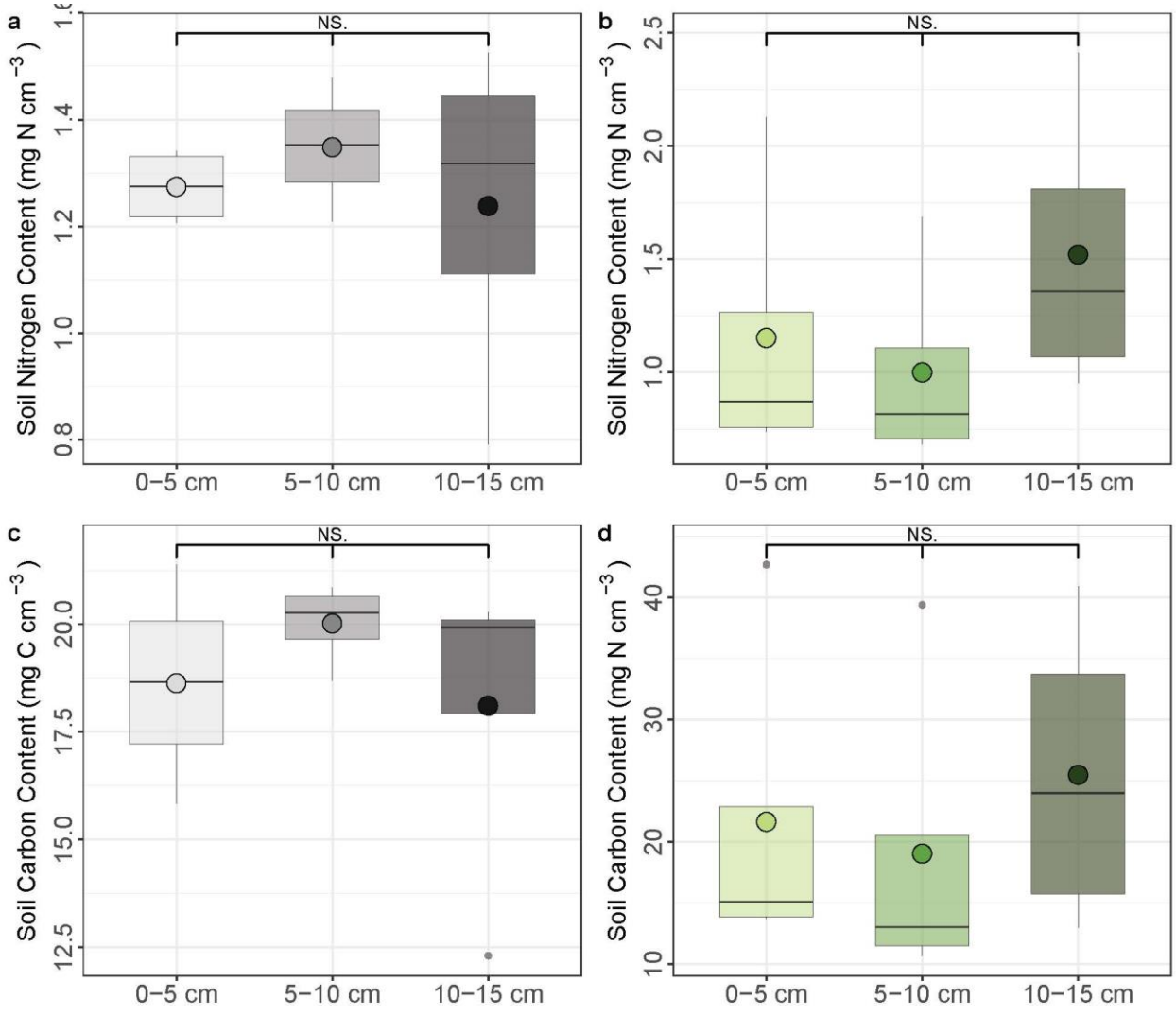

Figure S11. Comparisons of soil content per volume of N (a & b) and C (c & d) and soil depth at vegetated and unvegetated areas on collapsing polygon features. NS. indicates no significance.

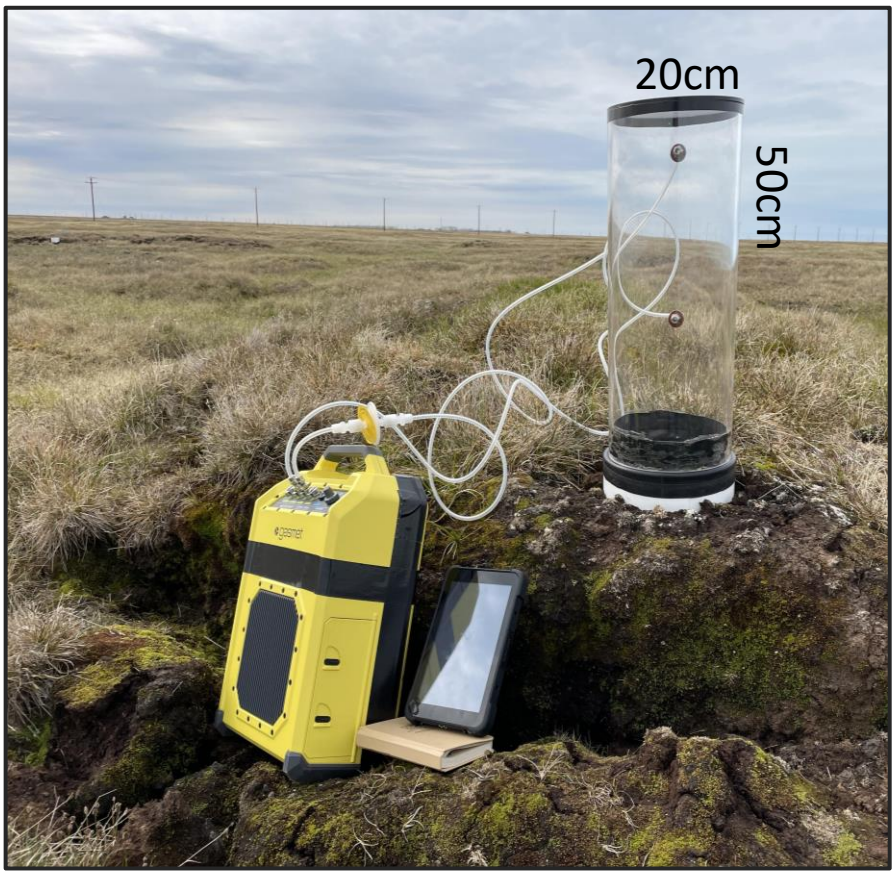

Figure S12. Photo of FTIR GGA and chamber setup with dimensions on collapsing high centered polygon feature.

Supplementary Tables

Table S3. Multivariate regression model performance with log transformed N_2O fluxes. Fluxes are means per collar location (models 1 & 2) and single point measurements (model 3).

	Coefficient	Std. Error	95% CI	*t*-Statistic	Significance	VIF
Model 1						
Constant	6.13	1.96	1.99 to 10.27	3.14	0.006	-
BD	-13.24	7.3	-28.75 to 2.23	-1.81	0.08	1.61
Mean SWC	-0.05	0.02	-0.09 to -0.003	-2.25	0.039	2.31
Mean TS	0.15	0.2	-0.28 to 0.58	0.76	0.46	1.62
R-squared	***0.67***					
Adj. R-squared	***0.61***					
F-Statistic	***10.95***					
p-value	***<0.001***					
Model 2						
Constant	7.57	0.47	6.58 to 8.56	16.1	<0.001	-
BD	-12.78	7.18	-27.94 to 2.37	-1.78	0.08	1.59
Mean SWC	-0.05	0.02	-0.09 to -0.02	-3.25	0.005	1.59
R-squared	***0.66***					
Adj. R-squared	***0.62***					
F-Statistic	***16.6***					
p-value	***<0.001***					
Model 3						
Constant	0.92	0.31	0.3 to 1.54	2.92	0.004	-
SWC	-0.07	0.007	-0.08 to -0.05	-9.14	<0.001	1.09
TS	-0.001	-0.02	-0.04 to 0.04	-0.05	0.96	1.09
R-squared	***0.34***					
Adj. R-squared	***0.33***					
F-Statistic	***45.64***					
p-value	***<0.001***					
Abbreviations: SWC - soil water content; BD - Bulk Density; TS - soil temperature						

Acknowledgements

This work was funded by the National Science Foundation—Office of Polar Programs (Nos. 1204263, 1702797, & 1932900) and the NASA ABoVE Program (No. NNX16AF94A). Additional logistical support was funded by the National Science Foundation—Office of Polar Programs, the NASA ABoVE Program, NOAA CESSRST EPP (No. NA16SEC4810008), the European Union's Horizon 2020 research and innovation program (No. 629727890), and from the Natural Environment Research Council (NERC) UAMS Grant (No. NE/P002552/1). The corresponding author was supported by the Joint Doctoral Program in Ecology at San Diego State University and the University of California – Davis. We would like to thank the Ukpeaġvik Inupiat Corporation (UIC) for the ability to conduct this research on UIC owned land.

References

Abbott, B. W., & Jones, J. B. (2015). Permafrost collapse alters soil carbon stocks, respiration, CH4, and N2O in upland tundra. *Global Change Biology*, *21*(12), 4570–4587. https://doi.org/10.1111/gcb.13069

Ahlmann-Eltze, C., & Patil, I. (2021). ggsignif: R Package for Displaying Significance Brackets for 'ggplot2'. PsyArxiv. doi:10.31234/osf.io/7awm6

Andresen CG, Lara MJ, Tweedie CE, Lougheed VL. Rising plant-mediated methane emissions from arctic wetlands. (2017). *Global Change Biology* ; 23 (3):1128-1139. doi: 10.1111/gcb.13469

Bernhardt, E. S. et al. Control points in ecosystems: moving beyond the hot spot hot moment concept. Ecosystems 20, 665–682 (2017).

Bruhwiler, L., Parmentier, FJ.W., Crill, P. *et al.* The Arctic Carbon Cycle and Its Response to Changing Climate. *Curr Clim Change Rep* **7,** 14–34 (2021). https://doi.org/10.1007/s40641-020-00169-5

Butterbach-Bahl, K., Baggs, E. M., Dannenmann, M., Kiese, R., & Zechmeister-Boltenstern, S. (2013). Nitrous oxide emissions from soils: How well do we understand the processes and their controls? *Philosophical Transactions of the Royal Society B: Biological Sciences*, *368*(1621). https://doi.org/10.1098/rstb.2013.0122

Commane, R., Lindaas, J., Benmergui, J., Luus, K. A., Chang, R. Y.-W., Daube, B. C., … Wofsy, S. C. (2017). Carbon dioxide sources from Alaska driven by increasing early winter respiration from Arctic tundra. *Proceedings of the National Academy of Sciences*, *114*(21), 5361–5366. https://doi.org/10.1073/pnas.1618567114

Davidson, S. J., Sloan, V. L., Phoenix, G. K., Wagner, R., Fisher, J. P., Oechel, W. C., & Zona, D. (2016a). Vegetation Type Dominates the Spatial Variability in CH4 Emissions Across Multiple Arctic Tundra Landscapes. *Ecosystems*, *19*(6), 1116–1132. https://doi.org/10.1007/s10021-016-9991-0

Davidson, S. J., Santos, M. J., Sloan, V. L., Watts, J. D., Phoenix, G. K., Oechel, W. C., & Zona, D. (2016b). Mapping arctic tundra vegetation communities using field spectroscopy and multispectral satellite data in North Alaska, USA. *Remote Sensing*, *8*(12). https://doi.org/10.3390/rs8120978

Diáková, K. et al. (2016). Variation in N2 fixation in subarctic tundra in relation to landscape position and nitrogen pools and fluxes. Arct. Antarct. Alp. Res. 48, 111–125.

Dowle, A. and Srinivasan, A. (2021). data.table: Extension of `data.frame`. R package version 1.14.2. https://CRAN.R-project.org/package=data.table

Elpelt-Wessel, I., Reiser, M., Morrison, D., & Kranert, M. (2022). Emission determination by three remote sensing methods in two release trials. *Atmosphere*, *13*(1), 53.

Euskirchen, E. S., Bret-Harte, M. S., Shaver, G. R., Edgar, C. W., & Romanovsky, V. E. (2017). Long-Term Release of Carbon Dioxide from Arctic Tundra Ecosystems in Alaska. *Ecosystems*. https://doi.org/10.1007/s10021-016-0085-9

Gil, J., Pérez, T., Boering, K., Martikainen, P. J. & Biasi, C. Mechanisms responsible for high N2O emissions from subarctic permafrost peatlands studied via stable isotope techniques. Glob. Biogeochem. Cycles 31, 172–189 (2017).

Harden, J. W., Koven, C. D., Ping, C. L., Hugelius, G., David McGuire, A., Camill, P., … Grosse, G. (2012). Field information links permafrost carbon to physical

vulnerabilities of thawing. *Geophysical Research Letters*, *39*(15), 1–6. https://doi.org/10.1029/2012GL051958

Hebbali, A. (2020). olsrr: Tools for Building OLS Regression Models. R package version 0.5.3. https://CRAN.R-project.org/package=olsrr

Hinkel, K. M., Eisner, W. R., Bockheim, J. G., Nelson, F. E., Peterson, K. M., & Dai, X. (2003). Spatial Extent, Age, and Carbon Stocks in Drained Thaw Lake Basins on the Barrow Peninsula, Alaska. *Arctic, Antarctic, and Alpine Research*, *35*(3), 291–300. https://doi.org/10.1657/1523-0430(2003)035[0291:SEAACS]2.0.CO;2

Hodge A, Robinson D, Fitter A. Are microorganisms more effective than plants at competing for nitrogen? Trends Plant Sci. 2000 Jul;5(7):304-8. doi: 10.1016/s1360-1385(00)01656-3. PMID: 10871903.

Hugelius, G., Strauss, J., Zubrzycki, S., Harden, J. W., Schuur, E. A. G., Ping, C. L., … Kuhry, P. (2014). Estimated stocks of circumpolar permafrost carbon with quantified uncertainty ranges and identified data gaps. *Biogeosciences*, *11*(23), 6573–6593. https://doi.org/10.5194/bg-11-6573-2014

IPCC 2014 Climate change 2014: synthesis report Contribution of Working Groups I, II and III to the Fifth Assessment Report of the Intergovernmental Panel on Climate Change

Jorgenson, M. T., & Shur, Y. (2007). Evolution of lakes and basins in northern Alaska and discussion of the thaw lake cycle. *Journal of Geophysical Research: Earth Surface*, *112*(2). https://doi.org/10.1029/2006JF000531

Jorgenson, M. T., Racine, C. H., Walters, J. C., & Osterkamp, T. E. (2001). Permafrost degradation and ecological changes associated with a warming climate in central Alaska. *Climatic Change*, *48*(4), 551–579. https://doi.org/10.1023/A:1005667424292

Liimatainen, M., Voigt, C., Martikainen, P. J., Hytönen, J., Regina, K., Óskarsson, H., & Maljanen, M. (2018). Factors controlling nitrous oxide emissions from managed northern peat soils with low carbon to nitrogen ratio. Soil Biology and Biochemistry, 122, 186-195.

Liljedahl, A. K., Boike, J., Daanen, R. P., Fedorov, A. N., Frost, G. V., Grosse, G., … Zona, D. (2016). Pan-Arctic ice-wedge degradation in warming permafrost and its influence on tundra hydrology. *Nature Geoscience*, *9*(4), 312–318. https://doi.org/10.1038/ngeo2674

Lipson, D. A., & Zona, D. (2011). Water table height and microtopography control biogeochemical cycling in an Arctic coastal tundra ecosystem. *Biogeosciences Discussions*, *8*(4), 6345–6382. https://doi.org/10.5194/bgd-8-6345-2011

Lipson, D. A., Zona, D., Raab, T. K., Bozzolo, F., Mauritz, M., & Oechel, W. C. (2012). Water-table height and microtopography control biogeochemical cycling in an Arctic coastal tundra ecosystem. *Biogeosciences*, *9*(1), 577–591. https://doi.org/10.5194/bg-9-577-2012

Martin A F, Lantz T C and Humphreys E R. (2018). Ice wedge degradation and CO2 and CH4 Northwest Territories Arct. Sci. 4 130–45

Marushchak, M. E., Kerttula, J., Diáková, K., Faguet, A., Gil, J., Grosse, G., … Biasi, C. (2021). Thawing Yedoma permafrost is a neglected nitrous oxide source. *Nature Communications*, *12*(1). https://doi.org/10.1038/s41467-021-27386-2

Marushchak, M. E., Pitkämäki, A., Koponen, H., Biasi, C., Seppälä, M., & Martikainen, P. J. (2011). Hot spots for nitrous oxide emissions found in different types of permafrost peatlands. *Global Change Biology*, *17*(8), 2601–2614. https://doi.org/10.1111/j.1365-2486.2011.02442.x

Mastepanov, M., Sigsgaard, C., Tagesson, T., Ström, L., Tamstorf, M. P., Lund, M., & Christensen, T. R. (2013). Revisiting factors controlling methane emissions from high-Arctic tundra. *Biogeosciences*, *10*(11), 5139–5158. https://doi.org/10.5194/bg-10-5139-2013

McEwing, K.R., Fisher, J.P. and Zona, D. (2015) Environmental and vegetation controls on the spatial variability of CH_4 emission from wet-sedge and tussock tundra ecosystems in the Arctic. Plant and Soil, 388 (1-2). pp. 37-52. ISSN 0032-079X

McGuire, A. D., Christensen, T. R., Hayes, D., Heroult, A., Euskirchen, E., Kimball, J. S., … Yi, Y. (2012). An assessment of the carbon balance of Arctic tundra: Comparisons among observations, process models, and atmospheric inversions. *Biogeosciences*, *9*(8), 3185–3204. https://doi.org/10.5194/bg-9-3185-2012

Miner, K. R., Turetsky, M. R., Malina, E., Bartsch, A., Tamminen, J., McGuire, A. D., … Miller, C. E. (2022). Permafrost carbon emissions in a changing Arctic. *Nature Reviews Earth and Environment*, *3*(1), 55–67. https://doi.org/10.1038/s43017-021-00230-3

Nadelhoffer, K. J., Giblin, A. E., Shaver, G. R. & Laundre, J. A. Effects of temperature and substrate quality on element mineralization in six arctic soils. Ecology 72, 242–253 (1991).

Natali, S. M., Watts, J. D., Rogers, B. M., Potter, S., Ludwig, S. M., Selbmann, A. K., … Zona, D. (2019). Large loss of CO2 in winter observed across the northern permafrost region. *Nature Climate Change*, *9*(11), 852–857. https://doi.org/10.1038/s41558-019-0592-8

Natali, S. M., Holdren, J. P., Rogers, B. M., Treharne, R., Duffy, P. B., Pomerance, R., & MacDonald, E. (2021). Permafrost carbon feedbacks threaten global climate goals. *Proceedings of the National Academy of Sciences of the United States of America*, *118*(21), 1–3. https://doi.org/10.1073/pnas.2100163118

Oelke, C., Zhang, T. & Serreze, M. C. Modeling evidence for recent warming of the Arctic soil thermal regime. Geophys. Res. Lett. 31, L07208 (2004).

Oechel, W. C., Laskowski, C. A., Burba, G., Gioli, B., & Kalhori, A. A. M. (2014). Annual patterns and budget of CO 2 flux in an Arctic tussock tundra ecosystem. *Journal of Geophysical Research: Biogeosciences*, *119*(3), 323–339. https://doi.org/10.1002/2013JG002431

Olefeldt, D., Goswami, S., Grosse, G. et al. Circumpolar distribution and carbon storage of thermokarst landscapes. *Nature Communications* 7, 13043 (2016). https://doi.org/10.1038/ncomms13043

Palmer, K., Biasi, C. & Horn, M. A. Contrasting denitrifier communities relate to contrasting N_2O emission patterns from acidic peat soils in arctic tundra. ISME J. 6, 1058–1077 (2012).

Post, W., Emanuel, W., Zinke, P. *et al.* Soil carbon pools and world life zones. *Nature* **298,** 156–159 (1982). https://doi.org/10.1038/298156a0

R Core Team 2019 R: a language and environment for statistical computing Vienna, Austria: R Foundation for Statistical Computing accepted (available at: www.R-project.org/)

Ramm, E., Liu, C., Ambus, P., Butterbach-Bahl, K., Hu, B., Martikainen, P. J., … Dannenmann, M. (2022). A review of the importance of mineral nitrogen cycling in the plant-soil-microbe system of permafrost-affected soils—changing the paradigm. *Environmental Research Letters*, *17*(1), 013004. https://doi.org/10.1088/1748-9326/ac417e

Repo, M. E., Susiluoto, S., Lind, S. E., Jokinen, S., Elsakov, V., Biasi, C., … Martikainen, P. J. (2009). Large N"2O emissions from cryoturbated peat soil in tundra. *Nature Geoscience*, *2*(3), 189–192. https://doi.org/10.1038/ngeo434

San Martin Ruiz, M., Reiser, M., & Kranert, M. (2021). Nitrous Oxide Emission Fluxes in Coffee Plantations during Fertilization: A Case Study in Costa Rica. *Atmosphere*, *12*(12), 1656.

Siewert, M. B., Lantuit, H., Richter, A., & Hugelius, G. (2021). Permafrost Causes Unique Fine-Scale Spatial Variability Across Tundra Soils. *Global Biogeochemical Cycles*, *35*(3), 1–19. https://doi.org/10.1029/2020GB006659

Stewart, K. J., Lamb, E. G., Coxson, D. S. & Siciliano, S. D. (2011) Bryophyte-cyanobacterial associations as a key factor in N_2-fixation across the Canadian Arctic. *Plant Soil* 344, 335–346

Stewart, K. J., Brummell, M. E., Coxson, D. S. & Siciliano, S. D. (2013). How is nitrogen fixation in the high arctic linked to greenhouse gas emissions? Plant Soil 362, 215–229

Stewart, K. J., Grogan, P., Coxson, D. S. & Siciliano, S. D. (2014). Topography as a key factor driving atmospheric nitrogen exchanges in arctic terrestrial ecosystems. Soil Biol. Biochem. 70, 96–112

Subbarao, G. V., Nakahara, K., Hurtado, M. P., Ono, H., Moreta, D. E., Salcedo, A. F., … Ito, O. (2009). Evidence for biological nitrification inhibition in Brachiaria pastures. *Proceedings of the National Academy of Sciences of the United States of America*, *106*(41), 17302–17307. https://doi.org/10.1073/pnas.0903694106

Tamocai, C., Canadell, J. G., Schuur, E. A. G., Kuhry, P., Mazhitova, G., & Zimov, S. (2009). Soil organic carbon pools in the northern circumpolar permafrost region. *Global Biogeochemical Cycles*, *23*(2), 1–11. https://doi.org/10.1029/2008GB003327

Taş, N., Prestat, E., Wang, S., Wu, Y., Ulrich, C., Kneafsey, T., … Jansson, J. K. (2018). Landscape topography structures the soil microbiome in arctic polygonal tundra. *Nature Communications*, *9*(1). https://doi.org/10.1038/s41467-018-03089-z

Taylor, M. A., Celis, G., Ledman, J. D., Bracho, R., & Schuur, E. A. G. (2018). Methane Efflux Measured by Eddy Covariance in Alaskan Upland Tundra Undergoing Permafrost Degradation. *Journal of Geophysical Research: Biogeosciences*, *123*(9), 2695–2710. https://doi.org/10.1029/2018JG004444

Treat, C. C., Marushchak, M. E., Voigt, C., Zhang, Y., Tan, Z., Zhuang, Q., … Shurpali, N. J. (2018). Tundra landscape heterogeneity, not interannual variability, controls the decadal regional carbon balance in the Western Russian Arctic. *Global Change Biology*, *24*(11), 5188–5204. https://doi.org/10.1111/gcb.14421

Turetsky, M. R. et al. Permafrost collapse is accelerating carbon release. *Nature* 569, 32–34 (2019).

Voigt, C., Lamprecht, R. E., Marushchak, M. E., Lind, S. E., Novakovskiy, A., Aurela, M., … Biasi, C. (2017). Warming of subarctic tundra increases emissions of all three important greenhouse gases – carbon dioxide, methane, and nitrous oxide. *Global Change Biology*, *23*(8), 3121–3138. https://doi.org/10.1111/gcb.13563

Voigt, C., Marushchak, M. E., Abbott, B. W., Biasi, C., Elberling, B., Siciliano, S. D., … Martikainen, P. J. (2020). Nitrous oxide emissions from permafrost-affected soils.

Nature Reviews Earth and Environment, *1*(8), 420–434. https://doi.org/10.1038/s43017-020-0063-9

Walker, D. A., Raynolds, M. K., Fred J. A. Daniëls, Einarsson, E., Elvebakk, A., Gould, W. A., Adrian E. Katenin, Sergei S. Kholod, Carl J. Markon, Evgeny S. Melnikov, Natalia G. Moskalenko, Talbot, S. S., Yurtsev, B. A., & CAVM Team. (2005). The Circumpolar Arctic Vegetation Map. *Journal of Vegetation Science*, *16*(3), 267–282. http://www.jstor.org/stable/4096690

Webber P J 1978 Spatial and temporal variation of the vegetation and its production, Barrow, Alaska Vegetation and Production Ecology ofan Alaskan Arctic Tundra ed L L Tieszen (New York: Springer) 37–112

Wickham, H. (2016). ggplot2: Elegant Graphics for Data Analysis. Springer-Verlag New York.

Wilke, C. (2020). cowplot: Streamlined Plot Theme and Plot Annotations for 'ggplot2'. R package version 1.1.0. https://CRAN.R-project.org/package=cowplot

Wilkerson, J., Dobosy, R., Sayres, D. S., Healy, C., Dumas, E., Baker, B., & Anderson, J. G. (2019). Permafrost nitrous oxide emissions observed on a landscape scale using the airborne eddy-covariance method. *Atmospheric Chemistry and Physics*, *19*(7), 4257–4268. https://doi.org/10.5194/acp-19-4257-2019

Zona, D., Lipson, D. A., Richards, J. H., Phoenix, G. K., Liljedahl, A. K., Ueyama, M., Sturtevant, C. S., and Oechel, W. C. (2014). Delayed responses of an Arctic ecosystem to an extreme summer: impacts on net ecosystem exchange and vegetation functioning, Biogeosciences, 11, 5877–5888, https://doi.org/10.5194/bg-11-5877-2014

Zona, D., Gioli, B., Commane, R., Lindaas, J., Wofsy, S. C., Miller, C. E., … Oechel, W. C. (2016). Cold season emissions dominate the Arctic tundra methane budget. *Proceedings of the National Academy of Sciences*, *113*(1), 40–45. https://doi.org/10.1073/pnas.1516017113

Zuidhoff, F. S., & Kolstrup, E. (2005). Palsa development and associated vegetation in northern Sweden. *Arctic, Antarctic, and Alpine Research*, *37*(1), 49–60. https://doi.org/10.1657/1523-0430(2005)037[0049:PDAAVI]2.0.CO;2

Zulueta, R. C., Oechel, W. C., Loescher, H. W., Lawrence, W. T., & Paw U, K. T. (2011). Aircraft-derived regional scale CO2 fluxes from vegetated drained thaw-lake basins and interstitial tundra on the Arctic Coastal Plain of Alaska. *Global Change Biology*, *17*(9), 2781–2802. https://doi.org/10.1111/j.1365-2486.2011.02433.x

Conclusion

The works presented here outline the importance of spatial and temporal variability to GHG dynamics. Seasonality, moisture status, and vegetation composition work in tandem to direct the potential of Arctic tundra to have a variable strength in terms of climate forcing potential. Emissions of CO_2, CH_4, and N_2O are all temporally and spatially specific both in emission strength and controls on production.

I show the importance of mesoscale carbon budget variability, in terms of CO_2, CH_4 and their combined climate forcing potential by using a continuous four-year dataset of eddy covariance measurements. The timing and magnitude of carbon fluxes significantly vary over only a few kilometers. Drier upland tundra exhibits increased carbon sink strength relative to drained lake basins and polygonized tundra during the growing season. This is due to both increased GPP and decreased CH_4 emission at drier areas. However, CO_2 emissions during the fall zero-curtain period offset most of the growing season uptake in these areas, showing that growing season GPP is negatively associated with annual carbon sink strength due to interseasonal variability. I also show that CH_4 emissions during the zero-curtain are equal across three diverse landscape types, outlining the need to investigate dynamics that regularize the zero-curtain CH_4 budget, despite hydrological variability. Though each of these landscape types are an annual net carbon source, polygonized tundra are the strongest mean carbon source. This is owing to having both areas of high growing season CH_4 emission and strong zero-curtain CO_2 emission. This is of particular importance as polygonized tundra make up 65% of the landscape (Hinkel et al., 2003) and are highly sensitive to temperature (Liljedahl et al., 2016). This work supplies further evidence that finer scale

heterogeneity should be taken into consideration in regional budget estimates as climate projections show a significant reduction in model error when representing moisture status (Lara et al., 2020).

I present evidence of active methanogenesis during the zero-curtain period in Arctic tundra by comparing soil CH_4 storage during the onset of this period to eddy covariance emissions throughout its duration. Mean seasonal CH_4 emissions are an order of magnitude higher than soil storage, indicating that CH_4 inputs into the soil during the zero-curtain must occur. As warming is most pronounced during the winter (Bekryaev et al., 2010) and the zero-curtain period is increasing in duration (Arndt et al., 2019), this work shows that emissions due to microbial activity during the non-growing season will likely increase as well. I also show evidence that plant mediated CH_4 transport occurs during this time, likely identifying one of the dominant pathways of CH_4 emission during the non-growing season. This outlines the need for future work investigating plant mediated methane transport during the non-growing season. These dynamics may reveal information regarding relationships of methanotrophy and methanogenesis, and contributions to CO_2 emissions during the zero-curtain period.

Finally, I show the first evidence of strong N_2O sources from Arctic Alaskan tundra, formerly thought regionally negligible. Areas of the landscape in polygonized tundra that undergo block erosion expose areas of unvegetated soil that emit N_2O at a rate more than an order of magnitude higher than previously estimated. This work identifies an important and unaccounted-for feedback in the climate forcing potential of Arctic tundra, introducing both the need to understand regional N_2O emission dynamics and a multitude of research directions. These directions include mapping areas of

potential N_2O sources, analyzing the development and increase of these features over time, understanding seasonal emission dynamics, and understanding their importance in the global N_2O burden. Moreover, this work outlines the need to include Arctic N_2O dynamics in global climate simulations.

Arctic regions currently make up the largest portion of uncertainty in climate global climate models (IPCC, 2014) due to their heterogeneity not being satisfactorily expressed in most climate models operating at low resolutions (Natali et al., 2019; Lara et al., 2020). Shifting patterns in vegetation, hydrology and GHG emissions invalidate historic dynamics currently used as benchmarks in estimating the warming potential and trajectory of these systems (Myers-Smith et al., 2011; Mastepanov et al., 2013; Liljedahl et al., 2016; Campbell et al., 2021). To this end, this work addresses crucial knowledge gaps regarding GHG dynamics in Arctic ecosystems and provides a framework for important future research directions. More work needs to be done on constraining uncertainty of the feedback potential that Arctic ecosystems may have on the Earth's climate. Collectively these chapters offer a contribution to reducing that uncertainty and open an array of research directions to begin to address it. A deeper understanding of the many processes and controls on Arctic emissions is the first step in their mitigation.

References

AMAP, 2021. Arctic Climate Change Update 2021: Key Trends and Impacts. Summary for Policy-makers. Arctic Monitoring and Assessment Programme (AMAP), Tromsø, Norway. 16 pp

Arndt, K. A., Oechel, W. C., Goodrich, J. P., Bailey, B. A., Kalhori, A., Hashemi, J., … Zona, D. (2019). Sensitivity of Methane Emissions to Later Soil Freezing in Arctic Tundra Ecosystems. *Journal of Geophysical Research: Biogeosciences*, *124*(8), 2595–2609. https://doi.org/10.1029/2019jg005242

Bekryaev, R. V., Polyakov, I. V., & Alexeev, V. A. (2010). Role of polar amplification in long-term surface air temperature variations and modern arctic warming. *Journal of Climate*, *23*(14), 3888–3906. https://doi.org/10.1175/2010JCLI3297.1

Butterbach-Bahl, K., Baggs, E. M., Dannenmann, M., Kiese, R., & Zechmeister-Boltenstern, S. (2013). Nitrous oxide emissions from soils: How well do we understand the processes and their controls? *Philosophical Transactions of the Royal Society B: Biological Sciences*, *368*(1621). https://doi.org/10.1098/rstb.2013.0122

Commane, R., Lindaas, J., Benmergui, J., Luus, K. A., Chang, R. Y.-W., Daube, B. C., … Wofsy, S. C. (2017). Carbon dioxide sources from Alaska driven by increasing early winter respiration from Arctic tundra. *Proceedings of the National Academy of Sciences*, *114*(21), 5361–5366. https://doi.org/10.1073/pnas.1618567114

Campbell, T. K. F., Lantz, T. C., Fraser, R. H., & Hogan, D. (2021). High Arctic Vegetation Change Mediated by Hydrological Conditions. *Ecosystems*, *24*(1), 106–121. https://doi.org/10.1007/s10021-020-00506-7

Hashemi, J., Zona, D., Arndt, K. A., Kalhori, A., & Oechel, W. C. (2021). Seasonality buffers carbon budget variability across heterogeneous landscapes in Alaskan Arctic tundra. *Environmental Research Letters*, *16*(3). https://doi.org/10.1088/1748-9326/abe2d1

Hinkel, K. M., Eisner, W. R., Bockheim, J. G., Nelson, F. E., Peterson, K. M., & Dai, X. (2003). Spatial Extent, Age, and Carbon Stocks in Drained Thaw Lake Basins on the Barrow Peninsula, Alaska. *Arctic, Antarctic, and Alpine Research*, *35*(3), 291–300. https://doi.org/10.1657/1523-0430(2003)035[0291:SEAACS]2.0.CO;2

Hugelius, G., Strauss, J., Zubrzycki, S., Harden, J. W., Schuur, E. A. G., Ping, C. L., … Kuhry, P. (2014). Estimated stocks of circumpolar permafrost carbon with quantified uncertainty ranges and identified data gaps. *Biogeosciences*, *11*(23), 6573–6593. https://doi.org/10.5194/bg-11-6573-2014

IPCC. Climate Change 2014: Synthesis Report. Contribution of Working Groups I, II and III to the Fifth Assessment Report of the Intergovernmental Panel on Climate Change.

Lara, M.J., McGuire, A.D., Euskirchen, E.S. *et al.* (2020). Local-scale Arctic tundra heterogeneity affects regional-scale carbon dynamics. *Nature Communications.* 11, 4925 https://doi.org/10.1038/s41467-020-18768-z

Liljedahl, A. K., Boike, J., Daanen, R. P., Fedorov, A. N., Frost, G. V., Grosse, G., … Zona, D. (2016). Pan-Arctic ice-wedge degradation in warming permafrost and its influence on tundra hydrology. *Nature Geoscience*, *9*(4), 312–318. https://doi.org/10.1038/ngeo2674

Mastepanov, M., Sigsgaard, C., Tagesson, T., Ström, L., Tamstorf, M. P., Lund, M., & Christensen, T. R. (2013). Revisiting factors controlling methane emissions from high-Arctic tundra. *Biogeosciences*, *10*(11), 5139–5158. https://doi.org/10.5194/bg-10-5139-2013

Myers-Smith, I. H., Forbes, B. C., Wilmking, M., Hallinger, M., Lantz, T., Blok, D., … Hik, D. S. (2011). Shrub expansion in tundra ecosystems: Dynamics, impacts and research priorities. *Environmental Research Letters*, *6*(4). https://doi.org/10.1088/1748-9326/6/4/045509

Natali, S. M., Watts, J. D., Rogers, B. M., Potter, S., Ludwig, S. M., Selbmann, A. K., … Zona, D. (2019). Large loss of CO2 in winter observed across the northern permafrost region. *Nature Climate Change*, *9*(11), 852–857. https://doi.org/10.1038/s41558-019-0592-8

Oechel, W. C., Laskowski, C. A., Burba, G., Gioli, B., & Kalhori, A. A. M. (2014). Annual patterns and budget of CO 2 flux in an Arctic tussock tundra ecosystem. *Journal of Geophysical Research: Biogeosciences*, *119*(3), 323–339. https://doi.org/10.1002/2013JG002431

Outcalt, S. I., Arbor, A., Nelson, F. E., & Hinkel, K. M. (1990). Region in Freezing Soil. *Water Resources*, *26*(7), 1509–1516.

Serreze, M. C., & Francis, J. A. (2006). The arctic amplification debate. *Climatic Change*, *76*(3–4), 241–264. https://doi.org/10.1007/s10584-005-9017-y

Stewart, K. J., Grogan, P., Coxson, D. S. & Siciliano, S. D. (2014). Topography as a key factor driving atmospheric nitrogen exchanges in arctic terrestrial ecosystems. Soil Biol. Biochem. 70, 96–112

Voigt, C., Lamprecht, R. E., Marushchak, M. E., Lind, S. E., Novakovskiy, A., Aurela, M., … Biasi, C. (2017). Warming of subarctic tundra increases emissions of all

three important greenhouse gases – carbon dioxide, methane, and nitrous oxide. *Global Change Biology*, *23*(8), 3121–3138. https://doi.org/10.1111/gcb.13563

Voigt, C., Marushchak, M. E., Abbott, B. W., Biasi, C., Elberling, B., Siciliano, S. D., … Martikainen, P. J. (2020). Nitrous oxide emissions from permafrost-affected soils. *Nature Reviews Earth and Environment*, *1*(8), 420–434. https://doi.org/10.1038/s43017-020-0063-9

Zona, D., Gioli, B., Commane, R., Lindaas, J., Wofsy, S. C., Miller, C. E., … Oechel, W. C. (2016). Cold season emissions dominate the Arctic tundra methane budget. *Proceedings of the National Academy of Sciences*, *113*(1), 40–45. https://doi.org/10.1073/pnas.1516017113